Radio Telescope Control System

Aaron Olsen, Zachary Martin

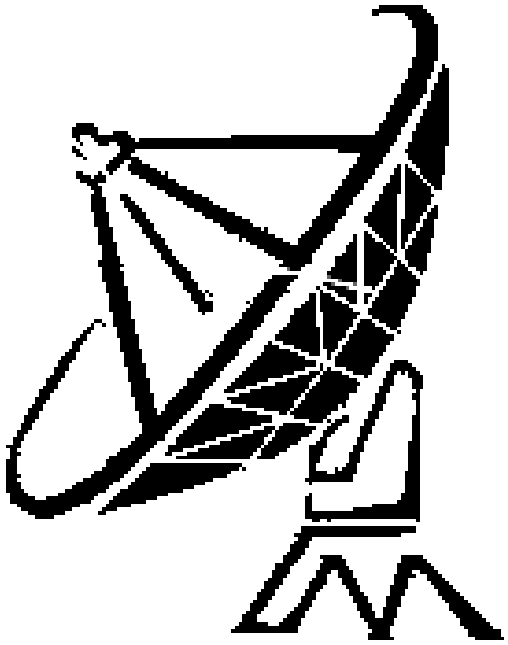

IEEE Susquehanna Section Regional Capstone Competition

Spring 2023

Abstract

Many people are familiar with the experience of looking up during a clear night and gazing at the stars. Whether through a telescope, binoculars, or with the naked eye, the night skies provide a provoking image of beauty and wonder as we observe the heavens. The night sky has long fascinated humankind, and observing celestial patterns has brought a wealth of information to mathematicians, physicists, and travelers.

The vast wealth of knowledge that can be obtained through examining the universe has prompted billions of dollars in investment in sensitive and precise telescopes and observatories, telescopes mounted on spacecraft, and a host of radio astronomy observatories. These radio astronomy observatories help us to understand another perspective of the universe: the naturally occurring radio waves emitting from stars, planets, and gases.

A low-cost, small-scale radio telescope can provide university undergraduate students with the ability to learn the basics of radio astronomy and astrophysics by taking measurements of radio frequency signals emitting from celestial objects. This paper presents the design, test, and creation of a control system that points a three-meter dish antenna at objects in the observable universe. The system was developed in accordance with the desires of a student astronomy club as well as a student chapter of the IEEE to provide students with an accessible and low-cost radio telescope system to use for research and experimentation.

This system was designed with an embedded subsystem that uses DC motor drivers in a closed-loop feedback configuration to control accurate pointing of a 3-meter dish antenna. The primary objective of the system design was to create a layer of abstraction for the main computer through a set of commands over a wired USB link that directs the dish antenna in an azimuth-elevation coordinate system. The system integrates an H-bridge to drive the motor, a microcontroller, a USB-UART converter, and more into a circuit board which was designed wholly by the capstone team and includes over 3,000 lines of C code and 100+ discrete and integrated electronic components. A manual override including an LCD display and pushbutton interface is provided so that users can perform calibrations and movements without the intervention of the computer. Power is supplied through a low-cost commercial off the shelf (COTS) module. This design resulted in a system that could accurately point the dish with a resolution of 0.1 degrees and near-perfect repeatability while seamlessly monitoring the states of the computer, local interface, and motor system. The resulting system was presented to the student clubs in such a way that anyone running the correct software can take astronomical measurements and expand on the system's capabilities for future measurements.

Table of Contents

Table of Figures

Table of Tables

Table of Equations

1. Introduction

1.1 Project Introduction

In early 2019, the scientific world was astounded by groundbreaking news: an international team of over 200 scientists presented the first image of a black hole. Using an array of radio telescopes and a technique known as "Very Long Baseline Interferometry (VLBI)," a telescope with an effective aperture size of the Earth was formed. This composite telescope, known as the "Event Horizon Telescope," not only created the first visual representation of a black hole, but confirmed physicist's simulations regarding the relativistic nature of black holes. This discovery comes as a drop in the bucket of a long lineage of scientific advances in astronomy.

Discovering the secrets of the universe has been a theme for much of recorded history. As humankind advanced, so too our discoveries in science, mathematics, and navigation advanced as a result of our innate curiosity of the heavens. Billions of dollars and entire lifetimes have been spent on measuring and recording stars, planetary motions, galaxies, and gases in the universe. The last few decades have seen numerous improvements to technologies that allow ever more accurate images of outer space. The Hubble and James Webb space telescopes, numerous ground-based observatories, and radio telescopes such as the ones that formed the Event Horizon Telescope have provided an increasingly large body of scientific measurements.

A radio telescope is a device which uses a directional antenna and control system to detect radio waves from astronomical sources in the sky. Much like with a traditional optical telescope, a radio telescope can be used to create a map of the position of stars and other objects which can be used for analysis by students, researchers, and amateur astronomers. Unlike an optical telescope, a radio telescope observes radio frequency emissions, which can lead to images of phenomena that are not visible, such as black holes, pulsars, and masars, in addition to new information on objects that are visible, such as the chemical composition of gases and stars.

Most radio telescopes are large, expensive, and custom-made for a specific lab, but the design documented in the following report is unique in that it is on a smaller scale than the radio telescopes of established research labs and at a much lower price than commercially available units. Because of this, the radio telescope project is accessible to a larger cohort of people who can accelerate crowdsourcing of astronomical data using VLBI and contribute to the citizen science movement. This project will bring a new experience to the members of the capstone design team in designing a radio telescope control system, and the end result is presented to a student astronomy club and an IEEE student chapter for their further use in astronomical research and experimentation.

1.2 Technical History

Humans have been trying to understand space and its relation to life on Earth for centuries. Almost 100 years ago, Karl Jansky of Bell Telephone Laboratories discovered that radio frequency waves from objects in space can be received by antennas on Earth. At this time, he conducted an experiment by assembling the first radio telescope-like system of a rotatable antenna from 1928 to 1930 [1]. His intention at the time was to observe radio interference as an experiment for Bell, yet he discovered that his system observed various radio sources that repeated exactly once for every rotation of the Earth.

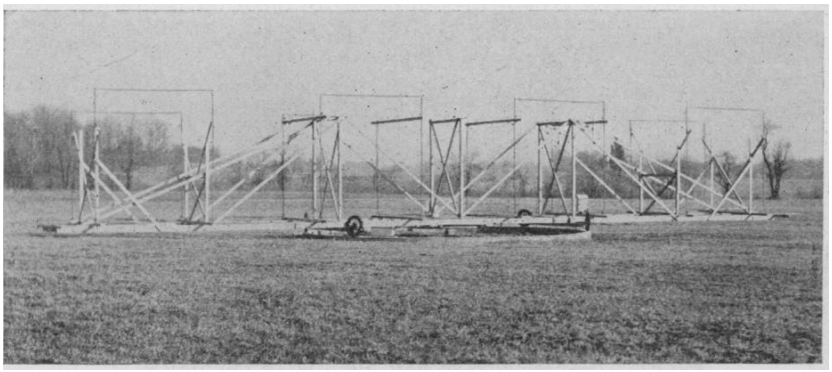

Figure 1: Karl Jansky's antenna array [2].

The system was not a dish antenna, rather it was the wire system in Figure 1 that captured waves of 14.6-meter wavelengths [1]. Other wavelengths were captured, but this was relevant to radio astronomy. The antenna was placed on a wooden turntable that was used to rotate the antenna to take measurements from multiple directions [2]. This was necessary to determine the direction of the interference for the new potential wavelengths for telecommunication. The turntable was rotated using four wheels from a Ford Model-T car and a chain drive to a small synchronous motor [2]. Quick speeds and directional accuracy were not necessary for the system because it was just trying to determine relative intensities of the measured wavelengths in a general direction. Today, radio telescopes want to create accurate intensity plots at very far distances; therefore, accurate directional movement is important. Jansky's system rotated completely every twenty minutes looking north, east, south, and west [3].

Using this system, Jansky measured the same electromagnetic interference every twenty-four hours from the same position in the sky, not originating from the sun as others previously believed it would be [4]. This was a clear indication that a source from space was creating noise in the antenna system. Thus, the start of studying space using these electromagnetic waves outside of the visible spectrum was born. He also demonstrated that the collected data could be used to plot radio maps of planets and the sun in the solar system [1]. However, it was not studied for many years due to astronomers not being radio engineers and radio engineers not being astronomers. The discovery was mostly ignored until after WWII except by Grote Reber [5].

Grote Reber studied Jansky's work and wanted to replicate the results with different wavelengths using a different system that provided greater angular resolution. The telescope built by Reber in 1940 was a paraboloidal reflector that was fully controllable and could

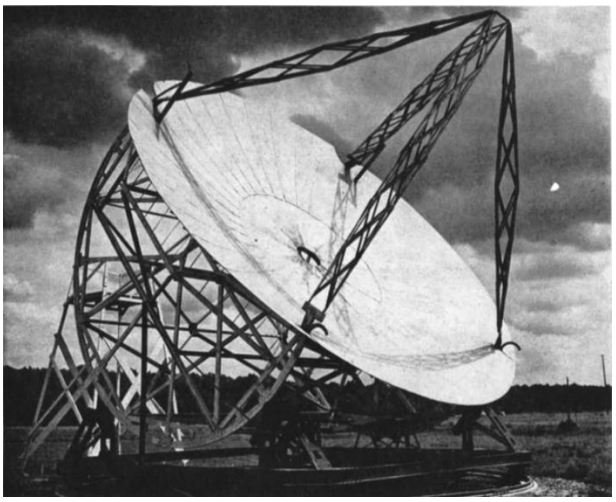

Figure 2: Grote Reber's radio telescope design with a parabolic antenna [7].

measure wavelengths in the submillimeter range [6]. This type of telescope became the main design for most telescopes following and is shown in Figure 2 [7]. The dish was 31.5 feet in diameter to get a larger angular resolution [5]. Angular resolution is the amount of radio waves that are intercepted for use in creating accurate measurements of intensity of that wavelength in the given direction. The control system must be designed to handle the dish and wavelength that needs to be measured.

In 1998 Haystack Observatory developed a Small Radio Telescope (SRT) to be used for educational purposes [8]. This introduced one of the earliest attempts at building a small radio telescope. The control system consisted of a rotor controller that was controlled by the main computer using RS-232 communication, and the system was custom made [8]. This device relied on the main computer to tell the control system how to move, and the control system just moved the antenna and converted the position data from the antenna rotor to data that the main computer could read [8].

This data is position data for antenna position correction and for the elevation/azimuth that corresponds to given intensity measured in the receiver part of the overall radio telescope system. It is used to create spectra plots that show what is in the sky in that measured location [8]. Radio telescopes are designed to make these with the greatest resolution possible to accurately study the universe.

The 1998 scopes went out of production due to CASSI going out of business and the telescopes being dwarfed by better and faster technology. This led to the development of an improved SRT in 2012 which instead of being produced by a company was assembled by the user with available blueprints and instructions [8]. The new SRT improved the signal-to-noise ratio and a better spectra resolution. This new scope also had a new system code which would send information about the target to the controller and receive position feedback [8]. The overall radio telescope system block diagram is shown in Figure 3.

This version uses a control system that only needs the desired position, and it will move to that position, reducing the strain on the main computer [8]. The main computer was reduced to storing collected data and giving commands of what positions to measure. The controller receives position data as feedback for the control loop to move the motor precisely to the desired location, and it receives position data of the rotor for recording the data with the corresponding intensity like the 1998 version [8].

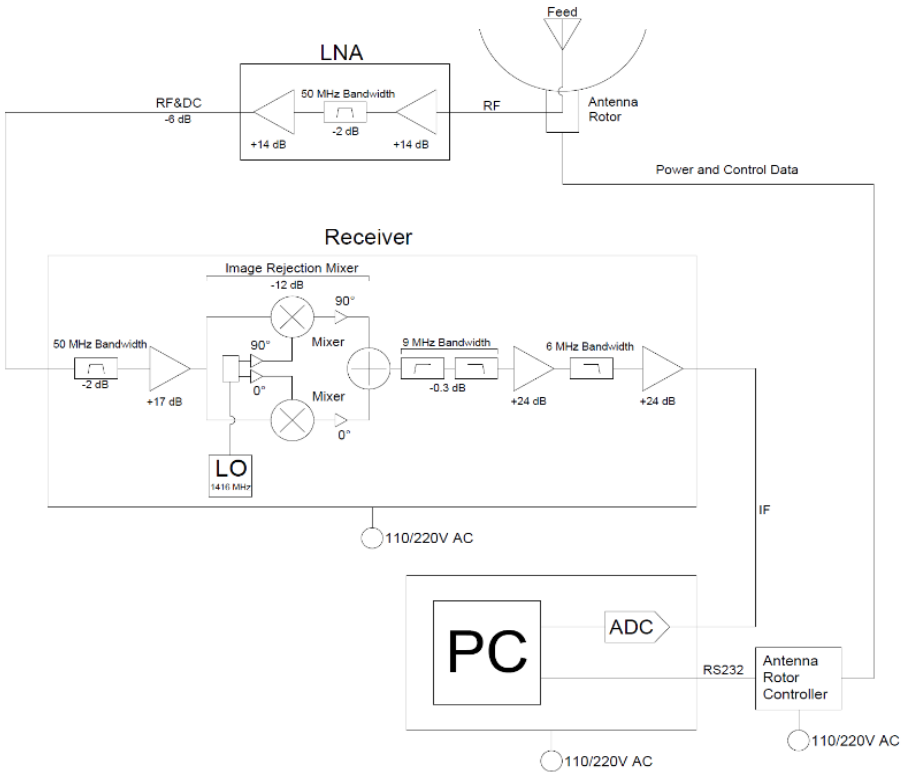

Figure 3: 2012 SRT radio telescope system block diagram from MIT [8].

Both telescopes were centered around the hydrogen line (1.42 GHz), a well-known frequency for detecting mass in the universe [8]. This discovery became a solid baseline because much of the universe consists of hydrogen or has hydrogen around significant mass that emits this frequency of electromagnetic radiation.

In 2005, the Atacama Large Millimeter Array (ALMA) radio telescope design team created a paper about this array of radio telescopes in the making. This array attempted the linking of over fifty radio telescopes into one system to increase angular resolution [9]. This increased the complexity of the control system. Each radio telescope needs its own control system, and the whole array requires a control system that unifies all of them together into a cohesive unit [9].

Each measurement and certain events need to occur at the same time. Therefore, time synchronization is key throughout the system which requires high speed communication and accurate clocks [9]. A GPS is used to support this time synchronization requirement. Also, each antenna transmits its measurement data to a central computer for analysis of all data as a whole [9]. This project is aimed to create a system like this to increase data resolution in the club project down the road. The block diagram of this array and its antennas is shown in Figure 4. This system is much more complicated than the MIT small radio telescope, but it is required because the goals of the system are to obtain high resolution images of further objects in space.

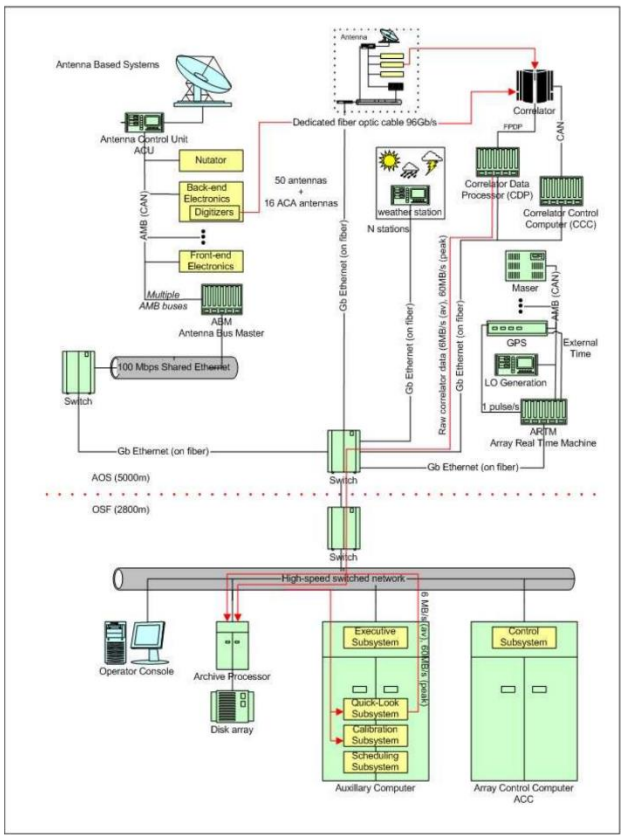

Figure 4: ALMA radio telescope array block diagram [9].

In April of 2019, the Event Horizon Telescope (EHT) comprised a global array of radio telescopes that released the first images of a supermassive black hole at the center of the Milky way, Sagittarius A* [10]. These images were made possible by the collective efforts of eight observatories to create a virtual global radio telescope. The radio telescopes array was set up in 2017 and the observations were started [10]. The innovation and collaboration of humanity made it possible to capture an image of a black hole which can be seen in Figure 5.

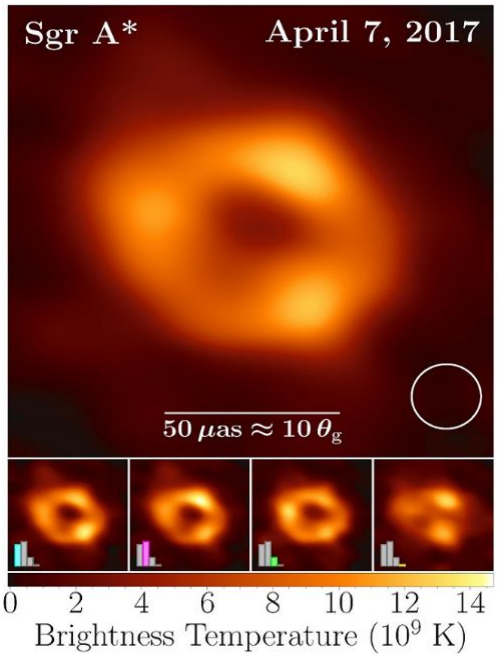

Figure 5: Picture of Sgr A by Event Horizon Telescope (EHT) in 2017, released in 2022 [24].*

1.3 Technical Literature

One of the more difficult aspects of designing a radio telescope is the control system. Accuracy of the measurement obtained by the antenna is only as good as the underlying confidence on the orientation of the antenna system.

Single-dish radio telescopes generally are reflector type antennas which consist of a reflector dish and a feed at the focal point of the dish to collect the signal. The dish antenna is positioned by virtue of two controls: altitude and azimuth [11]. These azimuth and altitude (also called elevation) positions are dictated by a main computer running a program which calculates the equatorial coordinates of the desired celestial body. This main computer directs the operation of the controller system for the angular position.

An example of a computer-controller relationship is given in the Giant Meterwave Radio Telescope (GMRT). This telescope system is an array of 30 large dish antennas of 45-meter diameter each. It uses counterweights to position the center of gravity over the motor for ease of rotation for these large dishes. The controller moves two sets of positioning motors at a constant speed, and the resulting angular position and limit switch status is fed back to the controller [11]. An overview of this Azimuth-elevation motor system is given in the figure below.

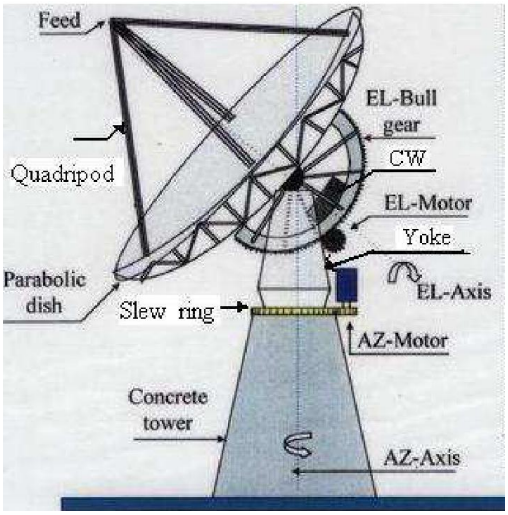

Figure 6: GMRT Servo System [12]

In this example, the controller for the antenna motion is the servo station computer (SSC). This unit controls the speed and angle of the azimuth and elevation motors (denoted AZ and EL below) and communicates that data over a wired link to the antenna base computer (ABC). The figure below shows the block diagram of the motor movement system consisting of azimuth and elevation motors, motor drive amplifiers, counter-torque system for backlash minimization, feedback of motor positioning, and the servo station controller. The SSC in this diagram has motor direction outputs, rotary encoder inputs, serial communication with the main computer,

and a human-machine interface for monitoring the status of the SSC. This SSC has since been replaced by a real-time embedded system, which is a similar approach to our system [13].

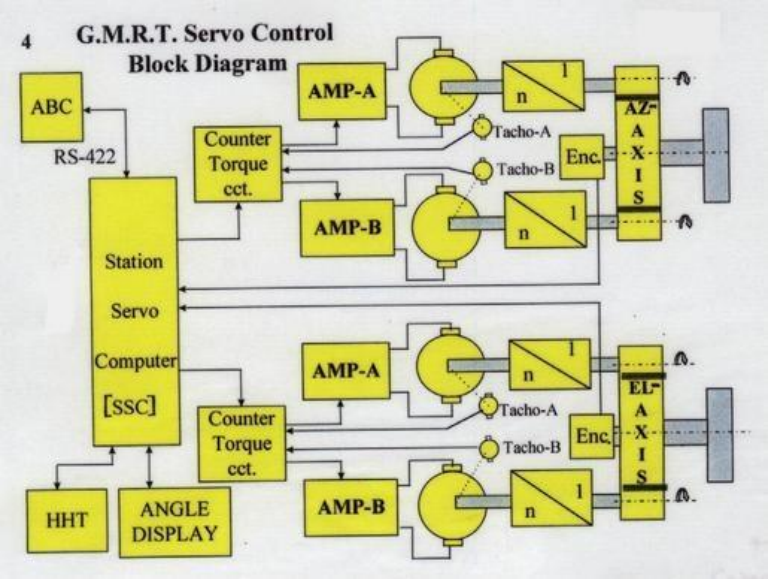

Figure 7: Block Diagram of the GMRT Control System [14]

The control loops contained in this system are shown in the diagram below. This system contains three nested control loops to control the motor current, motor speed, and the overall pointing position of the antenna. This system is given an angle via the command interface, as outlined in the simulation documentation published for this control system [12].

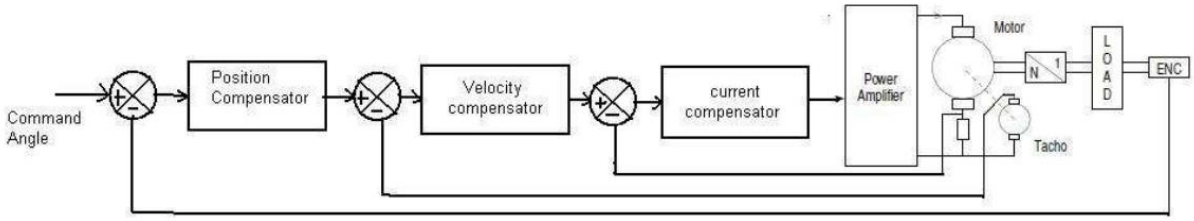

Figure 8: Control Diagram of GMRT [12]

In this proposed system, the control of the DC motor is handled by an H-Bridge designed from discrete components. This bridge can be used to move the Az-El pointing motors at slow speeds, via pulse width modulation, or at high speed with a bang-bang control. In other systems, such as the GMRT, the movement motor is a DC motor that is controlled through thyristor active AC rectifiers for speed control, as in Figure 9 [15]. This is a similar approach to other high-power servo controls in similarly sized radio telescope control systems. The proposed H-bridge will simplify the control to be adaptable to a low-cost commercial off the shelf (COTS) DC power supply module for use with single-phase utility power.

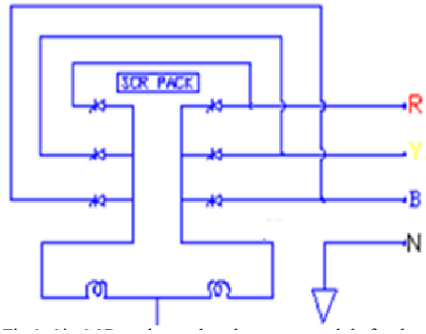

Figure 9: Thyristor Active Rectifier Motor Control [15]

Part of the challenge with designing a control system for a radio telescope is to know where the desired source is located. As the Earth is moving continuously, this becomes difficult since a fixed position relative to the earth is a variable position relative to the source itself. As these control systems are generally designed with two axes of rotation, namely altitude (vertical rotation) and azimuth (horizontal rotation), the antenna angle must be calculated—and adjusted—continuously to maintain a pointing position.

The coordinate system that is used for the command angles given to the control system is the Altitude-Azimuth system (Alt-Az), sometimes referred to as the Altitude-Elevation system. This system defines locations of celestial bodies relative to the angle above the horizon (Alt) and angle eastwards relative to the North Pole (Az). In Figure 10 (A), the celestial body (such as a star) is denoted by "X," the observer (such as a telescope) by "O," the zenith by "Z," and the horizon by the great circle formed by NMES. The altitude angle is shown by angle between the dotted line OX and the plane formed by the great circle NMES. This is marked "Alt" in the drawing. The azimuth angle is shown as the angle between the north pole and the point clockwise around the great circle, denoted by "Az" in Figure 10 (A) [16].

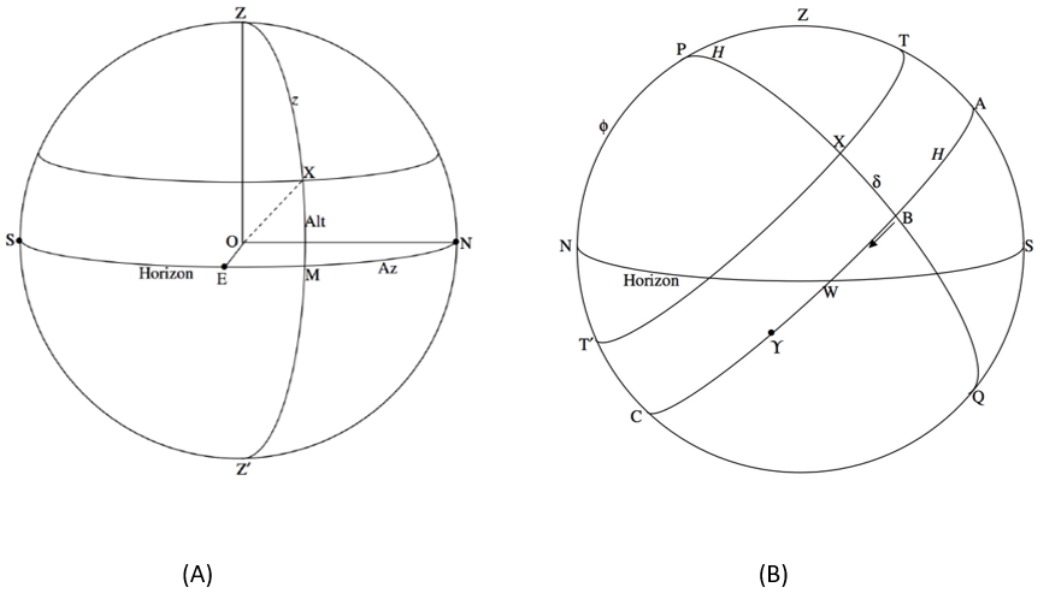

Figure 10: Alt-Az Coordinate System (A) and Equatorial Coordinate System (B) [16]

Since the earth is slowly rotating eastward, the entire sky as viewed from Earth toward the North pole is appearing to rotate counterclockwise. To track a celestial body, conversion must occur from the position given in Equatorial Coordinate System to Alt-Az coordinate system. The first part of an equatorial coordinate is the declination. This is given by δ in Figure 10 (B). The declination is given in degrees, from 0 to +90 for objects on or north of the equator, and from 0 to -90 for south of the equator. The second part of the coordinate system is the right ascension. This is denoted by the symbol α, and is given as the angle as measured eastward between γ and B on Figure 10 (B) [16]. This γ is the "First Point of Aires," which is a known reference point in the celestial sphere. Through trigonometric calculations and known sideral time, the coordinate systems can be converted from equatorial to Alt-Az, which provides the input needed for the proposed control system.

Generally, these radio telescope systems are each unique and created for a specific application by a research organization or government organization. Some of these systems use repurposed telecommunications systems with good results, such as the 7.3-meter hydrogen line Malaysian radio telescope developed for coordination with other such stations in very long baseline interferometry (VLBI) [17]. Others were able to purchase the dish, mounting, and controller directly from a research instruments supplier. One such case is the Sharjah five-meter radio telescope system, which uses the SPIDER 500A made by PrimaLuceLab [18]. This device, one of the few commercially available radio telescope systems, has a five-meter dish and very accurate control system for the price of $124,100 plus shipping [19]. On the other end of the spectrum, there are a handful of very basic kits available for hobbyist radio astronomy. One such device is the "itty-bitty telescope," which is a KU-band satellite TV dish mounted on a turntable. This kit uses the turntable as a crude azimuth control, and for the elevation it relies on adjustment of

the wing nut fastening the dish to its mount. For reception, it uses a simple power meter to indicate the relative intensity of the received signal. This device, for $269, is advertised as not for “serious” sky surveys. Indeed, it can be used mostly just for approximating the location of black body radiators.

1.4 Lifecycle of Similar Products

The lifecycle of a radio telescope can vary slightly depending on size but are mostly the same. Larger radio telescopes are in use for as long as possible because they are specifically designed for measurements at different frequencies (as many as feasible or as desired) and specific locations including space or around the globe. The larger telescopes also take a considerable cost to produce and typically only one is created due to being placed in a location that it is designed for. There is research specifically done to find new ways to increase accuracy and angular resolution through the control system and the array and antenna systems. Smaller radio telescopes are being attempted, although they are more difficult to create with higher angular resolution due to limiting the capture area. While the larger telescopes typically end up in a museum display, the smaller telescopes usually end up having parts repurposed because of the reduced cost. The smaller telescopes may be used in other projects that can benefit from a telescope with lower accuracy than the newest technology. The small radio telescope created by MIT was designed specifically so universities could have a radio telescope that can be used to demonstrate the function of them to university students [8]. This means the lifecycle of this type of radio telescope (like the control system being proposed in this document) is slightly different from the large radio telescopes.

The lifecycle of similar products can be found in Figure 11. The research and development stage of the cycle is to determine what has been attempted before and what could potentially be used to improve the radio telescope and its control system. This stage also includes the customer requirements, constraints and standards, and engineering requirements of the device to be made. When this is completed, it enters the design and simulate stage where a design for the system is created with potential real-world components in mind. This design is simulated on software such as PSpice to prove that there is potential for the device to function as desired. Then, the product is moved to the obtain materials and assemble stage where the materials that were considered in the design stage are obtained and the system is assembled. Using these, the prototype is created and tested in sections of the device and altogether.

After the produce and test stage, the product will need to be moved to the location at which measurements will be taken if not already there. This will typically be for telescopes that are moved to space. An extra stage here will be sales and marketing for the radio telescope that this control system will be a part of. This radio telescope will be used for the IEEE club’s radio telescope project and can be sold to other campuses to help them show students the function of radio telescopes like the MIT project.

The product moves to the consumer and end-of-life stage where it is used for as long as possible and then repurposed or sent to a museum depending on the scale of the telescope. A small radio telescope such as the one being proposed in this document will likely have its components repurposed. The research and development stage typically initiates the end-of-life of the telescopes because new discoveries lead to more accurate radio telescopes. This is seen in the small radio telescope designs from MIT where the first one in 1998 was replaced by the 2012 design due to new technology being developed [8].

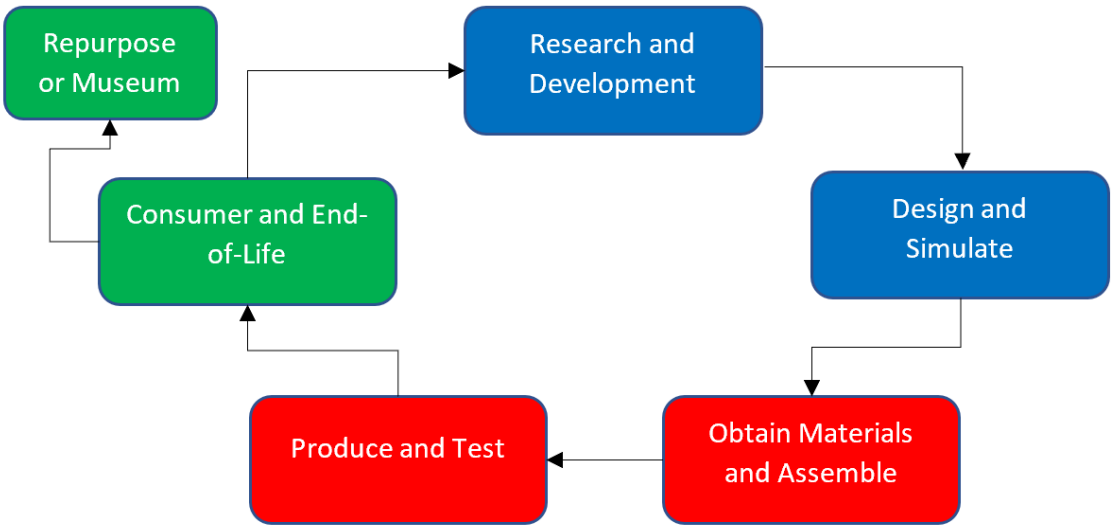

Figure 11: The product lifecycle of similar products to the radio telescope control system.

2 Experimental Method

2.1 Engineering Requirements Development

2.1.1 Customer Requirements

Meeting the requirements of the customer is crucial for the success of the product. To meet this need for the product, a customer survey was created and completed by potential customers to obtain an idea of the requirements the product must meet for a satisfied end user. The customer survey questions can be found in Appendix A at the end of this report. Based on customer ratings of the importance of different features, each feature was rated as either required (R) or desired (D). This list can be seen below. These will be weighted with respect to each other later in this section.

Measurement

- Accuracy to less than 0.5 degrees (R)
- Get result in less than 10 minutes (R)
- Automatically scan a section of the sky (R)
- Be able to measure hydrogen radiation (1.42 GHz) (R)
- Be able to measure other frequencies (D)

Access

- Price is less than $5000 (R)
- Easy access for student research, amateur astronomers, and researchers (D)

Product Use

- 120 V AC Power (R)
- 12 V DC Power (D)
- Control of device using USB standard (R)
- Option for local control at device location (D)

The three categories of features to be implemented are measurements, access, and product use as seen above. The measurements category is for degrees of accuracy, time to result, etc. The access category describes the ease of customer access to the device, and the product use relates to the user's experience using the device. The table below (Table 1) provides weighting for the relative importance of each category to the overall product. The measurements and product use are of equal importance (weight), and the access category trails both as the least important category.

Table 1: The pairwise comparison table of the categories of product features.

Categories	Measurements	Access	Product Use	Row Total	Weight
Measurements	1	3/2	1	3.5	0.38
Access	2/3	1	2/3	2.33	0.25
Product Use	1	3/2	1	3.5	0.38
			Total	9.33	1.00

The Measurements category includes the features listed below in Table 2. The most important features in this category are accuracy, automatically scanning the sky using control system feedback, and measuring hydrogen radiation. This design must be accurate, be able to move using commands that can be concatenated to scan a section of the sky, and it must be able to support an antenna that can measure the hydrogen line's radiation. Of less importance, the resulting measurements must be within ten minutes of starting, and the device would be better if it worked at a multitude of frequencies. This means the motor must move quickly, and the antenna and receiver system that can work for many frequencies around the hydrogen line must be supported by this system.

Table 2: The pairwise comparison table of the Measurements category of product features.

Measurements	Accuracy to < 0.5 degrees	Results in < 10 minutes	Auto-scan section of sky	Measure hydrogen radiation	Measure multitude of frequencies	Row Total	Weight
Accuracy to < 0.5 degrees	1	2	1	1	2	7	0.25
Results in < 10 minutes	1/2	1	1	1/2	1	4	0.14
Auto-scan section of sky	1	2	1	1	2	7	0.25
Measure hydrogen radiation	1	2	1	1	2	7	0.25
Measure multitude of frequencies	1/2	1	1/2	1/2	1	3.5	0.12
					Total	28.5	1.00

The Access category includes the features in Table 3. This shows the price maximum and easy access for students are of equal importance. The device must be affordable and easily accessible to students. So, the product must be available for all to use which means the control

system must only cost part of the $5000 maximum on the overall radio telescope. The lower the price, the easier it is for more people to access it.

As discussed in section Technical Literature, our target budget is much lower than commercially available products that incorporate automatic movement. Other available products had prices in excess of $120,000.

Table 3: The pairwise comparison table of the Access category of product features.

Access	Price < $5000	Easy access to student research, amateur astronomers, and researchers	Row Total	Weight
Price < $5000	1	1	2	0.50
Easy access to student research, amateur astronomers, and researchers	1	1	2	0.50
		Total	4	1.00

Lastly, Table 4 displays the features included in the Product Use category. The use of 120 V AC power and control using USB communication have the highest weights. It is best to use the 120 V AC power because the system would be best calibrated to a single position and consistently used there. 12 V DC power is less important because portability is not the primary concern with customer responses. The USB control is important because the telescope will be automatically operated via a main computer. The option for local control is less important, but still a significant weight as the user will be able to move the motor system without having to run a program on the main computer. Local control provides the user with the ability to test the system at the source and observe what is happening.

Table 4: The pairwise comparison table of the Product Use category of product features.

Product Use	120 V AC Power	12 V DC Power	Remote Control (USB)	Option for Local Control	Row Total	Weight
120 V AC Power	1	3	1	2	7	0.36
12 V DC Power	1/3	1	1/2	1/2	2.33	0.12
Remote Control (USB)	1	2	1	2	6	0.31
Option for Local Control	1/2	2	1/2	1	4	0.21
				Total	19.33	1.00

Also, Figure 12 shows the weights of each category and the features of each category in an overall, graphical form for easy visualization of the importance of each.

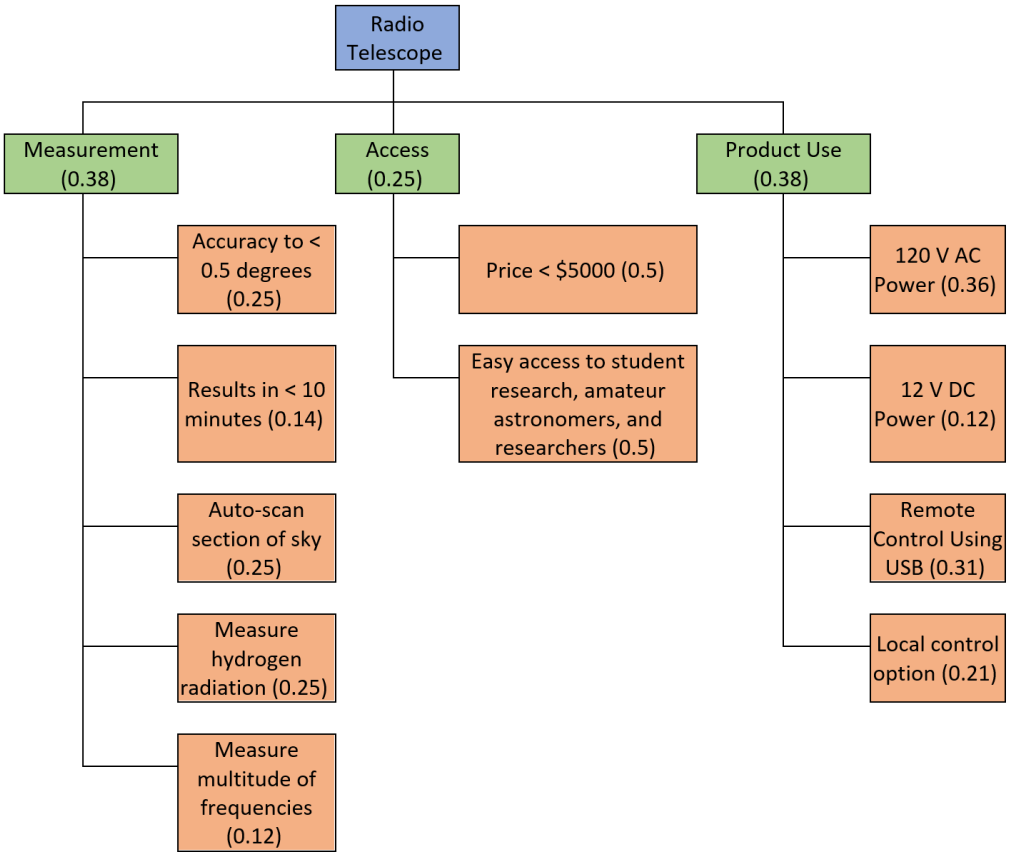

Figure 12: The objective tree including weights of the categories and features.

2.1.2 Environmental and Safety

One of the primary concerns for the deployment of a sensitive radio telescope system is the concern for minimizing external sources of interference. This concern can be so great that in certain cases, such as the green bank observatory in West Virginia, there has been established federal Quiet Zones where radio equipment is prohibited. This zone encloses approximately 13,000 square miles of land in Virginia and West Virginia, with particular emphasis in the area immediately surrounding the Green Bank observatory in West Virginia [20]. This concern for external interference limits the environment in which the radio telescope can be deployed, and in some cases mandates a quiet zone surrounding the area.

Another concern for the deployment of radio telescope systems is that generally speaking, they are quite large. In the case of the "A" configuration of the Very Large Array observatory, these systems can occupy surface area of 20 miles or more across [21]. In addition to other observatories, such as the Green Bank which limits radio emissions, these radio observatories limit resources that could be used for other purposes, such as farming, housing, or wildlife habitat. Hence, site location is a critical part of the planning of a radio telescope deployment project. In the case of the Very Large Array observatory, the location chosen was in the desert in a relatively remote area. Similarly, the Green Bank telescope is situated in a mountainous region and not near populous areas. However, as mentioned above, these radio telescope systems also limit the industrial and residential development in a larger area than just the site location, as they require a strict limit on radio emissions surrounding the installation site.

When selecting a site to install a radio telescope, prevailing weather conditions of the location should be considered. For example, areas of heavy winds or heavy snow and ice can cause mechanical and electrical failure in the system. Poor weather conditions can also affect the readings taken by the dish.

Safety concerns when operating a radio telescope system are almost entirely attributable to the concerns that arise from the movement of large dish antennas. Typical radio telescope systems are receivers only, in that they do not emit radio frequency energy and are not a source of danger in that way. However, in almost every case, the heavy antenna must be steered by a large motor and gearing system. While these antenna steering systems are typically very slow, in the order of a fraction of an RPM, the systems are large and powerful, so their movements must be considered. This safety concern led the team to observe the UL 60730-1 standard in developing the control system.

2.1.3 Political Concerns

One of the concerns that large radio telescope projects must address is the concern of political negotiation of site location. As radio telescope projects can take up enormous amounts of land, these projects may come at odds with the desires of locals and governments for that land. For example, the square kilometer array in South Africa has been the site of a political battleground. In some cases, international groups have attempted to pitch the project as a South African project in a push to get local acceptance [22]. However, local industry representatives have voiced concerns over the project being pushed on their community as it makes fracking, farming, and gas vehicle usage difficult in the surrounding area due to electromagnetic interference concerns. In vying for approval for the project in South Africa, the international astronomy societies had to make appeals to the culture and government of the area.

As the proposed design is for a small-scale radio telescope, many of the political concerns outlined above are not relevant. Since this project is small scale, the geographical footprint is small. However, should the project expand to include an array of dish antennas or backing by a governing authority, these concerns may be relevant in the case of land use and radio interference enforcement.

2.1.4 Sustainability

Sustainable designs include the three R's: reduce, reuse, and recycle. In the proposed project, all three of these factors are considered in creating a sustainable design. As the project is smaller in comparison to current designs, the component requirements were reduced overall. Throughout the design process, the participants made efforts to create minimally viable solutions to meet requirements without using excessive resources.

This project incorporates several examples of reusing. One of the biggest examples physically is the repurposing of a discarded 10-foot dish antenna designed for C band satellite television for the main reflector of the radio telescope. Similarly, a 3-foot dish designed for terrestrial wireless internet links was used for prototyping the project. Another example of reusing is the two-axis motor that is used for the control system. This motor was originally designed to point solar panels for maximum power tracking as the sun passes overhead. After the proposed radio telescope project reaches end-of-life, these components which were repurposed from their original intent can be returned to service in their original capacity. Similarly, there can be other uses for these components besides their original intent or the radio telescope project. For example, one of the options for a large C band satellite dish that was considered for this project was instead given to a farmer in Lancaster County PA to use as a hay feeder.

Unlike the larger components, the PCB will be difficult, if not impossible to reuse. Through open sourcing the design of the software and hardware for this project, anyone can observe the source files and potentially make changes to upload to the board. Since the board contains a

microprocessor and H-bridge motor driver circuit, it is conceivable that one could repurpose the microprocessor code and use the board to drive another motor system. However, the more likely outcome is that when the product reaches end of life, the PCB and its components will be recycled.

2.1.5 Constraints

Constraints are developed from the environment, time frame, cost, course requirements and customer requirements for the product. The constraints for this project are gathered from the course requirements for EE 405 and EE 406 (the Capstone Design report and implementation courses) and customer requirements. The report for the project must be completed by the end of the Fall 2022 semester according to the EE 405 course instructions. The overall project including the design and integration must be completed by the end of April of 2023 per EE406 course requirements. The overall cost of the radio telescope must be less than $5,000. A control system for this telescope should only represent a small part of this cost. Also, it must be able to support an antenna that can receive a frequency of 1.42 GHz and others in that frequency range. A result must be reached within ten minutes, so the motor must move quickly enough such that it can measure the plot of the intensity of reception in a certain resolution during that time. The accuracy must also be met in motor choice. This motor must be designed to move in both directions for both the azimuth and elevation aspects of the telescope, and it must protect against failure that could harm the user.

The overall control system must be easy to integrate with so the IEEE club can create the remainder of the radio telescope. This would include the radio receiving and processing of the information. It must also have the capability to be controlled from the location of the telescope and from a separate location where the data can be processed. It must also run on either 120 V AC or 12 V DC for common sources of power.

The following is the list of constraints that must be met in this project:

- Time:
    - Project must be completed by May 2023 (end of spring semester)
    - The report must be completed by the end of fall semester.
- Customer survey constraints:
    - Price: Under $5,000
    - Input frequency: 1.42GHz (Hydrogen measurement), secondary focus pulsars and deuterium.
    - Acquires result in less than 10 minutes.
    - Accuracy to less than 0.5 degrees
    - Option for local control
    - Either 12V DC power or 120V AC power
- Protect against motor failure.
- Bidirectional Motor Movement
- Connection for remote control via USB standard
- Integrate with IEEE club project.

2.1.6 Standards

In addition to the constraints, the following will be standards for this project:

- USB standard communication.
- UL 60730-1 standard for motor safety.
- I2C or SPI standards for communication to an LCD display.

USB is a standard form for communication which will allow a universal interface between the command computer and the proposed control system. This USB interface uses a popular integrated circuit to adapt UART characters to a USB interface, which can be accessed on the command computer via a virtual COM port in the command software. I2C standard is used to control a small LCD display for user visuals when using the local control option of the control system. The last standard that will be used is for the safety of the user. Efforts to follow the UL 60730 standard ensure that the control system is operated in a safe manner and avoids human injury. The movement of motors in this control system for the radio telescope must have redundancies to prevent harm to the user.

2.2 Engineering Requirements

The engineering requirements found in Table 5 were developed to assist in the process of developing the design of the radio telescope control system according to the marketing requirements. The marketing requirements are listed underneath the table. They are referenced in the leftmost column of the table according to which marketing requirement led to the engineering requirement. These engineering requirements were designed to be measurable to provide a method of demonstrating that the requirement is met by the end of the project.

Table 5: Engineering Requirements

Marketing Requirements	**Engineering Requirements**	**Justification**
1	Accurate to 0.5 degrees or better.	Know the antenna angle exactly
2	Minimum 1RPM Motor Speed	Obtain a measurement within 10 minutes
6	Microprocessor for <$15	Keep cost low
4	Directional dish antenna resonant at 1.42 GHz	Narrow beamwidth, higher accuracy
11	USB Communication with 115.2kbps baud rate	Communicate with main program computer.
10, 13	At least 32 Character LCD display	Ability to monitor local control.
12, 14	Limit Motor Current to 15A	Automatically shut down in case of damaged motor or wiring or in the case of human interference in the mechanical system for customer safety.
15	Bidirectional current for motor movement in either direction	Control motor speed & direction
10	Three or more buttons for local input	Control the device locally
16, 6	Subsystem PCB size < 200x200mm	Manufacturability & low price

Customer Requirements:

Measurement

1. Accuracy to less than 0.5 degrees (R)
2. Get result in less than 10 minutes (R)
3. Automatically scan a section of the sky (R)
4. Be able to measure hydrogen radiation (1.42 GHz) (R)
5. Be able to measure other frequencies (D)

Access

6. Price is less than $5000 (R)
7. Easy access for student research, amateur astronomers, and researchers (D)

Product Usability

8. 120 V AC Power (R)
9. Remote control of device using USB standard (R)
10. Option for local control at device location (D)

Standards:

11. USB standard communication.
12. UL 60730-1 standard for motor safety.
13. I2C or SPI standards for communication to an LCD display.

Constraints:

14. Protect against motor failure.
15. Bidirectional Motor Movement
16. Prototype PCB
17. Must be completed by May 2023
18. Integrate with IEEE club project.

2.3 Functional Decomposition

The radio telescope control system hierarchical chart is shown below in Figure 13. This chart includes the modules and sub-modules of the proposed design that categorize the functions of the control system. The radio telescope control system consists of four modules: the computer interface, local control, motor control, and power source. The inputs, outputs, and function of the control system, modules, and sub-modules are discussed in the subsequent level decomposition sections.

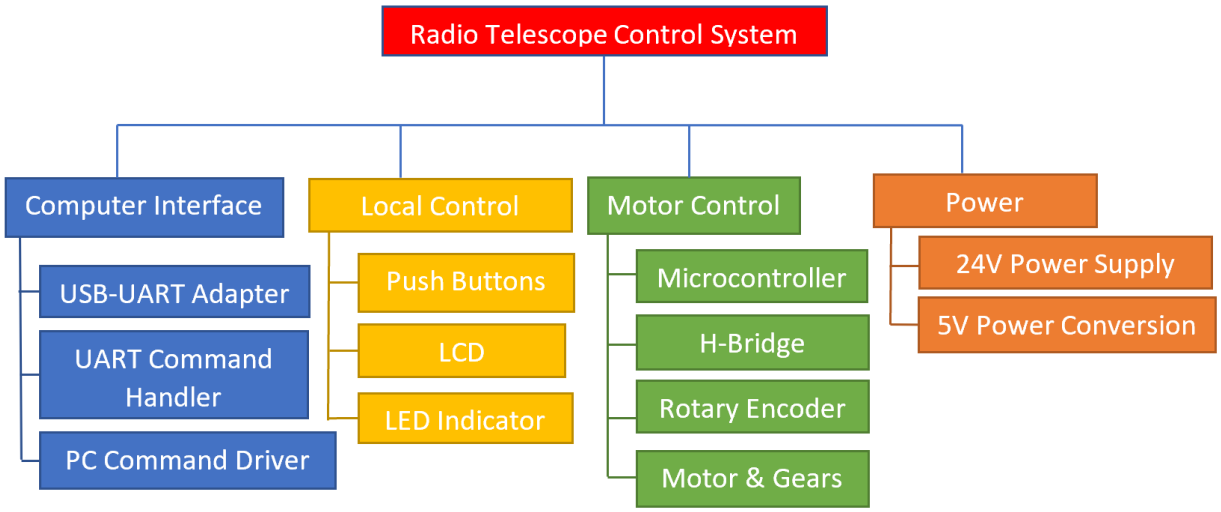

Figure 13: Hierarchical Chart

2.3.1 Level 0 Decomposition

The control system's level 0 functional decomposition is shown in Figure 14. This displays the overall inputs and outputs of the system. The power input supplies energy to the system from an outlet which will be down converted by a power module inside the system. The movement commands are a set of instructions given to the system by the user to reposition or locate different objects. These inputs are taken in by the control system which will process the commands to move accordingly. A local control system will allow a human operator to manually change the location of the telescope via a control pad. The output to the human operator includes the LCD and LED indicators to tell the user what is happening with the system. The motor location is the output that will be saved for later to create the plot of the intensity of the radio waves when the radio telescope is completed. This is not the same position that will be used as feedback to the control system. Motor movement is the other important output because the goal is to accurately move the motor to a desired position for measurement. This movement and its position will feed back into the system to determine if correction needs to be made.

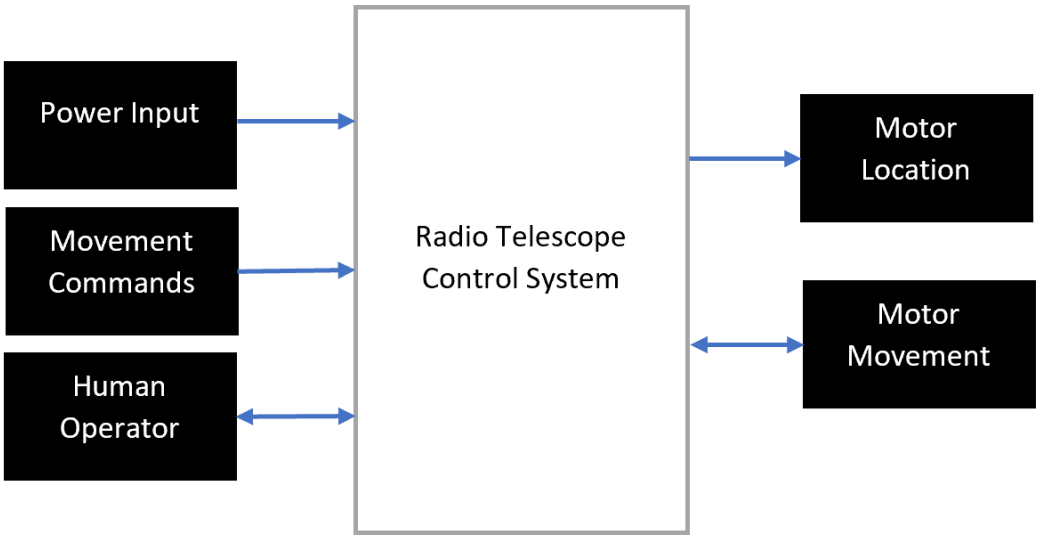

Figure 14: Level 0 Functional Decomposition

2.3.2 Level 1 Decomposition

The control system's level 1 functional decomposition is shown in Figure 15. The power module will convert the power source to the target voltages of 24V and 5V. The 24 V supply will be used for the motor, and the 5 V conversion will be used for the motor control system, the computer interface, and the local control. Motor rotation and control based on feedback will be handled by the motor control module. Motor movement input will provide feedback to the motor control. The motor control sends the position data back to the computer interface to be saved as the output for the motor location. Movement commands are sent to the computer interface to be processed and sent to the motor control microcontroller. This will send any converted signals to the designated outputs, such as the motors to move a certain direction. The local control input will be from the user which will be used to move the motors at the location and get immediate feedback to troubleshoot any problems. The local control output will be a system of LED indicators and an LCD so the user can be provided with extra information about motor movement.

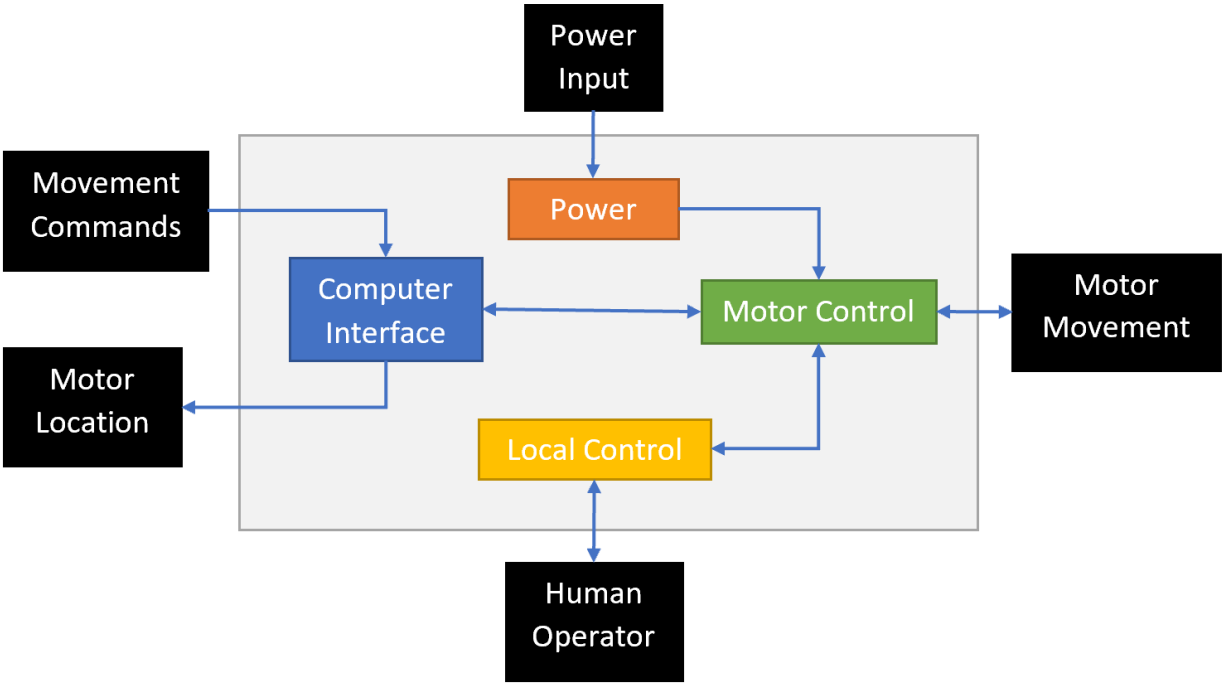

Figure 15: Level 1 Functional Decomposition

2.3.3 Level 2 Decomposition

The level 2 functional decomposition is shown in Figure 16. The connections between the sub-modules and the system's overall inputs and outputs are shown in this diagram. The specific inputs, outputs, and functions of each of the sub-modules are shown in the tables following the figure. The microcontroller is the center of most of the control in this system. The main PC is used for the input to the system, particularly the motor control, and saves motor location data. However, it will be used later to save intensity data along with the location data to plot an intensity plot of the measurements of electromagnetic waves from space.

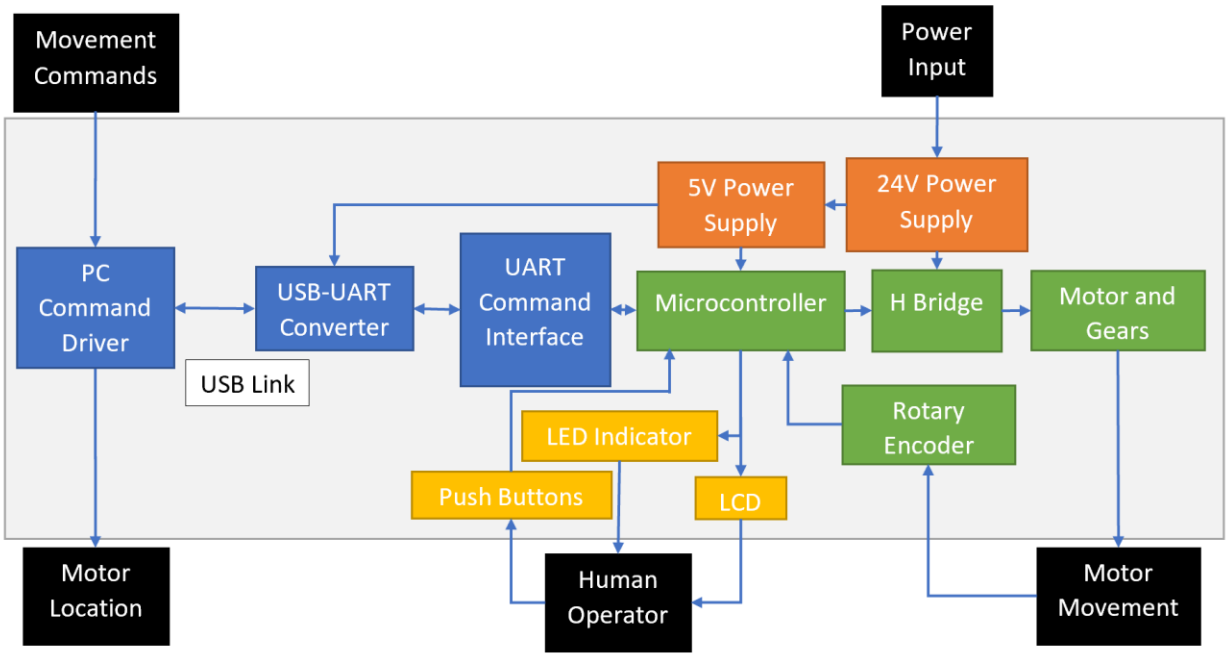

Figure 16: Level 2 Functional Decomposition

Table 6: Radio Telescope Control System Main Module

Radio Telescope Control System	
Inputs	• 120 V AC Power Supply • Movement commands for the motor from the main PC • Human Operator Commands • Motor position data for feedback to provide accuracy
Outputs	• Movement of the motors to a desired location • Information to a human operator at the system • Motor location to the main PC
Functionality	• To control and process information for motors used to rotate an antenna for a radio telescope to capture intensity of difference frequencies received from various objects in space.

Table 7: Computer Interface Module

Computer Interface	
Inputs	• Azimuth/Elevation Coordinate Commands from the main PC • Position data from the microcontroller
Outputs	• UART commands for motor control • Motor location data
Functionality	• To convert and transmit commands to the motor control subsystem. • To convert and transmit data of motor location to the main PC.

Table 8: PC Command Driver Sub-module

PC Command Driver	
Inputs	• Movement commands • PC power • USB protocol communication from USB-UART Converter module
Outputs	• USB protocol communication to USB-UART Converter module • Motor location data to the main PC
Functionality	• Controls the flow of commands and output data for motor location to the main PC.

Table 9: USB-UART Converter Sub-module

USB-UART Converter	
Inputs	• USB protocol communication from the PC command driver • +5 Volts DC power from the 5 Volt power supply • UART protocol communication from the UART command interface
Outputs	• USB protocol communication to the PC command driver • UART protocol communication to the UART command interface
Functionality	• Translate the USB communication to UART communication to provide the UART command interface with the movement commands. • Translate the UART communication to USB communication to provide the PC command driver with the motor location data for the main PC.

Table 10: UART Command Interface Sub-module

UART Command Interface	
Inputs	• Atomic movement commands • Status queries
Outputs	• Command acknowledgement to PC • Status to PC • Update movement states in microcontroller program
Functionality	• Interprets commands from main PC program in terms of current and desired states of the microcontroller program. Notifies the main PC program of command acknowledgement and current microcontroller system state.

Table 11: Power Module

Power Module	
Inputs	• 120 Volt AC Source
Outputs	• Power to each module, 24 V DC or 5 V DC
Functionality	• To provide power at 24 V DC or 5 V DC to all other modules, even if indirectly such as the supply of 5 V to the local control module through the microcontroller in the motor control module.

Table 12: 24 V Power Supply Sub-module

24 V Power Supply	
Inputs	• 120 Volt AC Source
Outputs	• +24 Volt DC to H-Bridge for motor power • +24 Volt DC to the +5 V voltage converter
Functionality	• To convert the 120 Volt AC source to +24 Volt DC.

Table 13: 5 V Power Supply Sub-module

5 V Power Supply	
Inputs	• +24 Volt DC supply from the +24 Volt power supply
Outputs	• +5 Volt DC
Functionality	• To convert +24 Volt DC to +5 Volt DC power for supplying the indicators and lower-level circuitry with power.

Table 14: Motor Control Module

Motor Control	
Inputs	• Power from the power module • Commands from local control • Commands from the computer interface • Position from the motor
Outputs	• Position data to the computer interface • Displayable information to the local control module • Motor movement
Functionality	• To provide any aspects of control for the motors from local control and the computer interface.

Table 15: H-Bridge Sub-module

H-Bridge	
Inputs	• Signals from the microcontroller to determine the direction of the current. • Power from the +24 Volt DC power supply
Outputs	• +24 Volt DC power to the motors and gears for movement
Functionality	• Provide bi-directional power to the motor and gears to move the motor in either direction.

Table 16: Motor and Gears Sub-module

Motor and Gears	
Inputs	• +24 Volt DC power from the H-bridge module.
Outputs	• Azimuth/Elevation angle.
Functionality	• Provide the movement of the antenna that will be attached to the system.

Table 17: Rotary Encoder Sub-module

Rotary Encoder	
Inputs	• Angular position and motion of the motors.
Outputs	• Position of the motors to the microcontroller.
Functionality	• To provide feedback to the microcontroller so the position can be changed for accuracy.

Table 18: Microcontroller Sub-module

Microcontroller	
Inputs	• The position of the motors from the rotary encoder as feedback for accuracy. • +5 Volt DC power as the supply of the microcontroller. • Commands from the UART command interface to control the H-bridge/motors. • Push button signals that the human operator causes for direct motor movement and direction.
Outputs	• Signals for the LED indicators and LCD to tell the human operator the status of the motor movement and possibly position. • 5V control signal to H-Bridge. • Position data to the UART command interface to be sent to the main PC.
Functionality	• The hub of data and controlling signals for most of the system. • To control the LED indicators and LCD display for human operator interaction. • Control the H-bridge direction of current flow that will provide power and desired direction of movement to the motors. • Send and receive data and commands with the main PC.

Table 19: Local Control Module

Local Control	
Inputs	• Human operator commands • Signals from the motor control module
Outputs	• Commands to the motor control module • Information to the human operator
Functionality	• Provide the user with the status of the motor movement and position. • Allow for control of the motors in any direction at their location.

Table 20: LED Indicators and LCD Display Sub-modules

LED Indicators and LCD Display	
Inputs	• Microcontroller control signals.
Outputs	• Signals and data to the user for debugging or testing.
Functionality	• Provide the user with the status of the motor movement and position.

Table 21: Push Buttons Sub-module

Push Buttons	
Inputs	• Human operator
Outputs	• Movement direction to the microcontroller.
Functionality	• Allow the user at the site of the system to move the motors in any of the four directions (azimuth and elevation).

2.4 Subsystem Design

This section contains explanations for the design process for the radio telescope control system. It begins with the design of the critical power components for the H-bridge DC motor driver, including simulation and testing of the H-bridge, and then continues to detail the design process for every other system in the block diagram given in section 2.3.3, Level 2 Decomposition.

Finally, this section contains an explanation of the general design approach for the embedded C code for the controller.

2.4.1 H-Bridge Design and Simulation

This project contains a DC motor driver subsystem which was designed using discrete components to meet the needs of the overall system function. Circuit simulation using OrCAD PSPICE was used to validate the circuit design and obtain reference parameters to compare with the results obtained during the integration and testing phase of the project. PSPICE was chosen since the vendors for many of the critical components provide PSPICE simulation models. Because these models are specific to each component that is in the subsystem, they provide circuit simulation results in a way that more simplistic generic component models in PSPICE or another simulation program such as MATLAB have trouble providing. Additionally, PSPICE is familiar to the members of the capstone team and using it for simulation reduces the design time of the project.

The DC motor driver subsystem was designed as a MOSFET H-bridge topology due to its simplicity and its ability to easily reverse the DC motors by passing current in either direction through the H-bridge. The original circuit model, given in Figure 17, displays a basic H-bridge configuration used to drive a purely resistive load. Other variations of the circuit can be seen later that include a more accurate motor model, flyback diodes as protection for the MOSFETs, and an RC snubbing circuit across the motor to reduce oscillations and cause faster settling time in the motor voltage. The goal of this simulation is to measure the time-domain response of the H-bridge switching circuit, particularly when transitions between on and off states occur. Of particular concern with a circuit of this type which switches a heavily inductive motor load is counter EMF (flyback voltage), gate coupling, and transistors fully turning on and off. This simulation looks at the voltage across the motor, voltages across the switching transistors from drain to source, and gate voltages of the transistors.

This simulation passes when the transistors do not turn on accidentally (their gate voltages are quiet), the counter EMF does not affect desired circuit operation, circuit oscillations do not affect operation, the transistors quickly reach saturation and cutoff with minimal time in the Ohmic region, and the transistors are not subjected to extreme currents or drain to source voltage greater than the datasheet recommends.

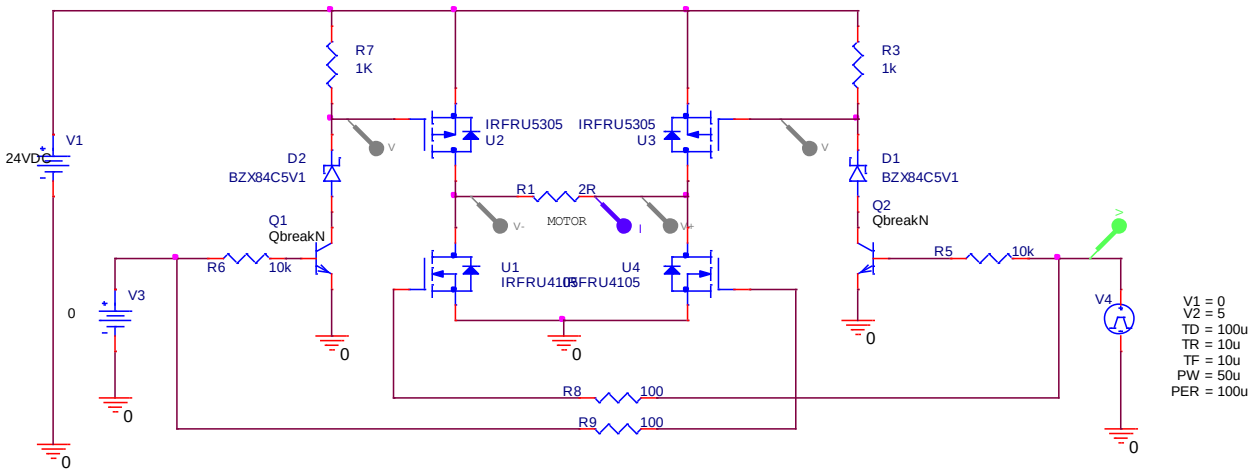

Figure 17: Schematic with imported vendor SPICE models of the H-bridge motor driver with a resistive load.

The simulation was first run with a simplified resistive load to validate the switching logic of the circuit. For this, one half of the H-bridge was turned off (zero volts applied), and the other half was alternated between on and off states. The U3 and U1 MOSFETs were turned on using the 5-V pulse generator in the bottom right of Figure 17. This allows the current to pass from the right side to the left side of the resistive load representing the motor. The other two MOSFETs (U2 and U4) must remain off to prevent a short circuit from the 24-V source to ground. While not tested in this simulation, the current will flow from the left to the right of the resistive load when the oppositive conditions are applied to the MOSFETs. This changes the voltage polarity to rotate the motor in the opposite direction.

The P-MOS transistors (U2 and U3) can be turned on by lowering the voltage on the gate such that the transistor is fully saturated. The voltage cannot be greater than 20 V from source to gate according to the data sheet, so the Zener diode protects against this. The N-MOS transistors (U1 and U4) follow similarly, except the gate needs to be raised to a large enough voltage with respect to the source, which is ground in this case. The gate voltage for the N-MOS transistors is connected through a small resistor to the 5-V pulse generator to provide a high enough voltage above its threshold voltage to ensure the transistor is fully on.

The 2-Ohm load was used because the highest current consumption of the desired motors for this system was 12A, which corresponds to a 2-ohm load. Similarly, the transistors and other critical components were selected to handle more than 12A. However, the motor system that was purchased requires only up to 2 A, so later simulations reflected this reduction in load current. This oversizing of the components allows for flexible installations should the larger motor become available in future iterations of the design.

The first simulation from Figure 17 resulted in the waveform in Figure 18 below, where the top plot shows the gates of the P-Channel MOSFETS U2 (green) and U3 (red). The bottom plot

shows the differential voltage applied to the resistor (red), the current through the resistor (blue), and the control signal applied (green).

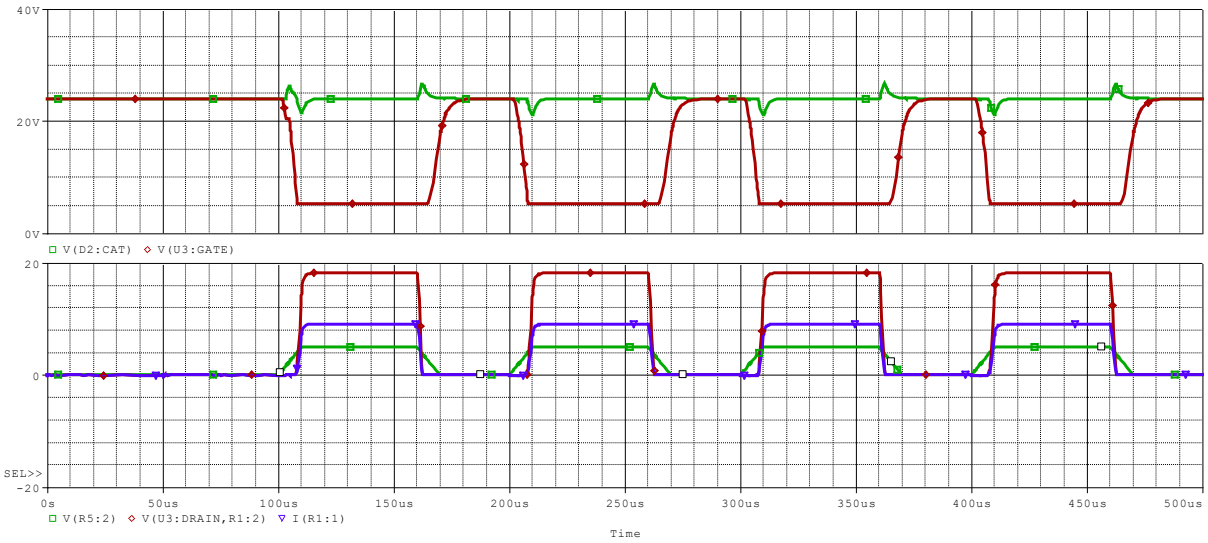

Figure 18: Top plot: Green trace is U2 gate voltage, red is U3 gate voltage. Bottom plot: Red trace is motor voltage, blue is current through the motor, green is control signal.

This simulation result proves a few things. First, it shows that the configuration of the H-bridge works for non-reactive (resistive) loads. This means that the switching logic is correct. In the plot, it is shown that the driven P-MOS transistor U3 is correctly turning on and off, while the gate of U2 is nearly quiet. However, it does show that some of the switching transients at the drain of U2 are coupling through the gate oxide layer and could inadvertently turn on the transistor if the transients are too large. This simulation shows that the N-MOS U1 is working exactly as expected. No oscillation is observed, and the transistor U3 is not turning off sharply due to the R-C time constant of R3 and the gate capacitance of U3, its rise time is sufficiently fast for a low speed (i.e., non-PWM) application. Improvements in rise time can be found by increasing the voltage of D1 or decreasing R3.

Further testing required a more accurate motor model that includes back EMF, armature inductance, and armature resistance. A paper proposes a model of a permanent magnet DC motor shown in (b) of Figure 19. This motor model has back emf, or a constant field flux, due to the permanent magnet [23]. Due to light loading, the back EMF should be around 70% (17 V) of the source voltage because the weight of the current antenna to be used is very small with respect to the high torque rating of the motor and gearing system. Due to not having the motor at the time of the simulations, the suggested armature inductance (0.12 H) from the paper was used. However, the expected current will be around 2 A or less, therefore a resistor of 10 Ohms was used to allow a current in this range. Figure 20 shows the H-bridge motor driver circuit with

the new motor model. Additional flyback diodes were added across the MOSFETs to protect them from reverse voltage upon turning the transistors off, thus cutting off in the input current.

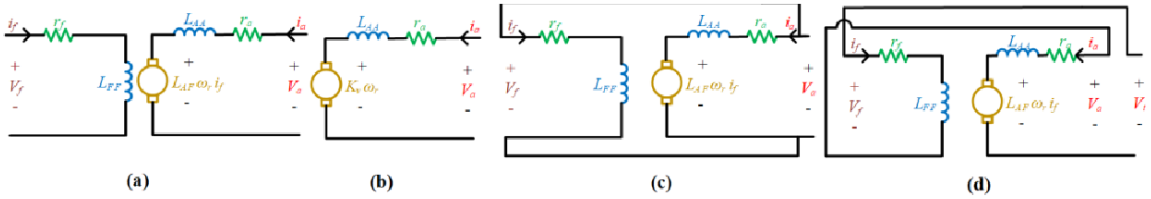

Figure 19: DC motor models: "Equivalent circuit of (a) separately excited, (b) permanent magnet, (c) shunt-connected and (d) series-connected DC motors" [23].

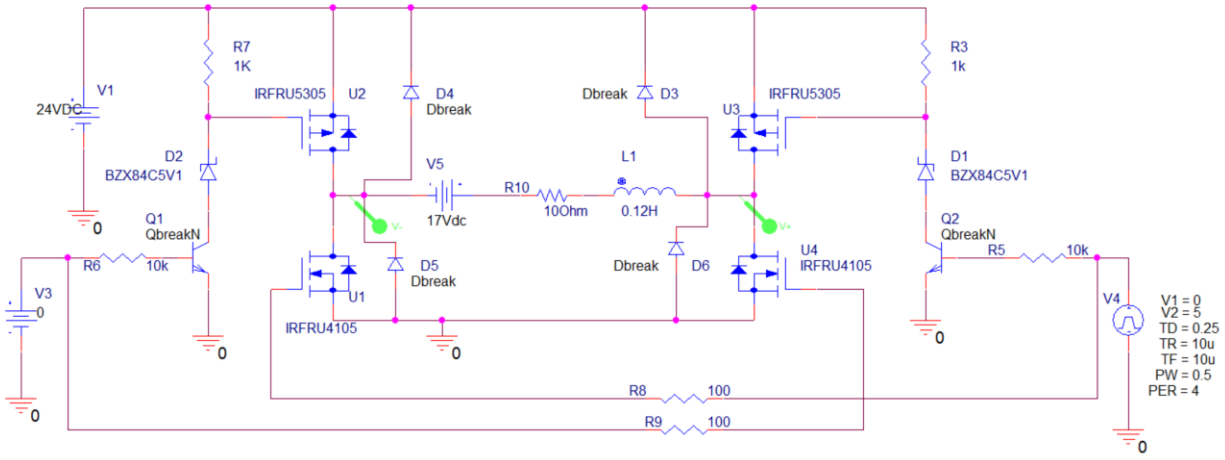

Figure 20: Schematic of the H-bridge motor driver with a motor model load. The green markers are the motor voltage which may not have the same color in the other simulation images.

Some traces are shown in Figure 21 and Figure 22 of the time domain simulation. The gate voltage of U2 has little noise. The source signal voltage and the gate voltage of U3 are behaving as expected. The motor voltage rises with no issues the first time it is turned on. Issues arise each time the transistors turn off. Upon shutoff, a large negative voltage of -25 V is across the motor model for 2 ms. This is handled by the flyback diodes D6 and D4 in this operation. After this, the motor voltage returns to 24 V briefly and starts a decaying oscillation to 17 V due to the back EMF. This oscillation likely does not matter because the current through the diodes and motor is essentially zero. In all, this transition lasts only 5 ms. The motor cannot switch on and off faster than 200 Hz using the below equation.

$$f = \frac{1}{T} = \frac{1}{5\ ms} = 200\ Hz$$

(1)

Most likely, the motor will not be able to be around 200 Hz because it will not have a predictable output if it is switched at this rate.

Figure 21: Various traces using the new circuit in Figure 20.

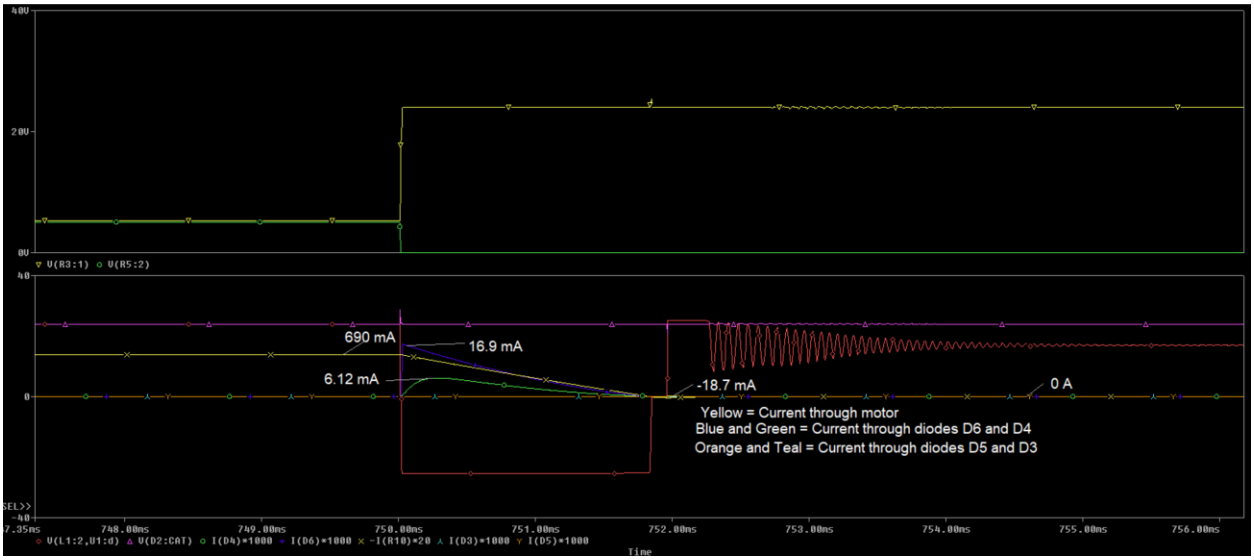

Figure 22: The same traces in Figure 21 zoomed in to view the traces at the turn off and on points more closely.

The oscillations can be removed if necessary. Adding an R-C snubber circuit across the motor with the appropriate RC time constant can eliminate the oscillations. Figure 23 shows the adjusted schematic. Figure 24 displays the resulting waveforms of the motor voltage, motor current, and current through the R-C circuit.

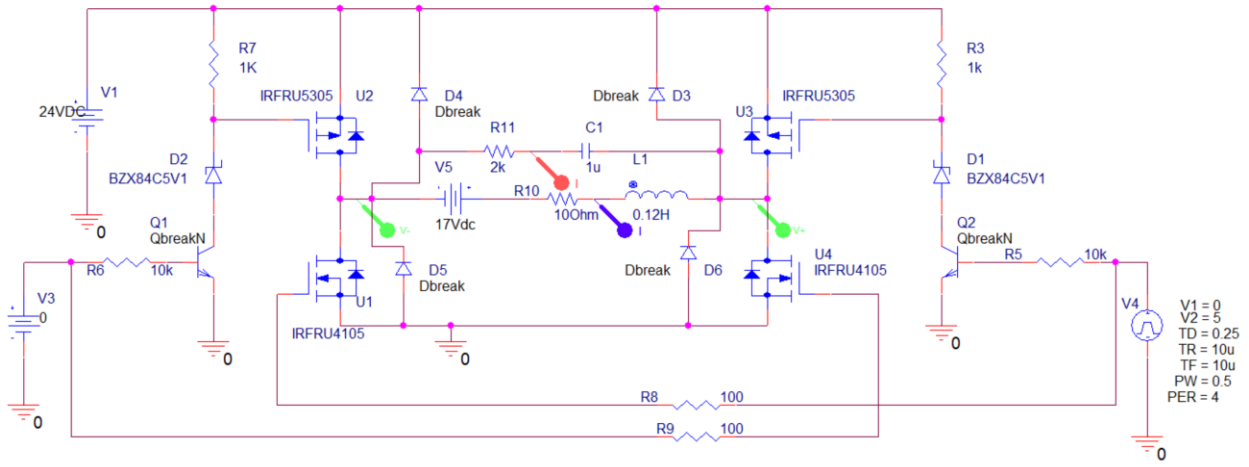

Figure 23: Schematic of the H-bridge motor driver with a motor model load and RC circuit across it.

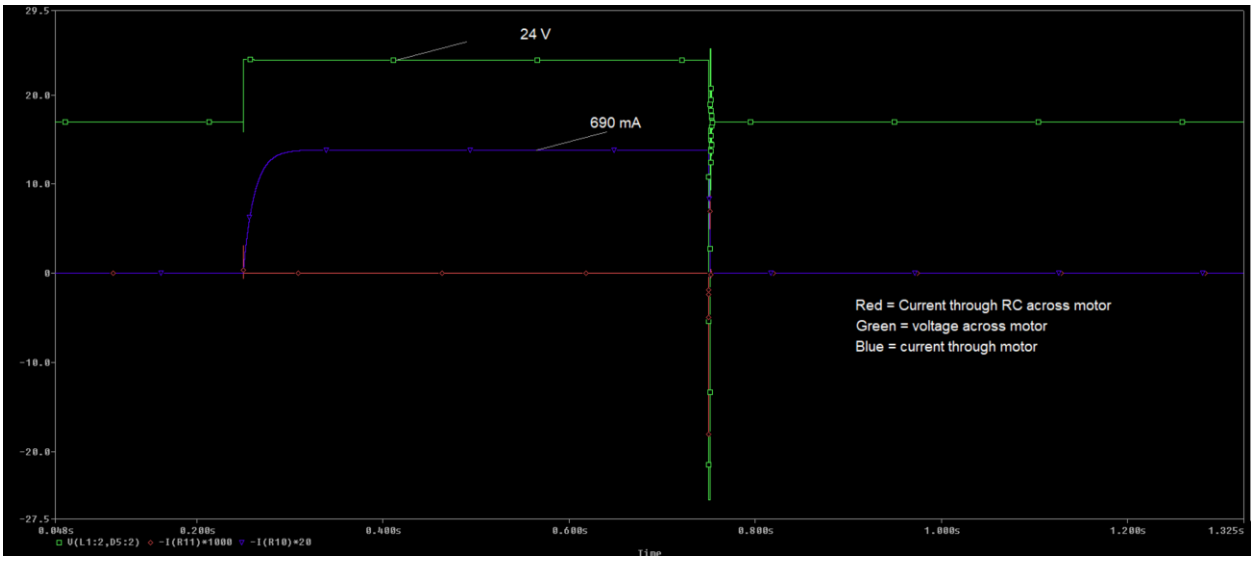

Figure 24: Overall response of the circuit with R = 1kOhm and C = 1nF. The traces are labeled in the image.

The effects appear to be similar to the initial chosen test values. To specifically design for the problem, the RC time constant and cutoff frequency of the added circuit could be calculated using the formulas below.

$$\tau = R * C \tag{2}$$

$$f = \frac{1}{2\pi\tau} \tag{3}$$

To determine the required cutoff frequency, the oscillation frequency of the signal is needed. The oscillation period was determined from the waveform in PSPICE and the frequency from equation (1).

$$f = \frac{1}{t_2 - t_1}$$

$$f = \frac{1}{752.425\ ms - 752.321\ ms} = 9.615\ kHz$$

To eliminate the oscillations, the cutoff frequency must be at or lower than the oscillation frequency. To start, the capacitance was chosen to be 1 µF and the frequency to be 9.615 kHz to match the oscillation frequency. The resistance was calculated to be 16.55 Ohms using equations (2) and (3). Figure 25 displays the motor voltage has oscillations worse than the oscillations previously. It has a longer settling time of around 30 ms. This is expected because the cutoff and oscillation frequencies closely match each other and may reinforce the other. The cutoff frequency needs to be lowered considerably to slow down the oscillations of the motor.

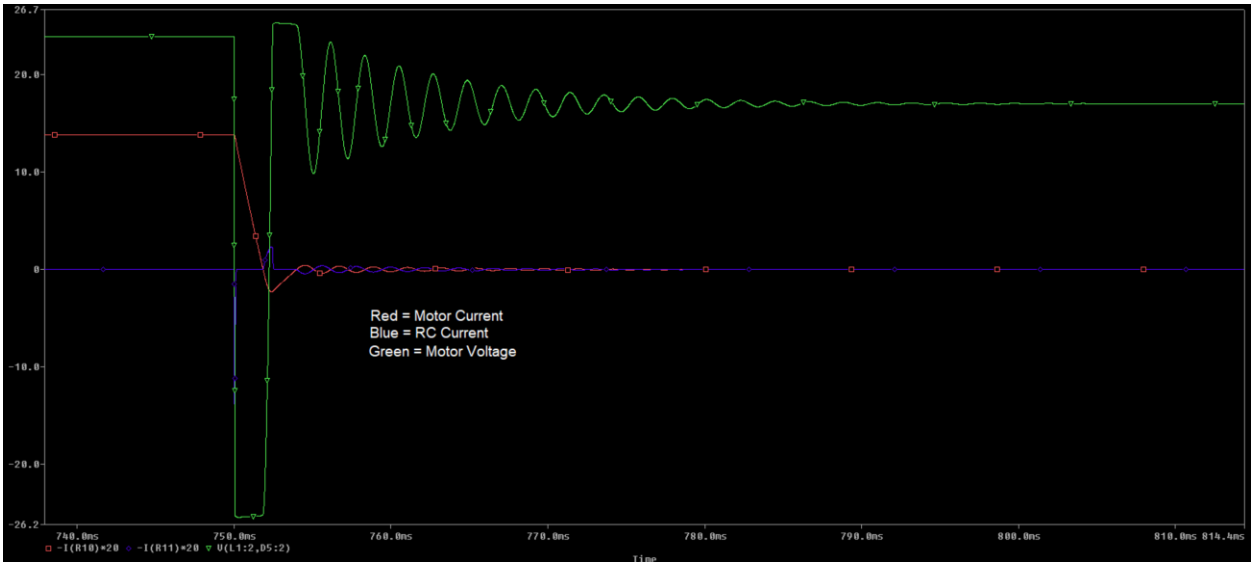

Figure 25: Response for R = 16.55 Ohm, C = 1 µF, and f_{RC} = 9.615 kHz.

Finding the right frequency to reduce oscillation was approached by experimenting with various resistances for the R-C circuit. The next resistance chosen was 200 Ohm with the same capacitance of 1 µF. The cutoff frequency was calculated to be 795.8 Hz using the same equations as before. The settling time improved and the oscillations were reduced as shown in Figure 26.

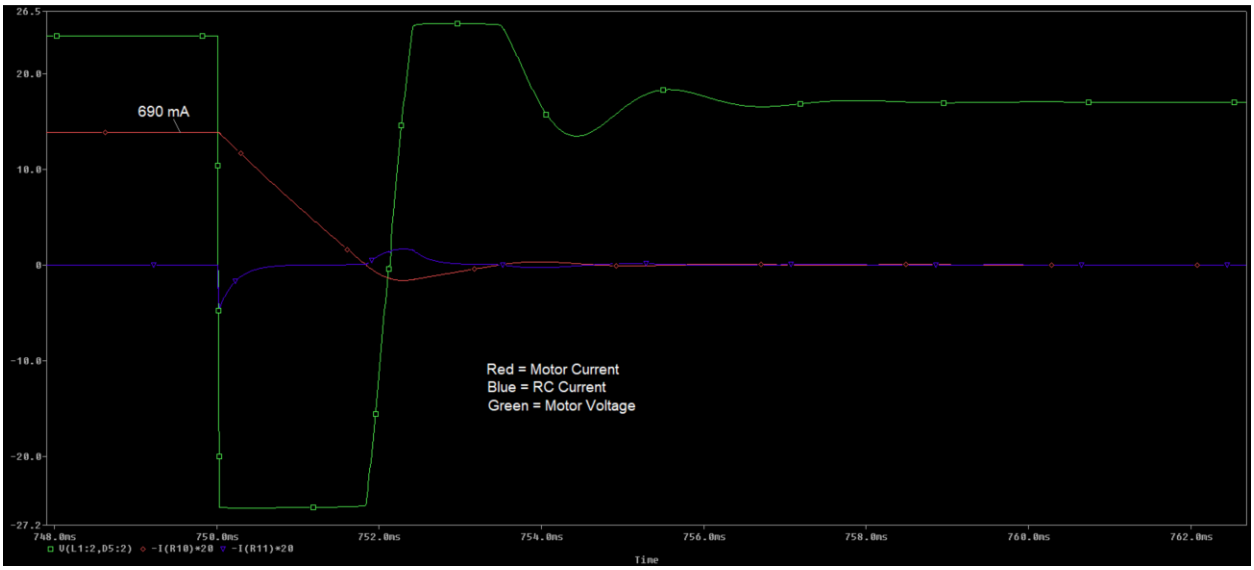

Figure 26: Response for R = 200 Ohm, C = 1 µF, and f_{RC} = 795.8 Hz.

The next resistance was chosen to be 1 kOhm with a capacitance of 1 µF resulting in a cutoff frequency of 159.2 Hz. The settling time was reduced and there is no oscillation occurring anymore. Figure 27 shows the new traces. This may be refined to reduce the overshoot, but due to an unknown inductance in the motor, this will be done later if needed.

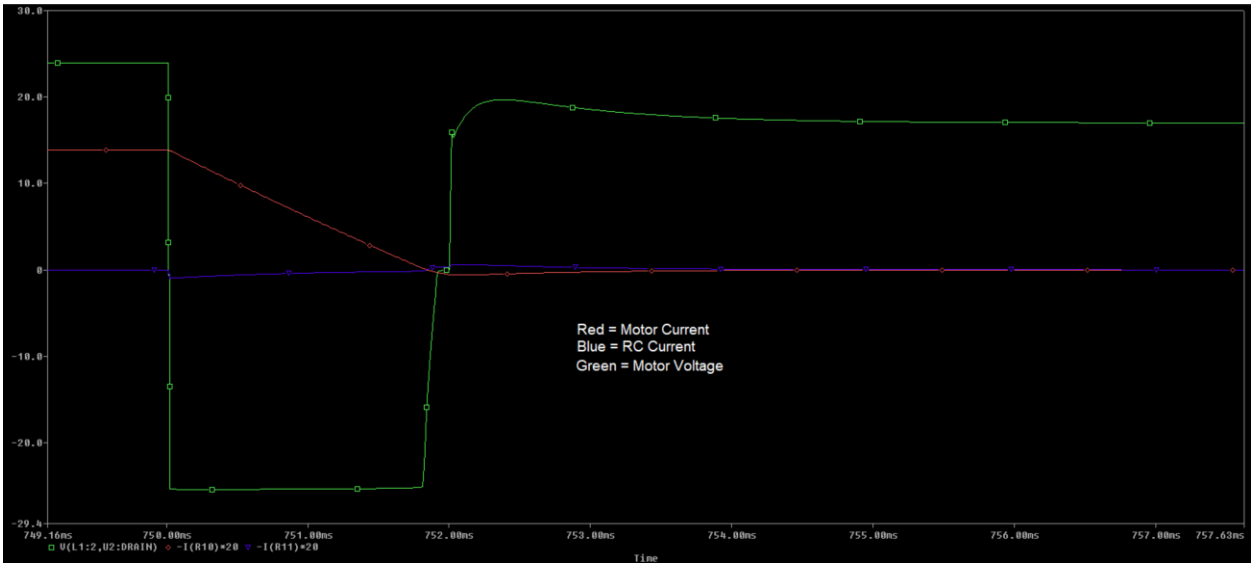

Figure 27: Response for R = 1 kOhm, C = 1 µF, and f_{RC} = 159.2 Hz.

To see the effects of increasing the resistance more, thus decreasing the cutoff frequency, it was increased to 2 kOhm with a capacitance of 1 µF giving a cutoff frequency of 79.58 Hz. The simulation is shown in Figure 28. The settling time is quicker than before, but there is a large overshoot in the beginning like the earlier RC circuits and the simulations without an RC circuit.

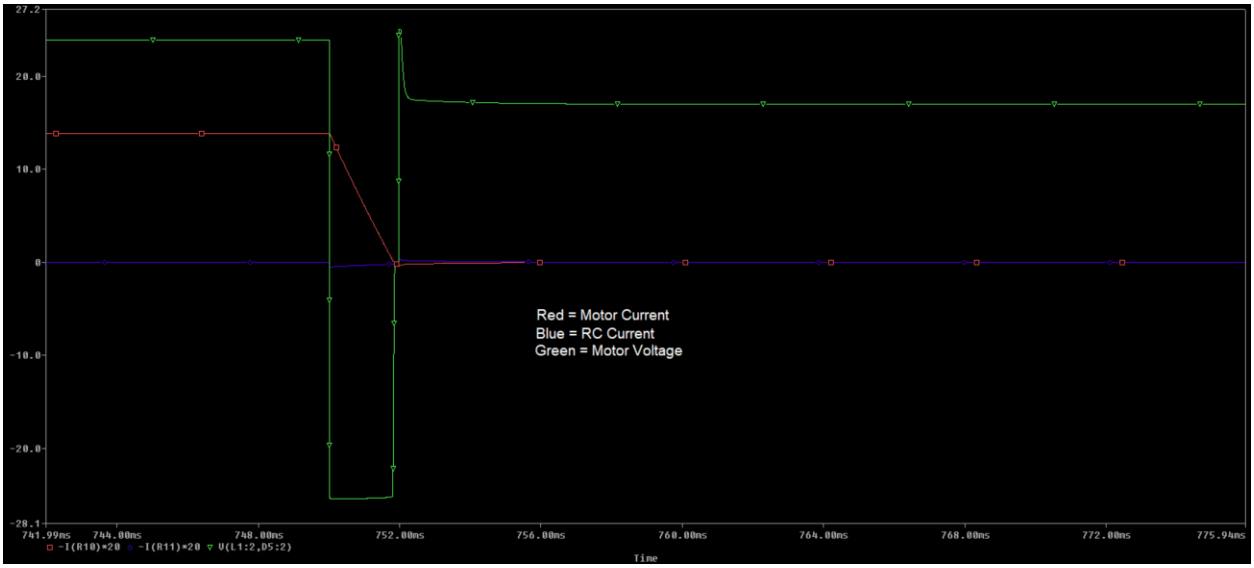

Figure 28: Response for R = 2 kOhm, C = 1 µF, and f_{RC} = 79.58 Hz.

To demonstrate the ability to run the motor in both directions, the motor model was flipped, and the other two transistors were turned on to cause current in the opposite direction. Figure 29 displays the new schematic. As Figure 30 shows, the response is the same as in the other direction. Therefore, the circuit follows the engineering requirement of bidirectional current through the motor.

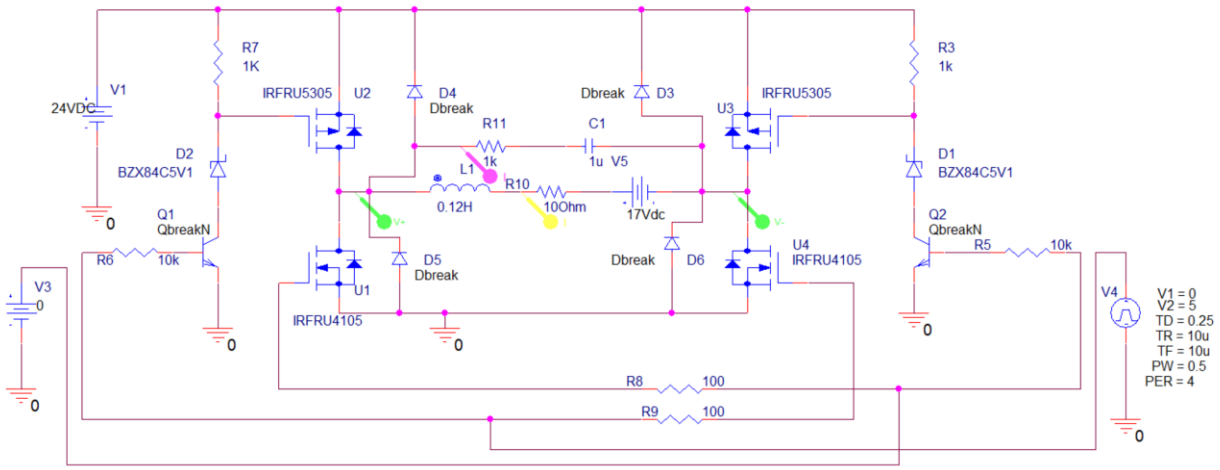

Figure 29: Schematic of the H-bridge motor driver with a motor model load with current traveling the other direction through the motor now.

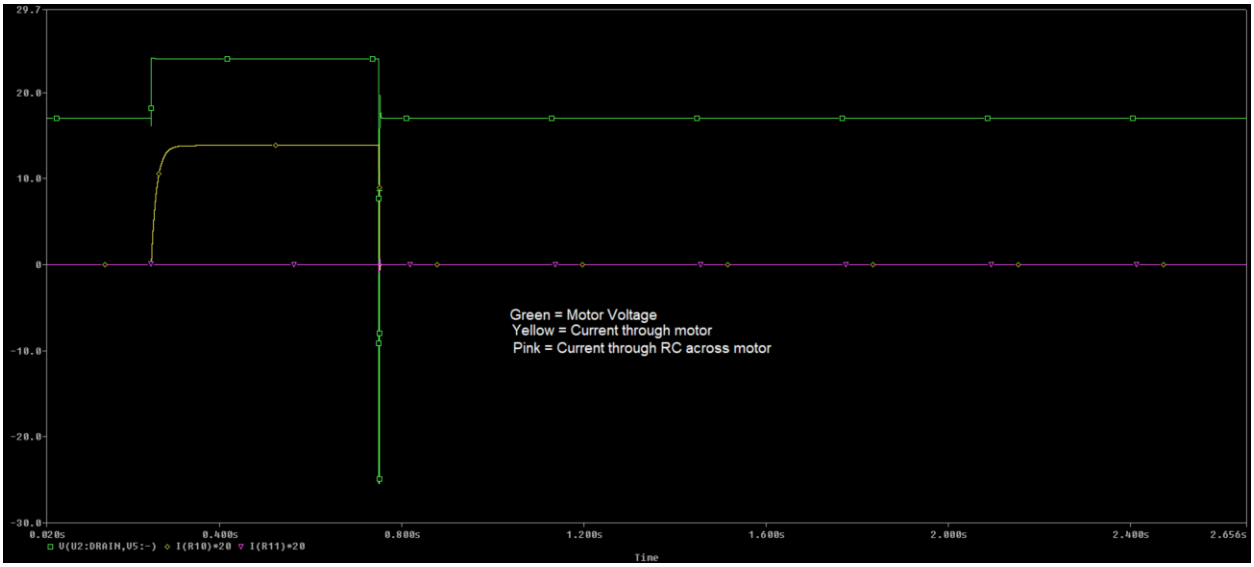

Figure 30: The response of the circuit in Figure 29.

2.4.2 General Description

The custom PCB for this project was developed as an integration of the motor control, local control, and computer (remote) control interface on one PCB. The power supply section was provided by external off-the-shelf modules. The circuit was designed for a DC motor with Hall-effect quadrature encoder feedback, which will be detected and controlled via a firmware control loop in a 16-bit PIC microcontroller. The microcontroller was designed to be the heart of the system, which decides how to move the motor and records the position of the motor, as well as communicates with the main computer as to the position and status of the controller system. The H-bridge section of the circuit was chosen as the subsystem to be designed using discrete components.

The software that was used for this PCB design process is the Cadence OrCAD package. This software was chosen as the student license contains PSPICE simulation, Capture schematic, and Allegro PCB Editor in one suite. The suite allows a simple transfer from designing and testing the schematic to laying out the PCB. Since this software was taught in courses, it seemed a logical choice for the project.

Figure 31 displays the schematic of one of the two identical H-bridge circuits. As explained in the simulation section of this report, the purpose of the H-bridge is to activate two of the four transistors in one of the two following combinations to control the direction of current in the motor. If Q8 and Q11 are on, and Q7 and Q12 are off, then the current flows from right to left through the load. If the opposite transistors are on, then the current flows from left to right through the load. If all the transistors are off, then the motor stops moving. One H-bridge

circuit is used for the motor that controls the elevation angle and the other H-bridge controls the azimuth angle. The microcontroller that controls the whole board including the H-bridges has a program that ensures the transistors are never on such that there is a short from 24 V to ground. One example would be Q8 and Q12 being turned on at the same time. This will break the system.

One of the changes that were made after the circuit was designed was the modification to use it for a lower current motor. Originally, the circuit was specified for a motor that could draw a peak current of 20A. High current transistors, wide traces, and large copper thermal area around the transistors were required to support this. The shunt current sensing circuit R46-49 and the operational amplifier U3 were configured to support a high peak current and a high average current. As the motor specification was later changed to support a motor that was slower but had a much lower peak and average current value on the order of 2 Amps, the circuitry was changed also. The current shunt resistors were then changed to have 100 mΩ instead of 50 mΩ values to increase the input gain to the amplifier U3. As the high current transistors were still in the circuit, the H-bridge could be returned to a higher current configuration later should a larger motor be desired in the future.

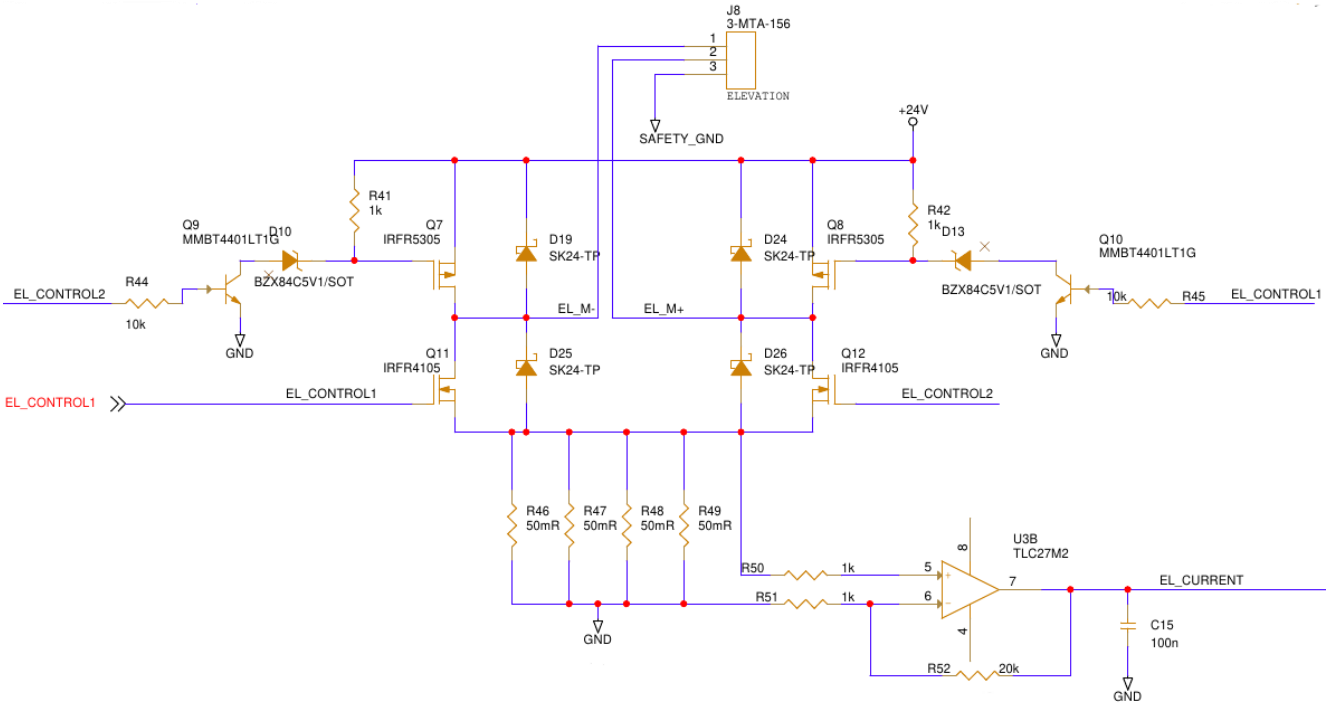

Figure 31: The schematic of one of the two H-bridge circuits. R46-49 are now 100 mOhm.

2.4.3 Step by Step PCB Design

Upon completion of the schematic design and mutual design approval by the capstone team, the first step of the PCB design was to associate footprints with schematic symbols. In general,

the footprints that were used could be easily found through the component manufacturer, online footprint libraries such as snap EDA, or through the small number of footprints supplied by OrCAD. After these footprints were added to the correct location in the project hierarchy and were added to the part properties of the part symbols they represented, the footprint pinouts had to be verified and adjusted to match what the schematic symbols and the part datasheet required. Additionally, some footprints had to be either created manually or modified. This was performed by using the allegro footprint drawing program and the allegro padstack creation program.

The next step in the PCB design process was to export the schematic to Allegro PCB editor and configure the PCB outline. The schematic export process used a netlist and some other information that was transferred to the Allegro PCB project. The PCB was chosen to have a board outline of 6 inches by 4 inches, based on the size of the component footprints and the desired enclosure.

Next, the connectors were added to the board so that their locations were on the edges of the board and near the sections to which they connected. After this, the high current traces were routed from the power connector to the H-bridge section.

The H-Bridge section was laid out in such a way that the connections between the transistors were short and direct and were as wide as reasonably possible to accommodate a large current. One trade-off with creating large copper areas attached to surface-mount pads was the issue of thermal conductivity. When populating the surface-mount components on the PCB, it is desired that there is moderately low thermal conductivity to the copper plane surrounding the component as the solder paste may not heat up evenly and may have issues flowing otherwise. However, during the operation of the circuit, it is desirable to have good thermal conductivity to provide a heat sink like function to the power transistors. It was decided to use thermal reliefs around power component pads to provide isolation for solder reflow at the cost of some heat sinking capacity.

The figure below shows the circuit layout and a 3-D render of the H-bridge section. It shows the connectors, the component placement, and the large copper traces that were used to connect the H-bridge section.

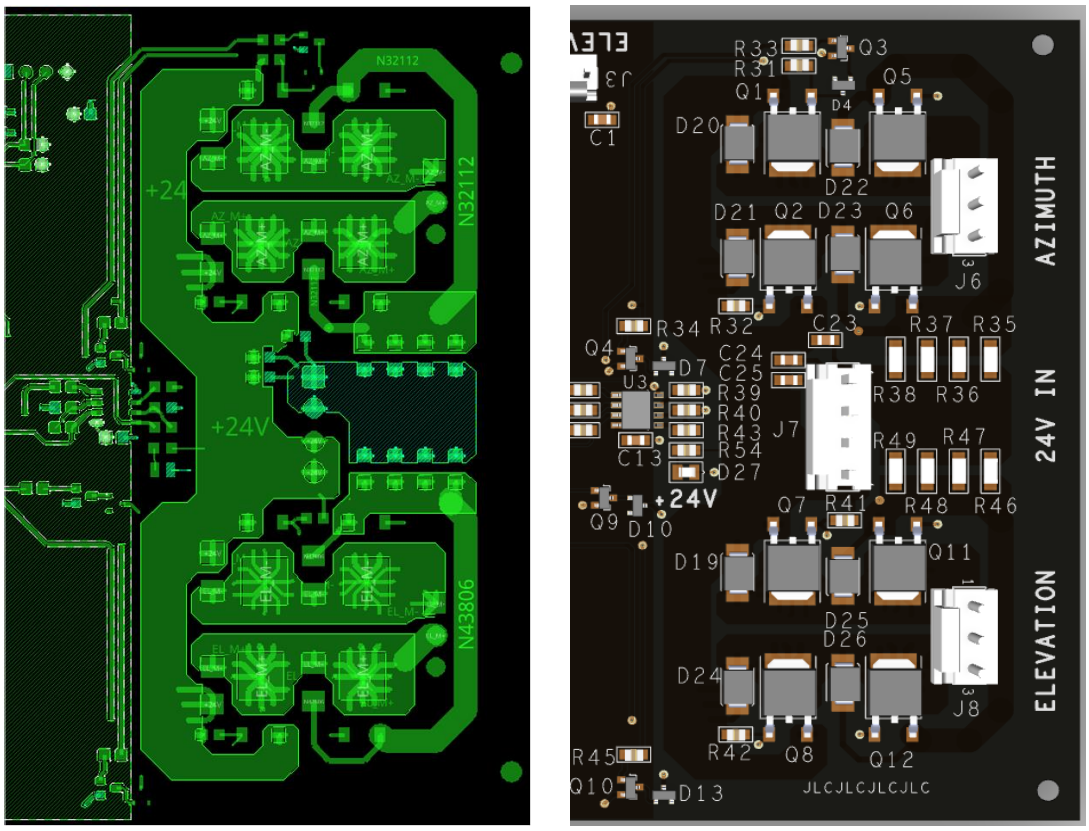

Figure 32: H-Bridge section PCB design (left) compared with 3-D render (right)

After the high current traces in the H-bridge section were completed, the low current sections including the microprocessor and digital inputs and outputs were laid out. Following that step, a ground plane was added to the bottom layer and a +5V plane to the top layer. These layers were inspected to ensure they had sufficient connections to each power pin on the circuit.

The last step in the PCB design process was to adjust the artwork such as reference designators, logo, and connector labels. Then the production Gerbers were exported per JLCPCB guidelines and sent to the factory for production.

During the testing phase it was discovered that the tradeoff between thermal isolation and solderability for the power components posed an issue when the average current through the H-bridge approached 10A. In this case, the N-Channel transistors (NMOS) got very hot and were in danger of self-destruction due to high junction temperatures. In that case, it may have been more useful to connect their larger pads directly to the copper fill surrounding the pad without thermal reliefs. An additional contributor to the high-power loss may be that the N-Channel transistors may not be turned on as fully as the P-Channel transistors (PMOS), which did not get hot at 10A. Although these transistors are marketed as usable with a logic-level signal, a signal well beyond the (2-4 Volt) threshold voltage may provide a lower on-state resistance from drain to source (R_{DS_on}). Using a MOSFET driver biased to around 10V instead of a 5V logic-level signal may improve high current performance.

2.4.4 PCB Comparison

When the entire PCB was completed, 3-D models were imported and associated with components so that a 3-D render of the PCB could be generated. This render shows how the PCB should look when it was populated with all the surface-mount and through-hole components. Figure 33 and Figure 34 show two views of the 3-D render from Allegro PCB editor.

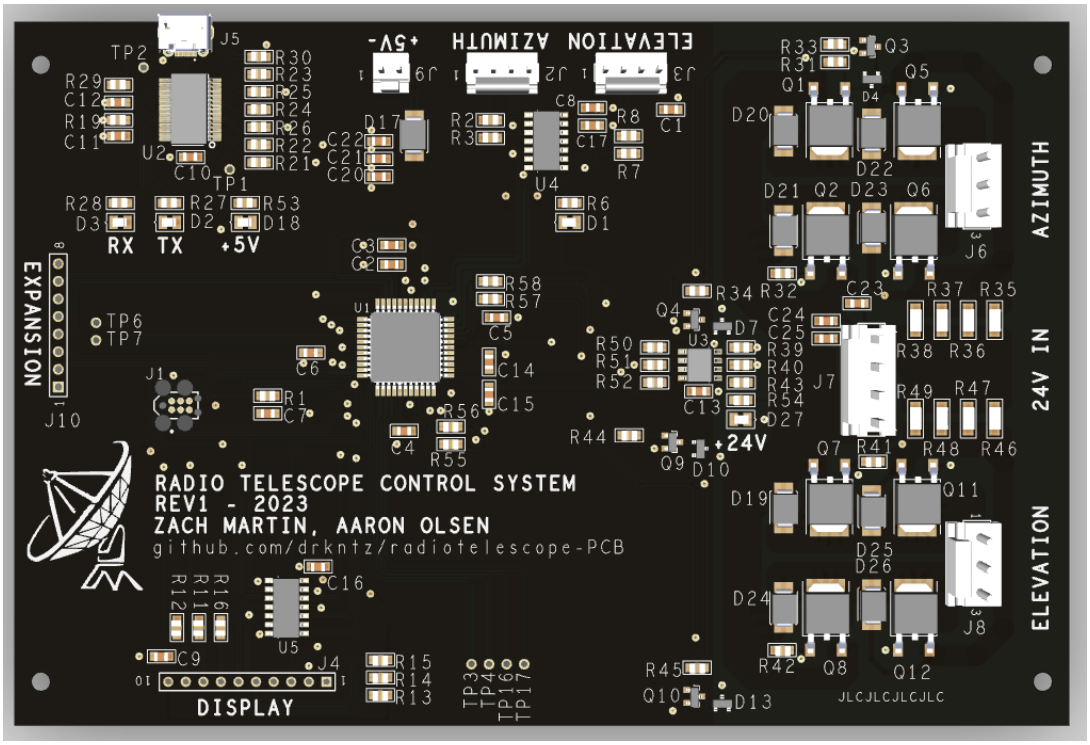

Figure 33: PCB with 3D rendered components (top view)

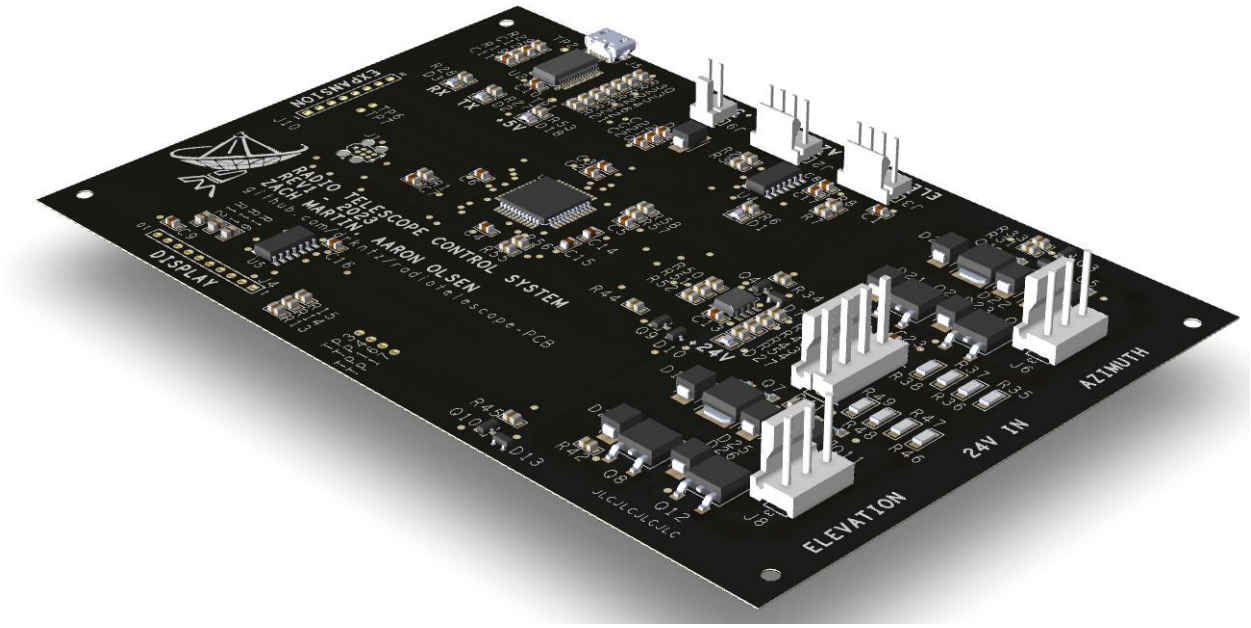

Figure 34: PCB with 3D rendered components (isometric view)

When the circuit board was received from the manufacturer, it was compared with the render given by the PCB program to ensure the layout and manufacture was correct. The manufactured PCB before populating it with surface-mount and through-hole components is given in the following image.

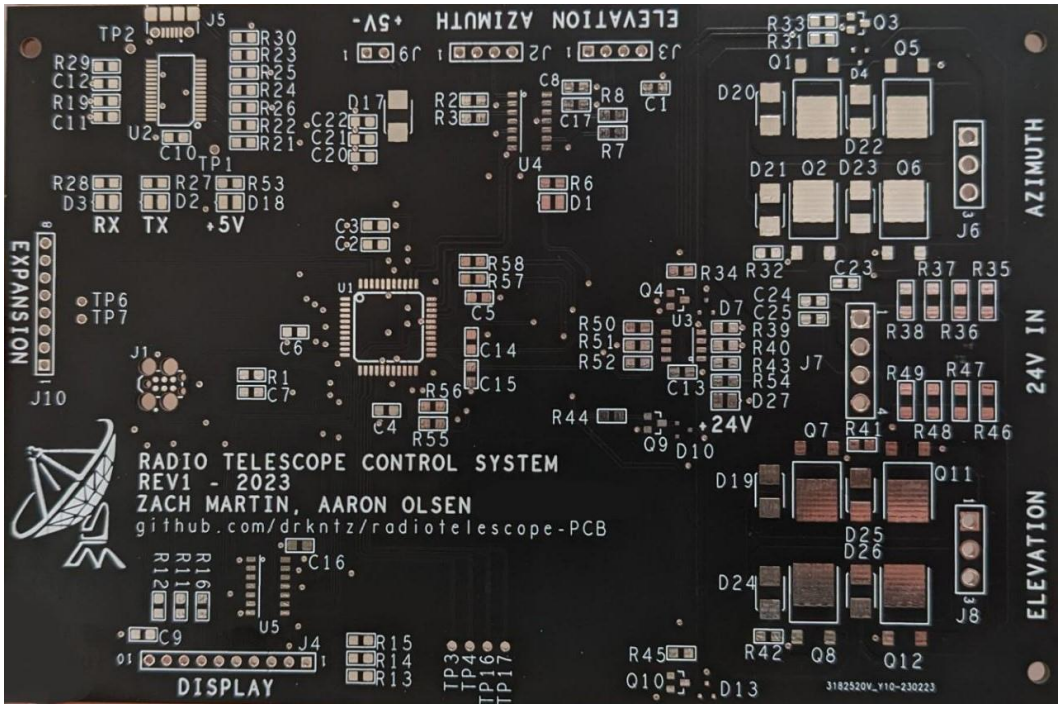

Figure 35: The unpopulated ordered PCB.

After the PCB components were assembled, the completed PCB was ready to test. This PCB is given in the image below.

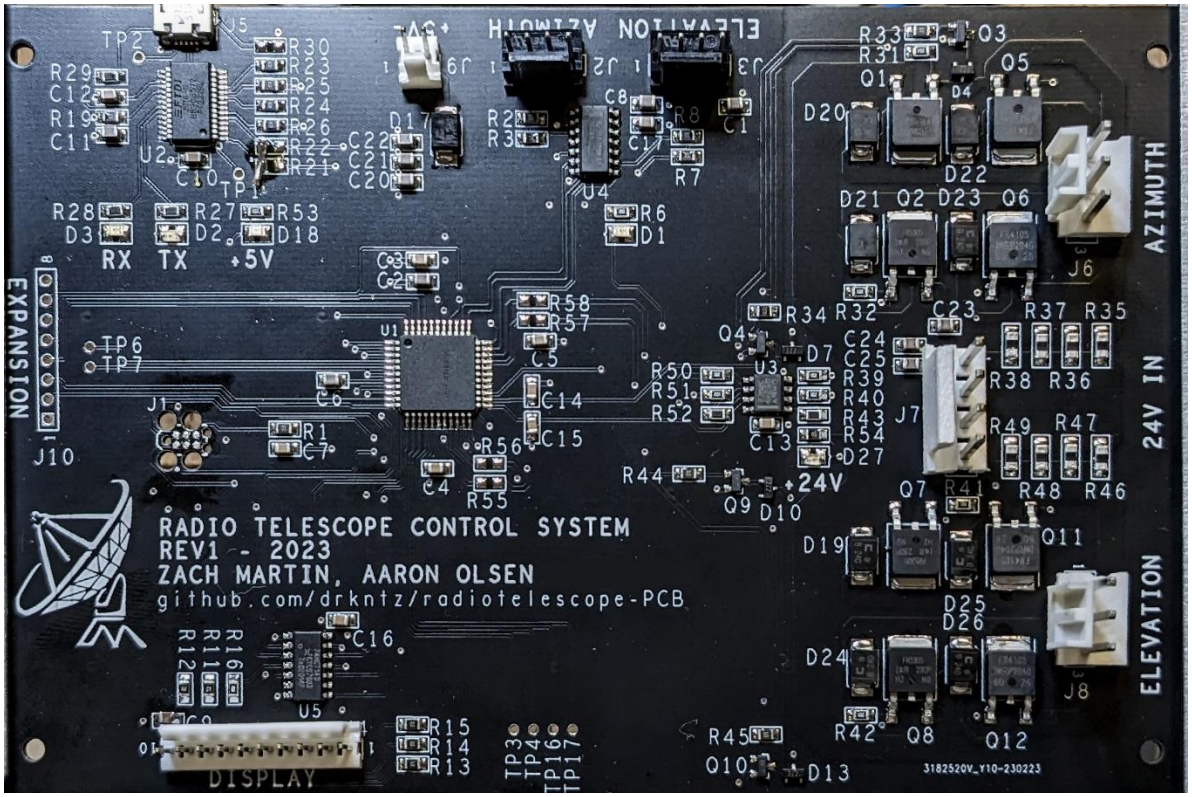

Figure 36: Assembled PCB

2.4.5 Testing of Populated PCB

When the components were populated on the PCB, testing began. This test followed the test plans that were developed during the design phase of the circuit, which included testing the H-bridge subsystem as well as testing the power modules, microprocessor, and the local control interface. An overview of the testing layout is shown in Figure 37, and a detailed close-up in Figure 38. Figure 39 includes the 24 V DC power supply that will later be used in the final design of the project as well as another view of the test setup.

For most of the testing, a power supply, debug connections, and oscilloscope were required. In some cases, the power supply used was a constant-current, constant-voltage supply that was set to a desired maximum current value around 50mA. This way, if there was an issue with the board subsystem under test, the current would be limited to a safe value that would minimize component damage. After these tests were completed at a low current limit, the entire system was tested with the high current Mean-Well power supply module installed.

Debug connections were used to program the microprocessor and control test functions via a command terminal on a laptop computer. As the microprocessor had two UARTs, one of them

was devoted to the USB-UART connection to the control PCB for radio-telescope operations, and the other was devoted to the debug header at J1 for testing. This UART was connected to a PC via an interface board that automatically selects between the PICkit programmer and the debug connector. The PICkit programmer was used to flash new programs to the board and can be used as a debugger to debug the PIC processor function.

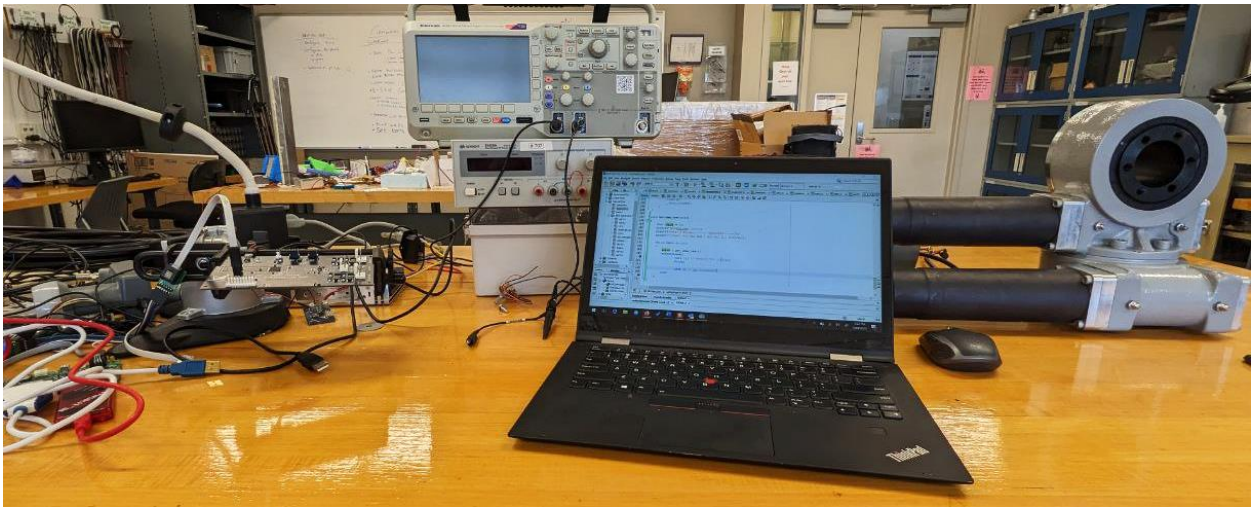

Figure 37: Overview of testing site, showing (L-R) PCB in vise, oscilloscope and power supply, laptop with terminal program, and two-axis motor.

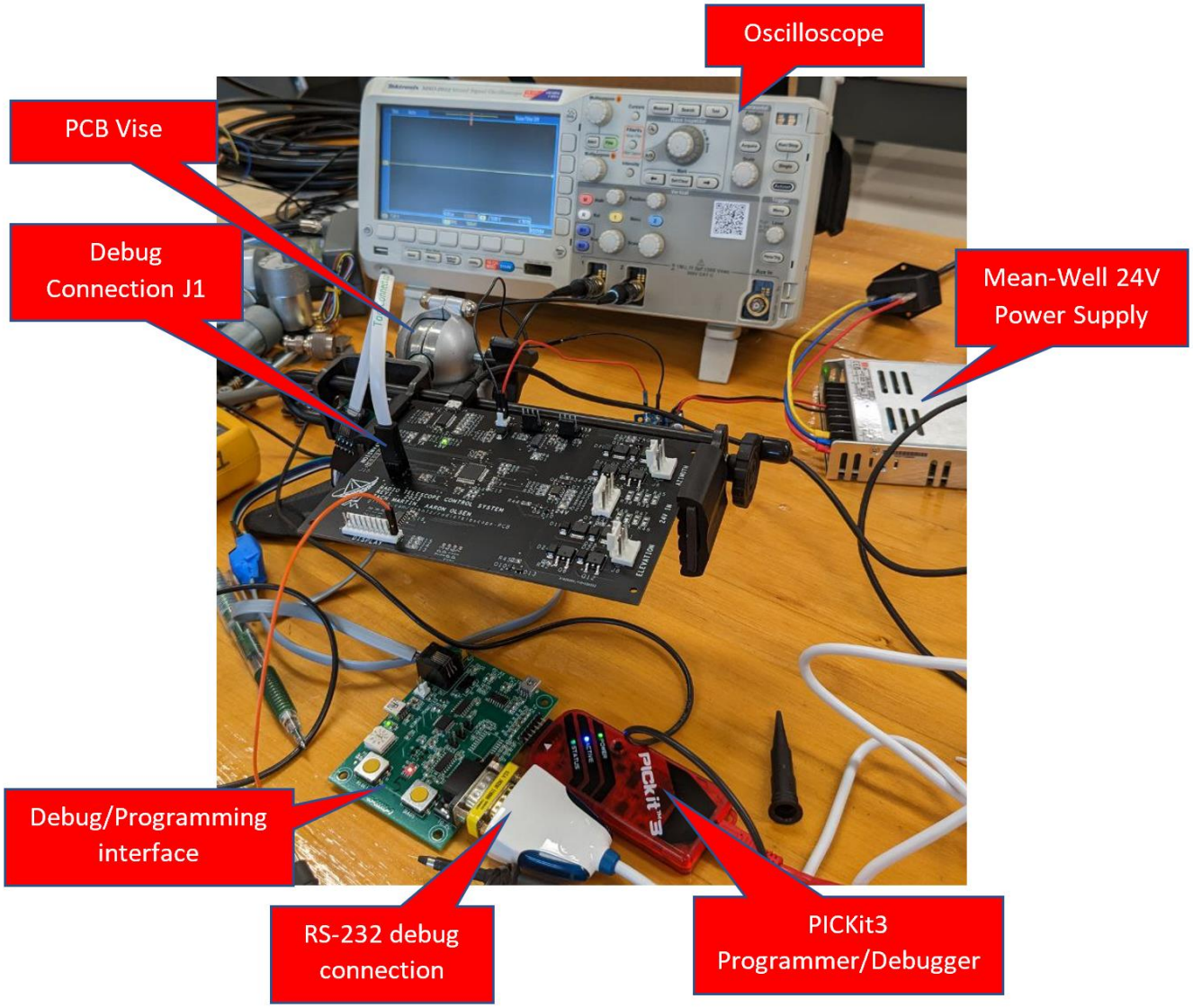

Figure 38: Test Setup Detail

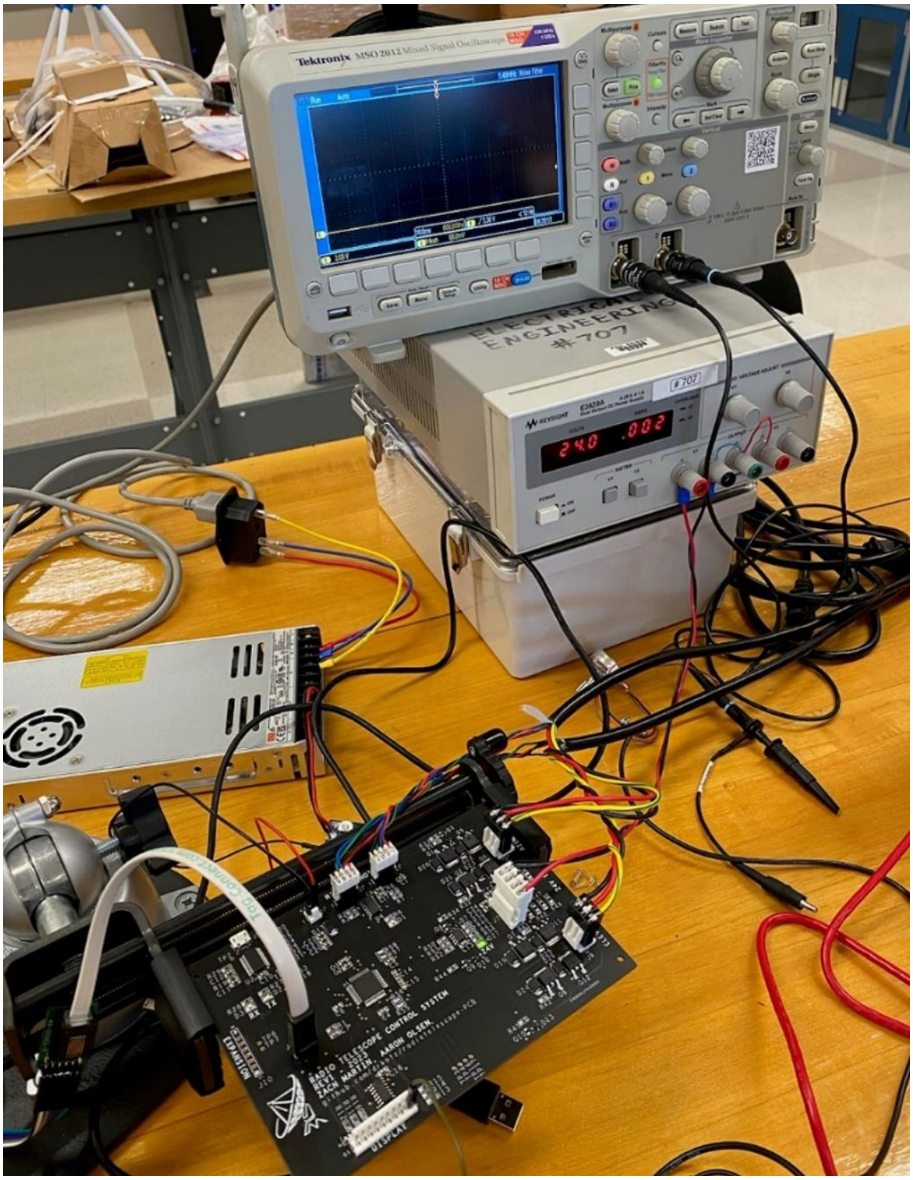

Figure 39: H-Bridge Test Setup.

The first set of tests utilized an 8-Ohm power resistor to determine the functionality of the H-bridge. Figure 40 shows the H-bridge turning on when trace 1 goes high (~4.6 V) and trace 2 goes low (5 V). It goes to ~4.6 V because of the diode in line with the 5 V source on the board. Figure 41 shows the gate of the PMOS that is off at 24 V and on at 5 V. There is ~250 mV of noise upon switching the motor on or off, likely due to gate coupling. This can be ignored for the purposes of this project because that voltage is not enough to turn on the PMOS.

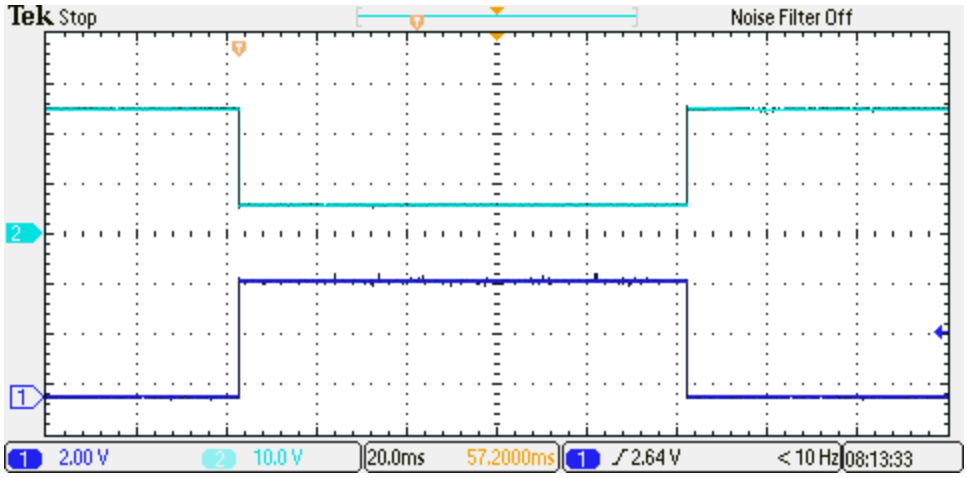

Figure 40: This is showing the gate of Q8 (PMOS) vs the gate of the NMOS (input signal). Trace 2 is Q8 gate.

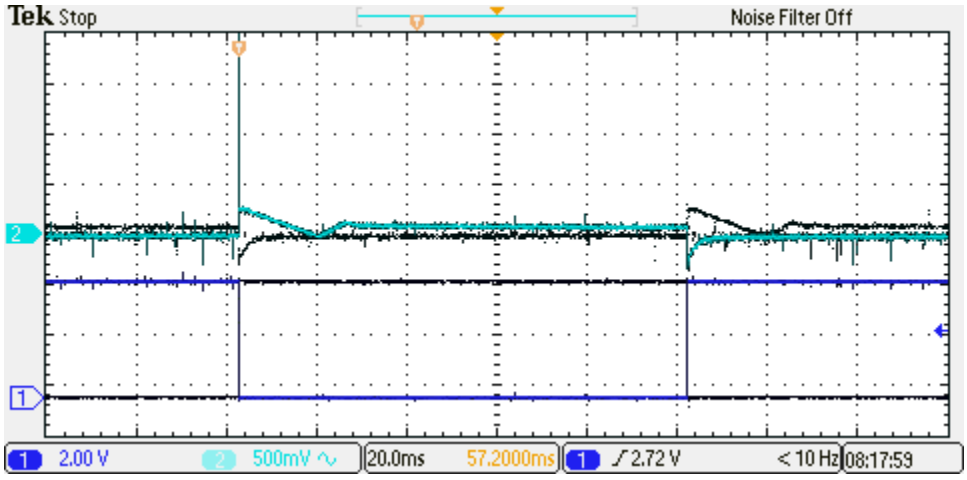

Figure 41: PMOS gate that should be quiet (Q7) and the input voltage wave.

The next set of tests used a 4-Ohm resistive load to test 6 Amps through the H-bridge. Once again, Figure 42 demonstrates the turn on and off of the current through the load as previously shown. The resistive load turns on and off essentially instantaneously from this view. Figure 43 shows the turn off transition of the PMOS and NMOS gates in use where the PMOS gate is not instantaneous and has some small oscillations. For the resistive load, this can be ignored because it is just 30 µs. The turn on transition is shown in Figure 44 with a ~1 µs switching time which can also be ignored.

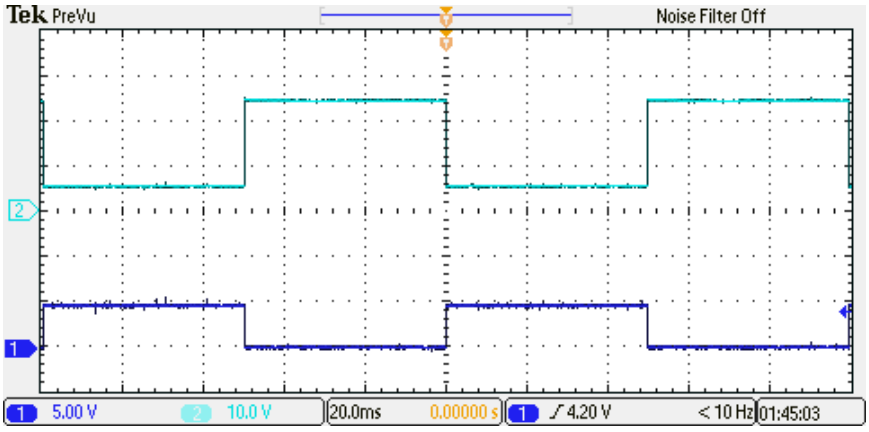

Figure 42: PMOS gate (cyan) vs NMOS gate (blue) with 100ms period and 50% duty cycle.

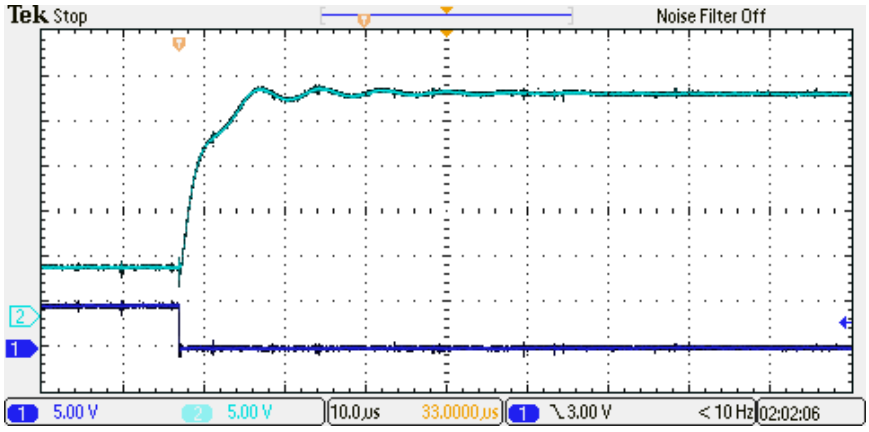

Figure 43: Turn off transition of Figure 42.

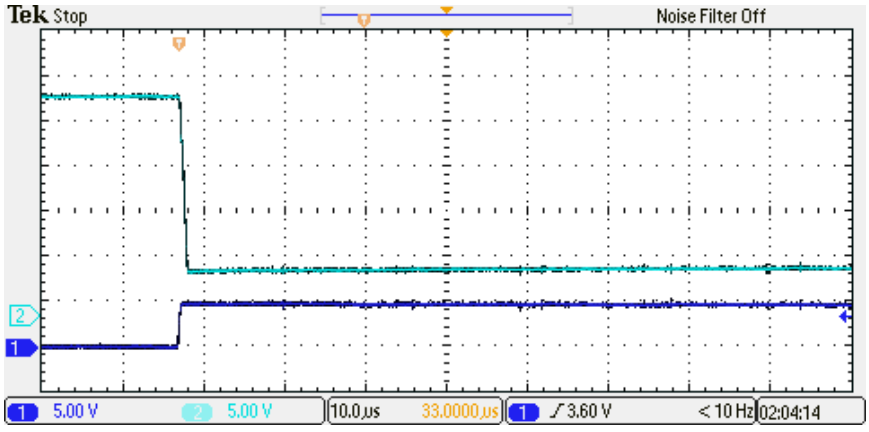

Figure 44: Turn on transition of Figure 42.

The voltage across the 4-Ohm resistive load is shown in red in Figure 45. The switching time is very quick for the applied voltage in red, while the turn off time for the two terminals of the motor individually take around 10 ms to decay. Without a current, the nodes share the same voltage. The turn on transition time is ~200 ns as shown in Figure 46 for the load voltage and positive node voltage. Figure 47 shows the decay to zero Volts is ~3ms for the node voltages, but the load voltage is turned off very quickly. These switching times demonstrate the capabilities of the H-bridge itself before being connected to the motor load. The limits of the H-bridge are needed to determine its ability to turn the load on or off quickly and switch directions quickly to reduce the time needed to change directions or just turn off. A short transition time is needed so the motor does not remain on where it would rotate to an undesired position past the desired position.

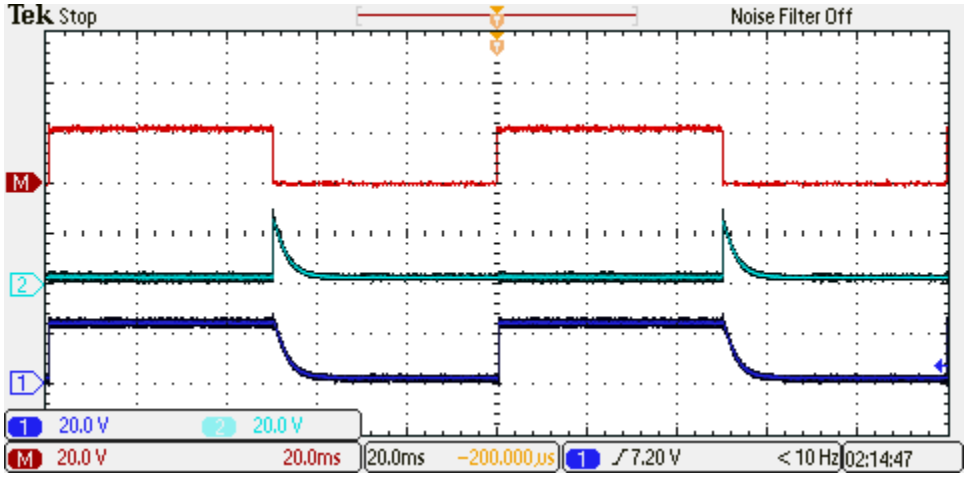

Figure 45: Positive side of motor voltage (blue), negative side of motor voltage (teal) and motor voltage (red = blue - teal) using a 4-Ohm resistive load.

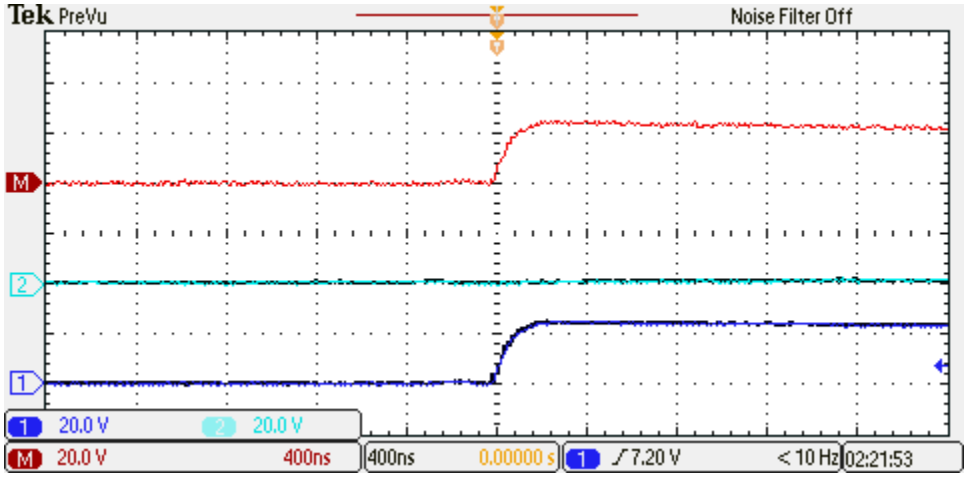

Figure 46: Zoom in of turn on transition in Figure 45.

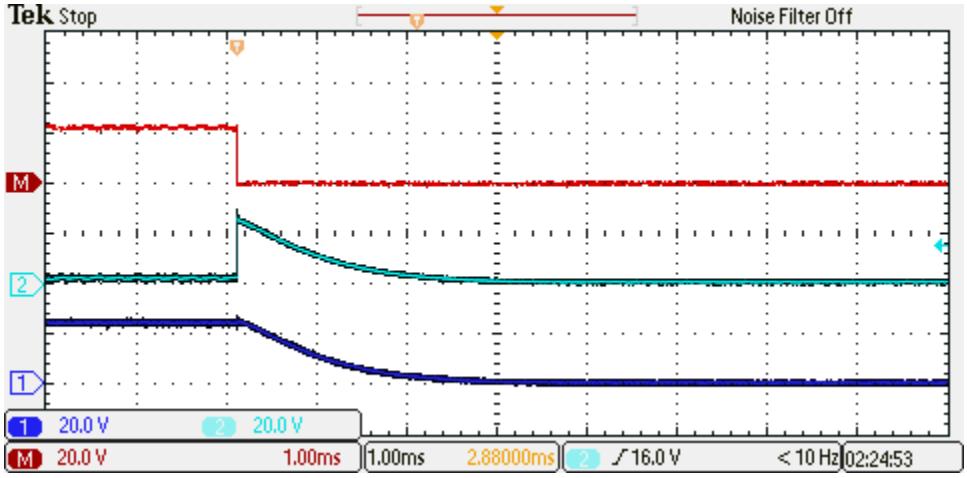

Figure 47: Zoom in of turn off transition in Figure 45.

A 2.4 Ohm resistor was used to test for larger current (10 A) capability. One engineering requirement is to limit the current to 15 A to protect the user from the motor in case the user gets caught in it or to protect the motor if it is damaged, thus this is a step to ensure that the transistors can handle such a current in the first place. Q11 got really hot, and smoke came from the board of unknown origin, although it is likely to be from Q11 or solder around that transistor. The datasheet of the NMOS transistor revealed that the temperature change per Watt was 30°C/W with an R_{DS_on} of ~45 mOhm. The maximum supported current is ~7.7 A with this information. A step back was taken to the 4 Ohm load. Figure 48 shows an IR image of the board where the transistor under 6 A is getting very hot and it continued to rise further risking damage. The junction temperature maximum is 170°C. The team's suspicion is that this is happening due to the NMOS transistor channel not being fully opened while the PMOS channel is. The PMOS has a V_{GS} of 19 V and the NMOS has a V_{GS} of 4.6 V. It is likely that the V_{DS} of the NMOS transistor is not close to zero which increases the power while the PMOS is driving a large current into it. A potential solution is to increase the V_{GS} of the NMOS transistor to see if the temperature decreases and supports the desired current.

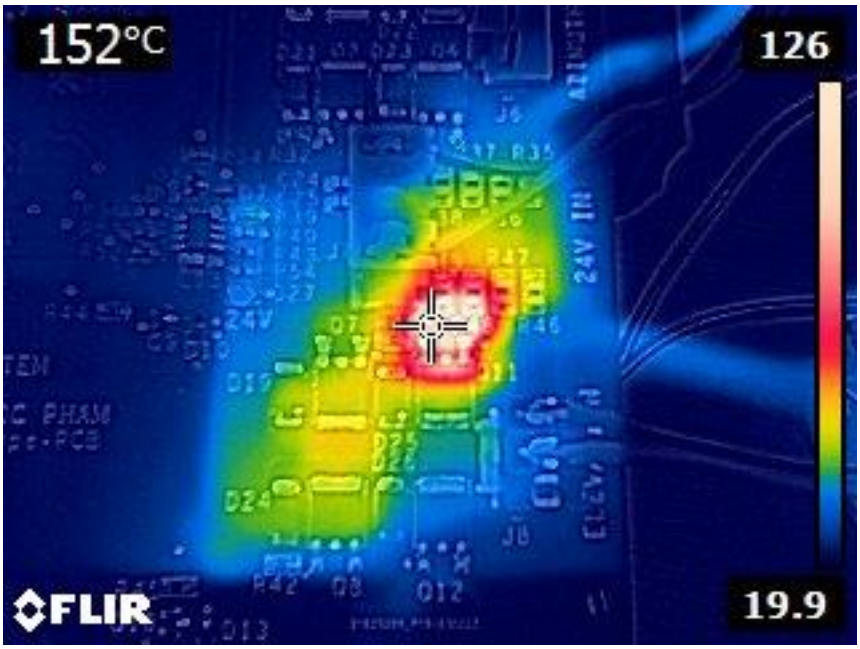

Figure 48: Temperature rose rapidly in Q11 (NMOS) with the 4 Ohm resistive load. It hit 152°C in this picture.

The final test used the motor as the load. The transition time to turn on the motor is very quick as shown in Figure 49. However, the turn off time of the motor is slow at about 600 ms. This seems like an extensive period, but it should not affect the purposes of the design. This time to turn off is caused by the motor itself as shown by the earlier resistive load results having a near instantaneous shut off from the H-bridge circuit. A separate motor would need to be considered to reduce this effect. Under the motor load, all components of the board remain under 35°C as seen in Figure 50. The H-bridge circuit, particularly the NMOS transistor of concern earlier, can support the current motor being used for the project.

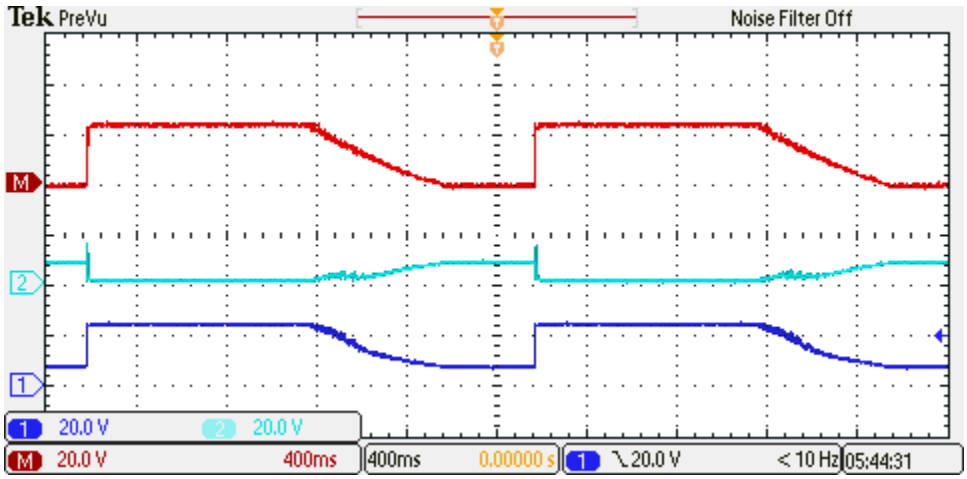

Figure 49: Motor voltage (red = blue-teal), positive terminal (blue), and negative terminal (teal).

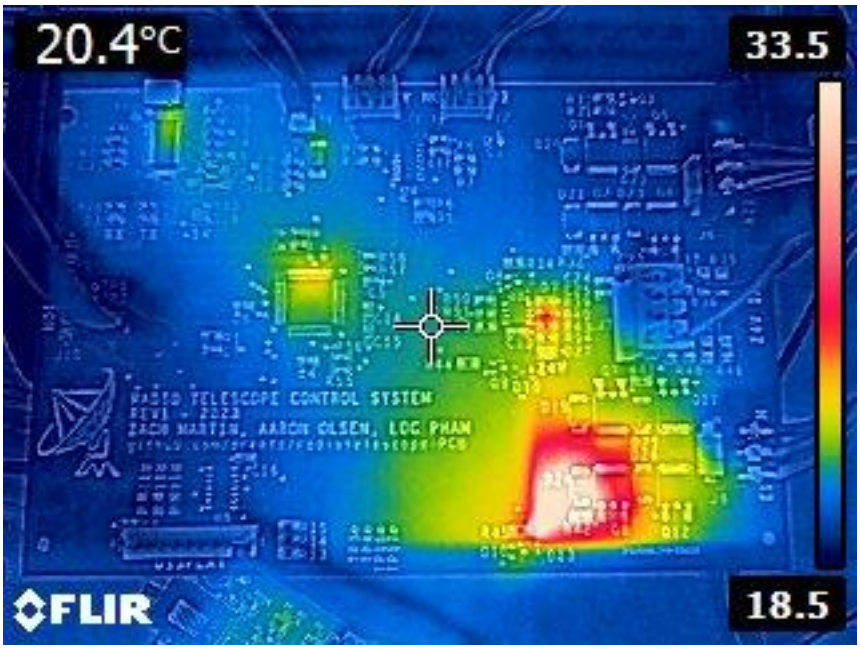

Figure 50: PCB temperatures when the motor is running.

2.4.6 Comparison of Testing with Simulation Results

In the simulation of this circuit, it was given that the simulation passes when the transistors do not turn on accidentally (I.E., their gate voltages are relatively quiet), counter EMF is handled by the protection diodes, transistors quickly reach saturation and cutoff with minimal time in the Ohmic region, and the transistors are not subjected to extreme currents or voltages beyond the datasheet recommendations. Similarly, the testing should follow the same goals and is expected to produce similar results to the simulation of the circuit.

One of the simulation results was the switching time of the P and N-Channel MOSFETS. In the simulation, it was found that the P-Channel MOSFETS turned on in about 10 µs and turned off in a little over 15 µs. The testing showed the turn-on time was much sharper, around 3 µs, while the turn off time was about the same with some small oscillations. The N-Channel MOSFETS turned on and off quickly, in only a few microseconds in simulation. Similarly in testing, these transistors had sharp transitions and passed through the Ohmic region quickly.

Simulation with a model more closely approximating a motor showed the result of driving a reactive load. This included a back EMF that was clamped by the flyback diodes and oscillation when the motor was turned off. The oscillations in simulation were found to be around 5 ms in duration, while in test the response was overdamped and did not oscillate, but instead decayed for approximately 10 ms until reaching steady state. It was then determined that with the 2 A motor that was used in test, R-C snubbers did not need to be added as they were added in simulation. Should they be needed with larger motors, a similar process to the one used in the simulation can be used to find the cutoff frequency that will dampen oscillations.

As expected from the design and simulation of this circuit, the protection diodes across the transistors in the circuit helped to prevent overvoltage damage to the transistors when the switches turned off. In the simulation, it was found that the motor voltage would very quickly flip polarity and approach -24V when the H-bridge was turned off, as expected. This flyback effect is due to the large negative change in motor current that occurs when the H-bridge switches off. In simulation as well as in testing, the protection diodes force the motor voltage to remain at 24V in either direction, with a small error due to the diode forward voltage. This prevents the MOSFETS from any appreciable voltage which could cause damage.

Overall, the testing supported general findings from the simulation of the circuit. In the places where the test diverged from the simulation, such as in the case of the oscillations, it was found that the actual circuit outperformed the simulation results.

2.4.7 USB-UART Converter

Part of the function of the circuit as given in the market requirements and engineering requirements portion of this document is to have a USB connection to a host computer. This connection was chosen to be a micro-USB connector on the side of the board, which is controlled by a USB-UART controller integrated circuit. With this method, the host computer

sees the USB device as a virtual COM port, while the microprocessor sees the integrated circuit as a UART transceiver.

The IC chosen was the ubiquitous FTDI FT-232RL chip. This IC cleanly handles the USB and UART protocols while offering a few additional features, such as power from USB or from controller, a programmable general-purpose set of pins, and additional UART features beyond RX and TX to enable smooth communications. For this configuration, the IC was set up with the internal oscillator source for USB, power from the PCB and not the host computer, and it was set up with only TX and RX going to the microprocessor. Additionally, there were two LEDs added to the board to indicate the TX and RX status of the FTDI FT-232. These LEDs were setup to flicker when TX and/or RX were active.

For a detailed drawing of the configuration of this chip, refer to Appendix C: Final Schematics, Layout, and Parts List.

2.4.8 UART Command Interface

Part of the requirements of this device is that it can interface over USB with the host computer software, so that commands can be sent via USB and responses in turn sent back.

This requirement was met in two ways: via a terminal-based menu and via a command-packet interface. The terminal-based menu was designed to be used by a user interfacing with the command computer so that they could select certain movements and calibration commands. For example, this was designed so that they could select a movement in the altitude direction.

The command-packet interface is a method by which a structured packet can be sent to the control PCB via the USB from the Python program running on the host computer. This interface, given in the code which is available in the appendix, is a system that has a structured packet size and type. The packet begins with a two-byte command, which is followed by the integer number of tenths of a degree for each axis. The degree value is also given in two bytes. The packet concludes with an EOT character, which indicates the packet is complete. This is given in the following diagram.

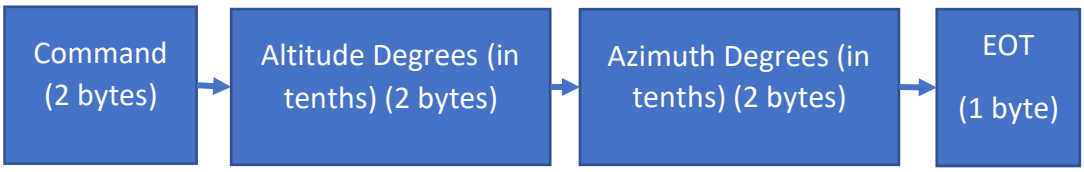

Figure 51: Automated command structure

To reference the terminal-based command method, refer to the program code in the appendix under the function update_pc_menu().

2.4.9 PC Command Driver

To interface with the control circuit board from the host computer, there must be software which can communicate over the USB interface. This is referred to as the “PC Command Driver” in this document. As mentioned in the previous section, UART Command Interface , the command interface was designed in the embedded system to support both connection via a terminal software and connection via a Python program.

The terminal software method is given in the previous section. The resulting terminal menu that is given is shown in the image below.

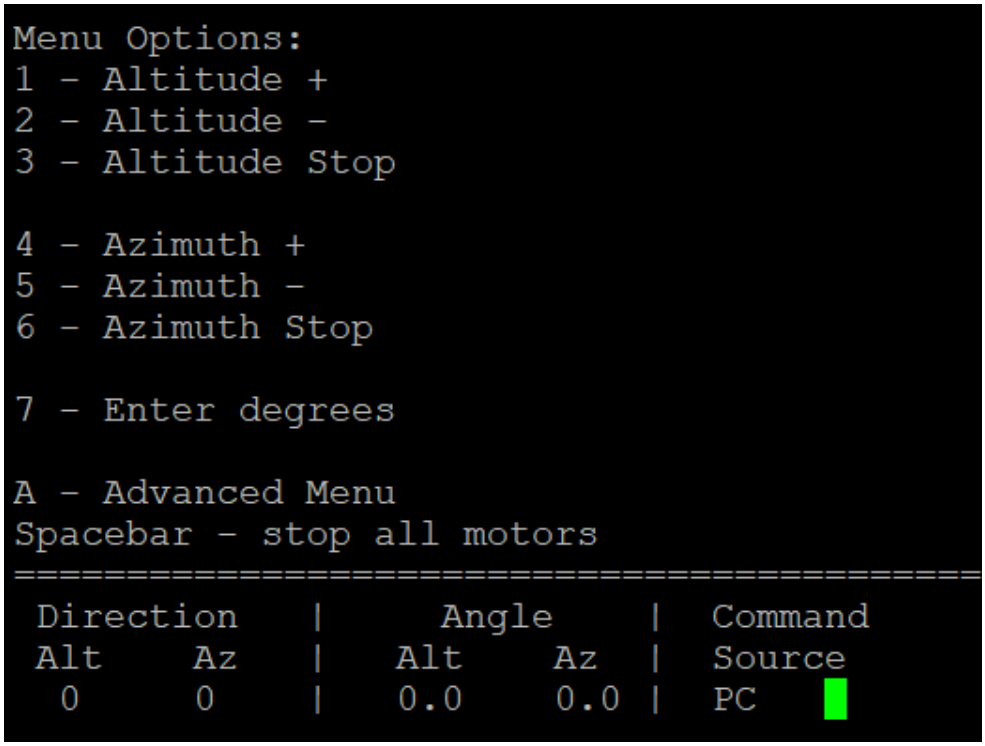

Figure 52: Terminal menu

This menu provides a pseudo-graphical method of interfacing remotely with the control PCB. It can be accessed via a simple terminal interface such as the popular “Putty” program via a virtual COM port set to 115.2kbps. There are two identical menus for altitude and azimuth. Each of these will turn the motor on in either direction for manual movement. There is a menu for entering a target degree value. Finally, there is a menu which has some additional commands, such as re-calibrating the home position and going to the home position.

Underneath the menu is a status section, which constantly refreshes the motor states, motor position, and the command source. As given in the engineering requirements, this device is meant to be controllable remotely over USB as well as locally via pushbutton interface and a

simple display. The former case is given by Command Source: PC, and the latter by Command Source: Local.

Automated control via a Python program is given in the program software as defined in the previous section. It handles a series of control packets streamed over the USB to UART interface. Each packet sent from the PC is a two-byte command followed by a two byte angle for altitude and a two byte angle for azimuth. The packet is terminated by an EOT character. The packets sent to the PC is a two-byte response followed by a two byte altitude angle and a two byte azimuth angle, terminated by an EOT character. This enables automation with a generic serial driver program written in Python.

2.4.10 24V Power Supply

The 24V power supply converts 120 VAC to 24 VDC for use in the H-bridge to drive the motors. The dual axis motors obtained for the elevation and azimuth rotation require 24 VDC to be driven. This supply was created by Mean Well with the model's name LRS-350-24. It provides a slightly adjustable 24 VDC supply at up to 14.6 A. This was suitable because the motors only take 2 A each at a maximum. The minimum input voltage is 90 VAC which is not a problem for standard outlets. The supply is shown in Figure 53, and the datasheet can be found in Appendix E: Datasheets.

Figure 53: The Mean Well 24 VDC Power Supply.

2.4.11 5V Power Supply

To provide a regulated 5V power rail for the low-voltage systems on the PCB, A 5 V buck regulator module was employed. The regulator converts the 24 V DC from the 24V power supply described above down to 5v for the circuit. Due to the reverse protection diode in series

with the 5v input connector on the PCB, the circuit on the PCB gets around 4.6 V. Future revisions would incorporate the 5v regulator onto the main PCB.

The 5V regulator that was used for this project was a module that was designed previously by one of the members of the capstone team. However, similar modules could be purchased off the shelf, such as those provided in the parts list section of this report. The regulator can be seen in Figure 54.

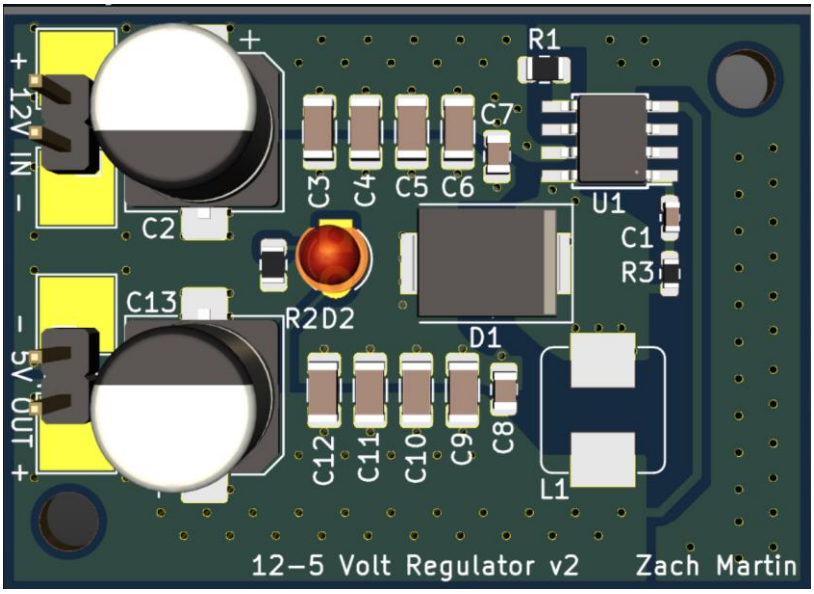

Figure 54: 5 V regulator designed by Zach.

2.4.12 Microcontroller

The microcontroller for this system is the heart of the entire control unit. The microcontroller chosen was a PIC24FV32KA304. Its configuration is given in the Schematics section in Appendix C: Final Schematics, Layout, and Parts List.

The reasoning behind the choice of the microcontroller is as follows. As the system required granular control over motor direction, interruptible pins, and several ADC inputs, as well as several serial interfaces and a host of GPIO pins and expandability, it was determined that a microprocessor of this size was necessary. As the capstone team members had done programming with PIC microprocessors, it was determined that a Microchip PIC part was the most logical choice. This microprocessor was selected from the available stock at the time of design.

As given in the system block diagram, the microcontroller had the duty of interfacing with the USB-UART converter interface, local control and an I2C display, as well as running a control loop between the H-bridge motor driver and the rotary encoder input.

2.4.13 Motor and Gears

The motor and gears came in a single off-the-shelf. A dual-axis motor was chosen to provide a single unit with both azimuth and elevation directional control in the final system. The chosen dual-axis motor was manufactured by Luoyang Jiawei Bearing Manufacturer Co., Ltd. This motor's datasheet can be found in Appendix E: Datasheets. The unit includes rotary encoders for each motor to determine the position. More on this in the next section. The output motor speed is ~17°/minute (0.048 rpm). This does not satisfy the engineering requirement of 1 rpm. The accuracy of the motor was favored over the speed of the result because a quick result has no meaning if the image is blurred. This speed is still quick enough because Earth only rotates at 15°/hour, thus changing your position by 0.25°/min which can be accounted for with the speed of the motors. The current antenna is light, but future antennas used for expansion of the project may not be as light. Thus, there is a need for the large gear reduction (575:1 and 62:1 in series for both motors) which increases the torque rating to 716 N-m.

2.4.14 Rotary Encoder

To determine precisely where the motor system was pointed, a motor and gearing system was selected that provided high rotary encoder resolution and low backlash.

The rotary encoders from these motors are given in the datasheet as two Hall-effect pulse encoders per axis, each 45 degrees out of phase. Each hall encoder transitions four times throughout the motor rotation, for a total of eight state transitions throughout a single motor rotation. This is given in the following drawing.

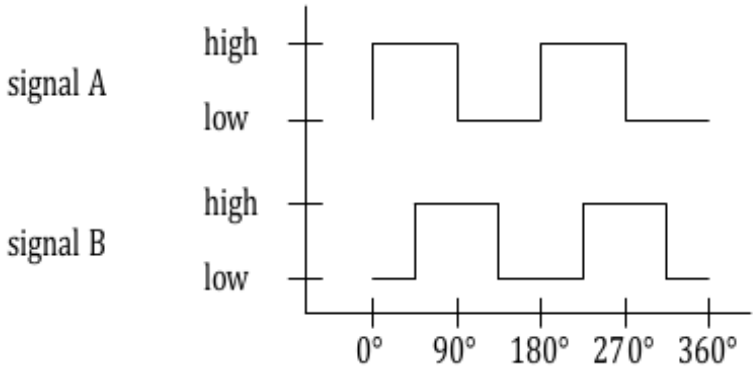

Figure 55: Hall rotary encoder pulses

As the motor (and rotary encoders) was positioned at the input of a precision gear box system, the hall encoder resolution was greatly increased by the very large gear ratio of the motor system. The previous section describes the motor and gearing system in-depth, but it is sufficient to note that the overall gear ratio is 35650:1, which increases our 8 transitions per 360 degrees (one rotation) figure to 792.2 transitions for every degree of movement at the

output. This means that our degree measurement resolution is around 0.0013 degrees, much more than the backlash spec given by the datasheet.

Each of these Hall effect encoders is an open-collector type encoder, so they were pulled up by a set of pull-up resistors to the 5V rail of the PCB. After that, the encoder pulses are passed through a Schmitt trigger buffer and sent to the microprocessor. In the microprocessor, interrupt-driven code increments a count of the number of pulse transitions for each axis, depending on the direction of rotation given in the motor driver code. This pulse counter is then converted to tenths of a degree in the main loop of the program, where it is used globally to communicate the pointing location of the system and to manipulate the motor movement control loop. The software for the encoder system can be found in the appendix.

2.4.15 Push Buttons

The push buttons are standard waterproof buttons that are mountable to the enclosure. Three buttons are connected in the pull-down form. When the buttons are pushed, the pin on the microcontroller is pulled down to ground which can be read and used for causing something in the firmware program. Currently, the center button is used to enter the local control which has multiple menus that can be rotated through using the same button. The left and right buttons are used as options in each respective menu.

2.4.16 LED Indicator and LCD

The LED indicator and LCD are used by the local control interface to indicate to the user the status of the radio telescope system. The LCD is a 2 row, 16 character (16x2) alphanumeric display which is driven by an I2C serial interface. This display shows the operating status of the unit including the antenna angles, the motor states, and the control input source (USB or local control, for example). The LED indicator displays the operation of the unit. It acts as a "heartbeat" to show that the unit is working. It is set to blink at a set rate while the unit is running through the main control loop. If the controller is stuck in another function at any point, the LED will stop blinking.

2.4.17 Embedded C Code Design

The C code for this project involved a number of processor peripherals and routines running throughout the operation of the device. The general approach to handling the runtime of the project was to use a "super loop," interrupts for time-critical functions, and interval checks for rudimentary scheduling.

After the device has configured itself and the peripherals that are used during the operation, including UART, interrupts, timers, I2C, and so on, the program enters an infinite "super loop." The super loop approach is one of the simplest methods of handling several operations

repeatedly. In the super loop approach, the processor handles several tasks sequentially, during which time it will update state machines for each task. If a task is desired to run at a particular rate, for example every 1 second, then the task will first check for an elapsed interval to be true, otherwise it will not run. The loop tasks are given in the following flow chart:

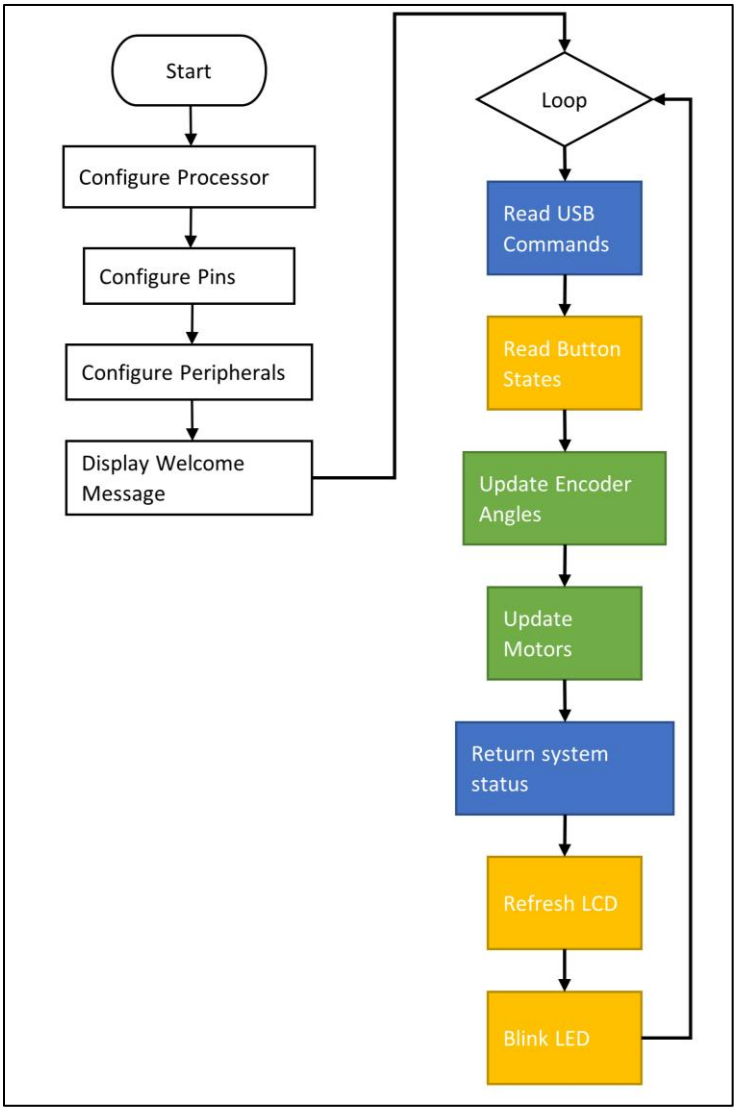

Figure 56: Software Flowchart

In the read USB commands task, the code will check a UART buffer for characters and decide what to do with the data. The read button states tasks polls the input buttons to check for changes. The encoder update task takes raw encoder pulses, which are incremented or decremented on interrupt, and converts it to a useable degree value in altitude-azimuth coordinates. The update motor task decides what to do with the local or remote control with consideration for the current angle and motor direction. The device then returns the system status via USB and displays the status locally using the LCD and the status LED.

As the encoder pulses are happening asynchronously, the device will interrupt at every transition of the encoder pulse inputs in order to avoid missing an encoder pulse transition. However, each function in the superloop has to be reentrant, so that the interrupts will not break the system function.

At the initial configuration of the device, the processor was configured using the microchip code configurator (MCC). This tool enables rapid development of peripherals using standard libraries. In some cases, however, the MCC tool was not sufficient or provided faulty code. This had to be fixed, as for example, the ADC reading the motor current would not work.

The program code for this project involves many routines and configuration functions beyond the super loop updater. For example, the LCD display updater calls several functions to convert the message to a bit stream and send the stream of bits out via I2C. This LCD driver had to be rewritten from a driver written in C++ for Arduino to C code optimized for PIC devices. As the entire program code involves thousands of lines, a link to the code repository is available in the appendix of this document.

3 System Integration, Test, and Results

This section contains the results of assembling and validating the entire design. In this section, the PCB assembly and enclosure setup are documented. The setup of the mechanical system using a dish antenna and the selected motor is also examined. In the testing section, each of the major subsystems of the design are tested separately, and then together as one system.

3.1 System Integration

This section documents the assembly of the system, beginning with the surface mount and through hole assembly of the printed circuit board, documenting the enclosure manufacturing and wiring, and concluding with the mechanical assembly of the motor and antenna system.

3.1.1 PCB Assembly

The printed circuit board used for this project was designed with surface-mount components for most of the electronics, while the connectors were through-hole. This approach allowed for higher component density and lower PCB size. As such, populating components on the PCB required use of surface mount solder techniques for most of the components.

The first step in populating the surface-mount components involved placing solder paste on the solder pads of each component using a stencil. This was accomplished by placing the PCB in a jig made of PCBs of the same height, as shown in Figure 57. The stencil was taped to the jig and solder paste applied to the stencil using a squeegee.

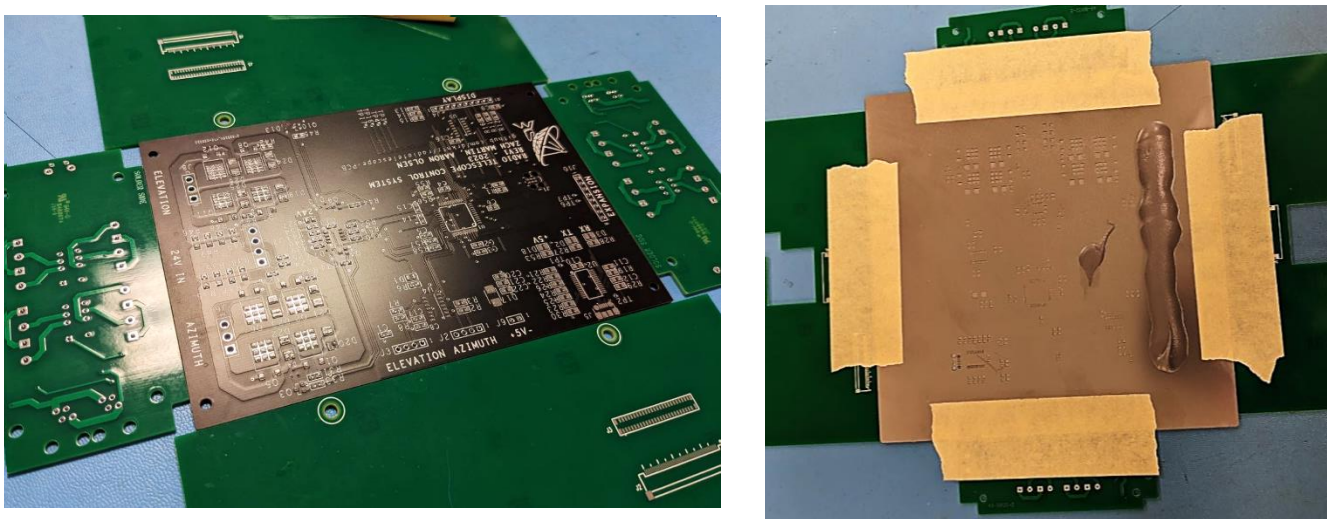

Figure 57: PCB in pasting jig (left). Stencil with paste on jig and PCB (right).

This stencil acts as a mask for the solder, which creates a print of solder paste neatly positioned on the component footprints on the PCB as shown in Figure 58.

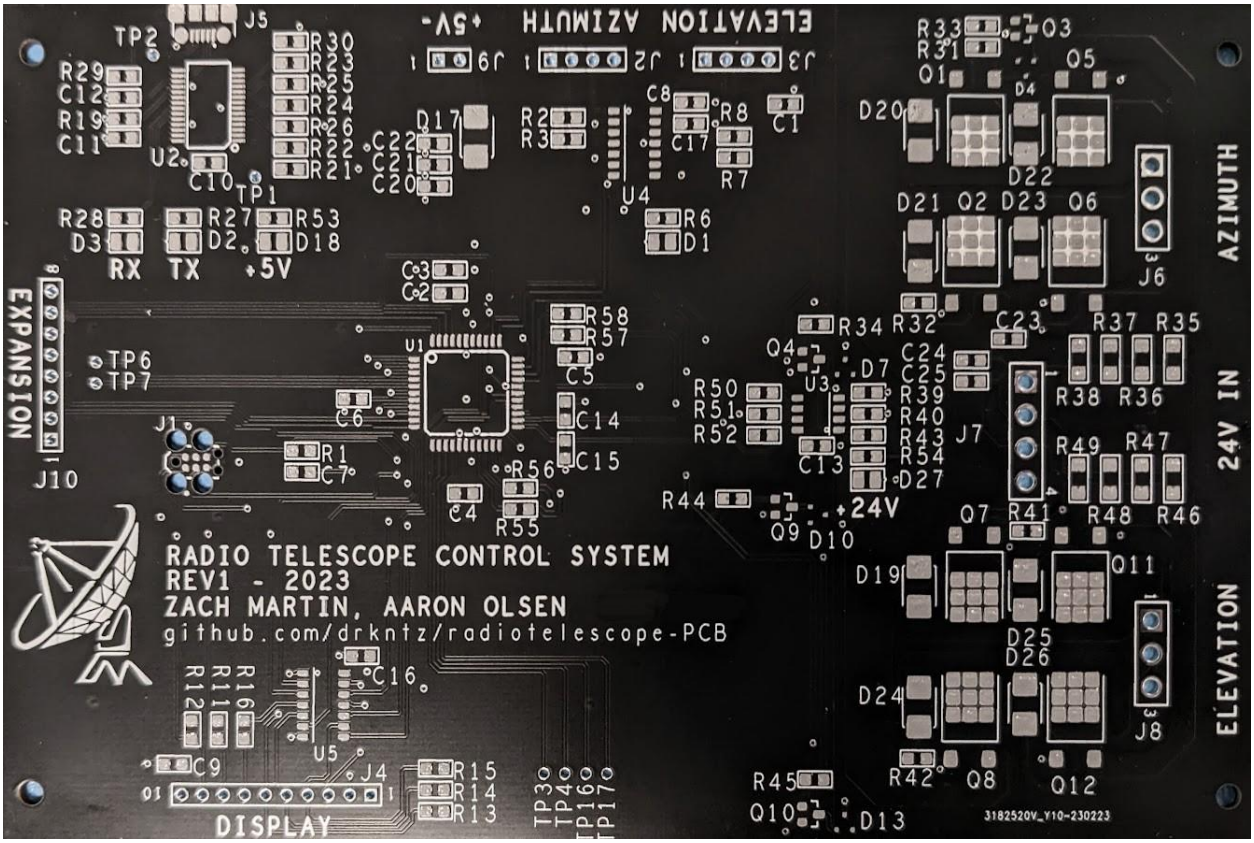

Figure 58: PCB with solder paste.

The next step in the surface-mount assembly was to place each surface-mount component on the solder paste according to the bill of materials and schematic. This was accomplished with the help of a stereoscopic microscope and several types of tweezers. The process is shown in Figure 59.

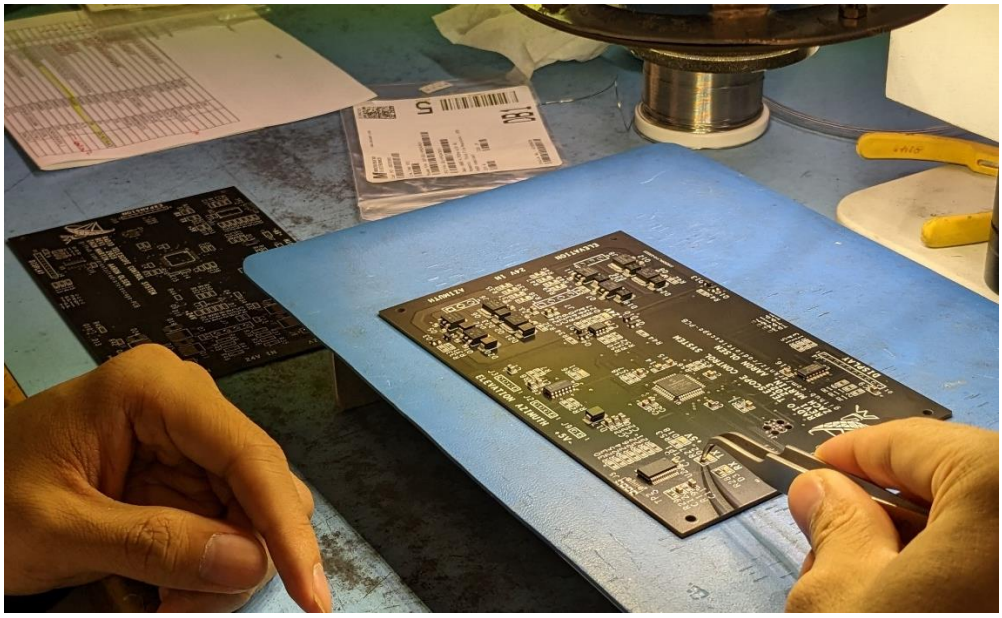

Figure 59: Surface-mount component placement.

The PCB, with the newly placed components on the solder paste, was then placed in a solder reflow oven set to a tin-lead solder heat profile. This oven melted the solder paste which flows between the component leads and their corresponding pads, completing the surface-mount soldering process.

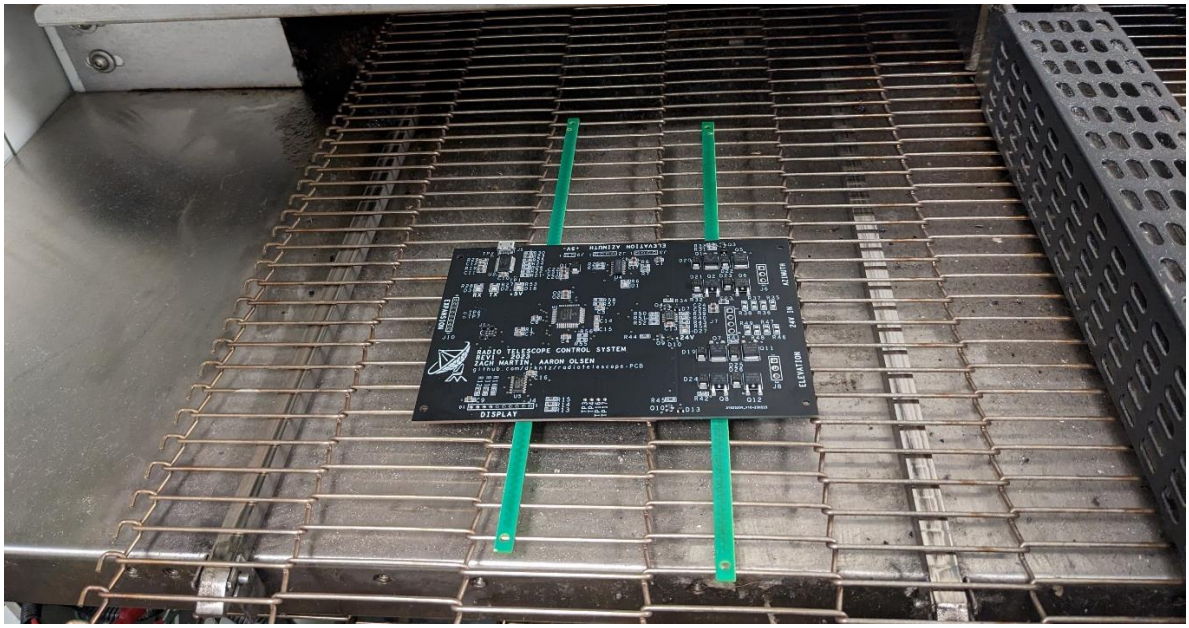

Figure 60: PCB placed in reflow oven.

The through-hole connectors were then soldered onto the PCB using tin-lead solder. This resulted in the completed PCB with both types of components as shown below.

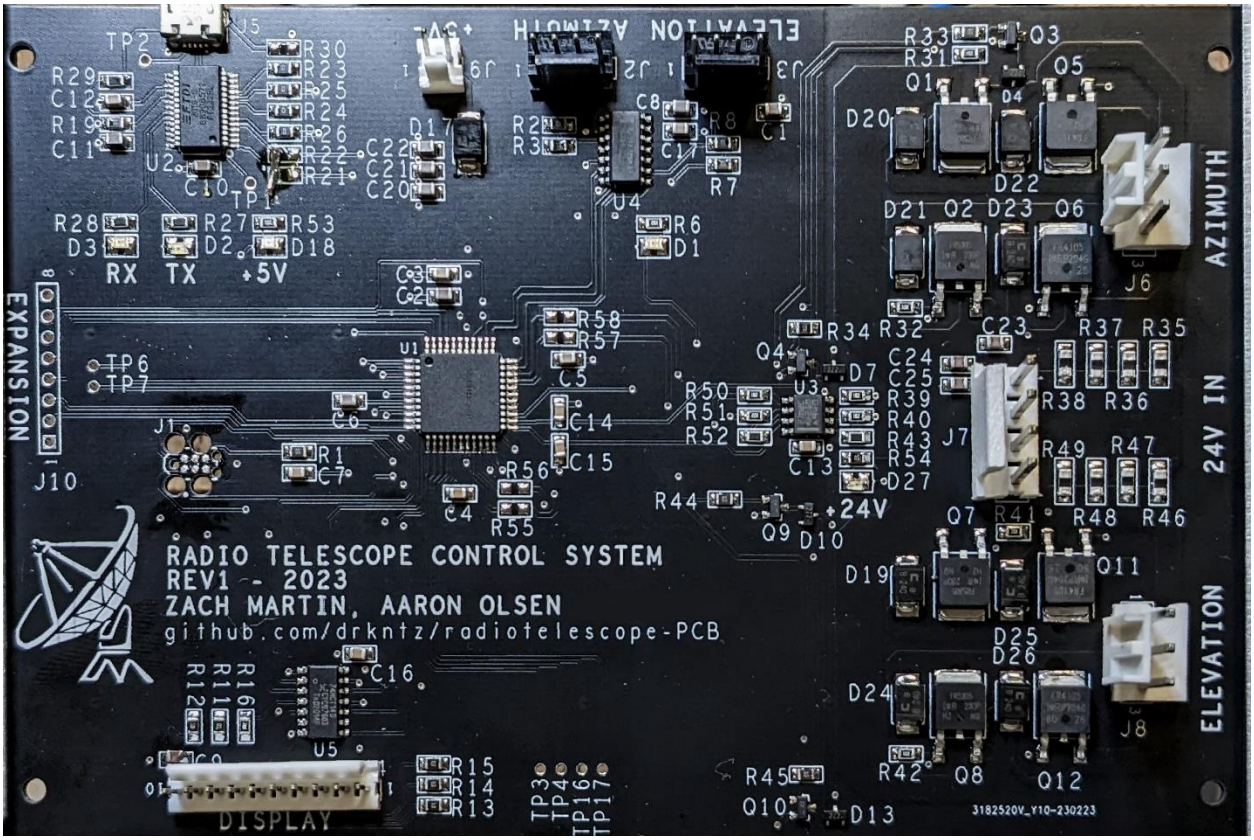

Figure 61: PCB With Through-Hole and surface mount components Installed.

3.1.2 Enclosure Assembly & Wiring

For much of the testing and validation process, the PCB was secured to the lab workbench via a PCB clamp. When the testing of the PCB and other subsystems was complete, the system was ready to be installed in the waterproof enclosure and have the remainder of the subsystems connected into one complete system. The first step of installing the system in the waterproof enclosure was to install the connectors into the enclosure to allow signal and power connection to the outside.

The side chosen for the connector placement was the side that would be the bottom of the enclosure, when mounted vertically at the installation site. This may help prevent water entry into the enclosure. Four connectors were added: two waterproof 8-pin M12 connectors for power and signal to the motors, a micro-USB connector for communication with the computer, and an IEC power socket for 120VAC. The holes for these connectors were cut into the case using drills and a plastic cutting tool. The assembled connectors are given in the following image.

Figure 62: Connectors installed in the bottom of the enclosure.

These connectors were attached to short pigtail wires which allowed connections to the PCB on the inside of the enclosure as shown below.

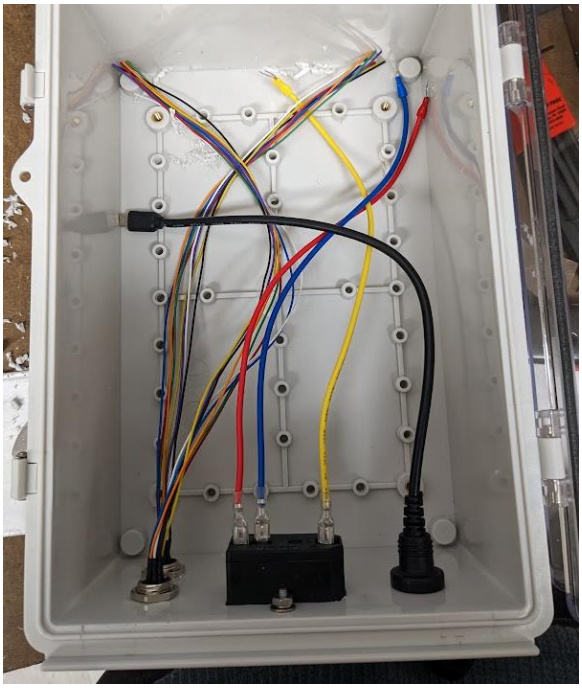

Figure 63: Connectors and pigtail wires inside of enclosure

The next step of installing the PCB in the enclosure was to add waterproof push buttons to the lid of the enclosure. This allows for local control without opening the box and exposing the electronics to the environment. Tape was placed along the bottom of the lid and holes were drilled into the lid to accommodate the waterproof buttons as shown below.

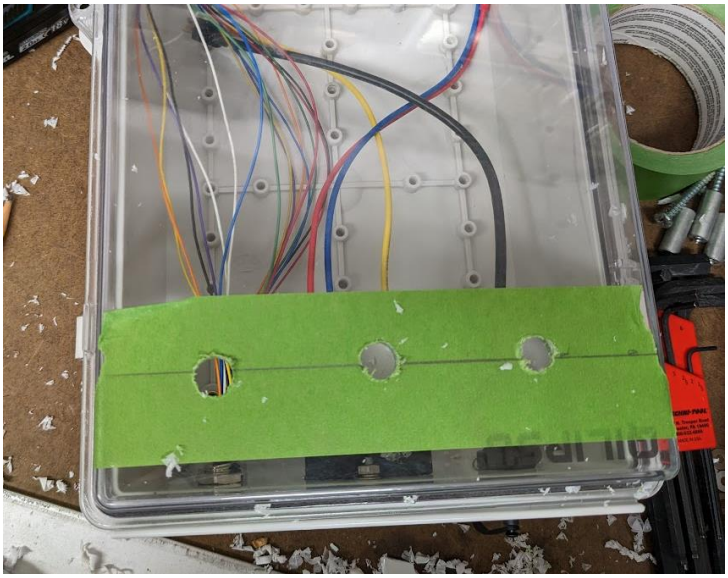

Figure 64: Pushbutton entry holes

The next step of the mechanical assembly was to secure the 24V power supply in the enclosure. This power supply was secured with small L-brackets to plastic standoffs in the bottom of the enclosure as shown below.

Figure 65: Power supply mounted in enclosure.

This resulted in the intermediate system as shown below, including the pushbuttons, connector inputs and outputs, as well as the 24V power supply secured to the bottom of the enclosure.

Figure 66: Enclosure with pushbuttons, connectors, and power supply

After this was completed, a plastic platform was mounted using standoffs to provide clearance above the power supply and provide easy access to the PCB. The PCB was then mounted to the plastic platform using brass PCB standoffs. Using similar standoffs, the display was mounted next to the PCB so that the user could see both the PCB and the display through the clear plastic cover of the box when the box was mounted vertically at the site. The +5V power supply module was installed in the enclosure using very high bond adhesive tape. The figure below shows the PCB and display installed on the plastic platform above the power supply.

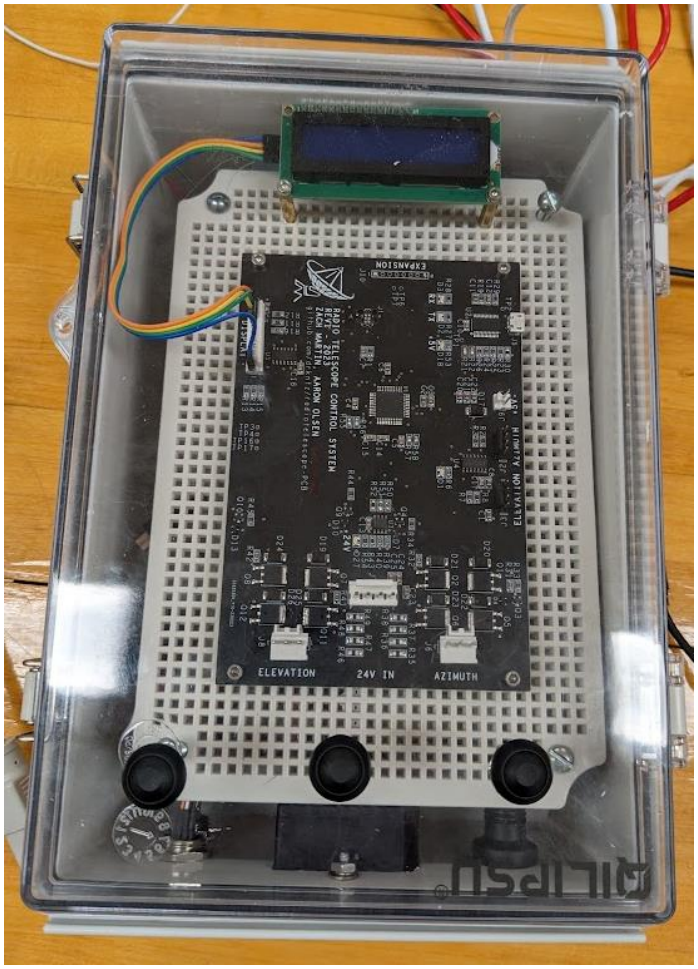

Figure 67: Completed mounting of PCB and display in enclosure.

The final step in assembling the control box was to add wiring for push buttons and connectors to the PCB. The altitude and azimuth waterproof M12 connector pigtails were terminated with header connectors and connected to their respective interfaces on the PCB. AC power from the IEC power connector was connected to the power supply using spade crimp connectors. Similarly, spade crimp connectors were used to interconnect the +24V power supply with the +5V power supply and the H-bridge sections of the board. The +5V and +24V wires were terminated on the PCB with their respective header connectors. As an additional safety measure, a 10A fuse was added in line with the 24V section of the wiring harness to prevent damage to the motor control in the event of a malfunction.

Finally, the pushbuttons were wired into the display/human interface header. These pushbuttons required a common ground and one signal line each, as pull-up resistors and buffers were already on the PCB. The image below shows the wiring bundles for the motor encoder inputs, motor power output, 24V and 5V power input, and pushbutton connection. It

also shows the USB cable connecting between the waterproof bulkhead USB connector and the PCB.

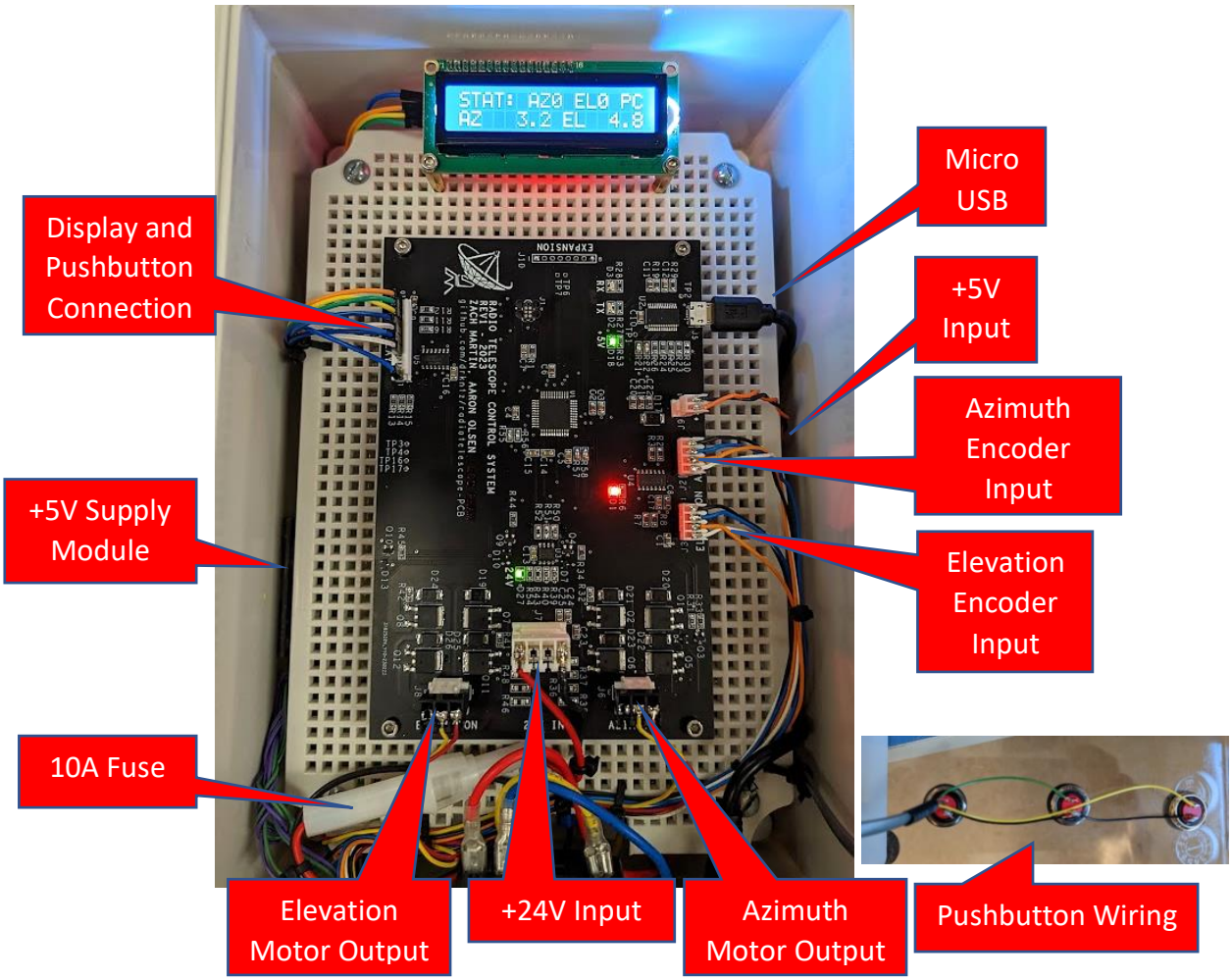

Figure 68: Complete control box assembly

3.1.3 Motor System and Antenna Assembly

To connect the motors to the control box, the unterminated wire from each motor had to be extended and terminated with an M12 plug. The wires were spliced to a suitable cable and protected with heat shrink insulation as shown in Figure 69.

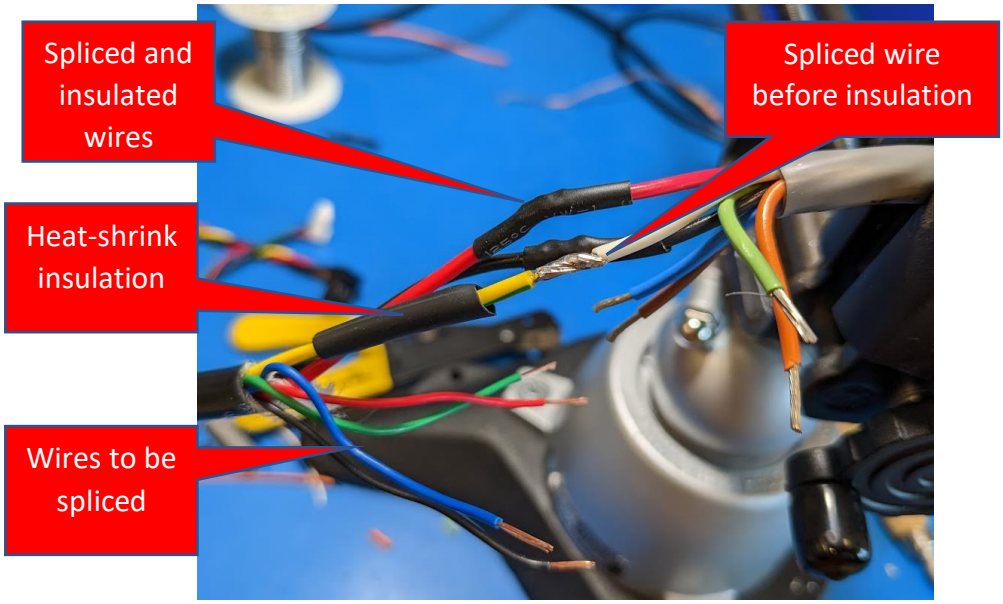

Figure 69: Motor Wire Splicing

When the splice was completed, the total splice shown below was covered with a large section of heat shrink tubing as shown in Figure 70.

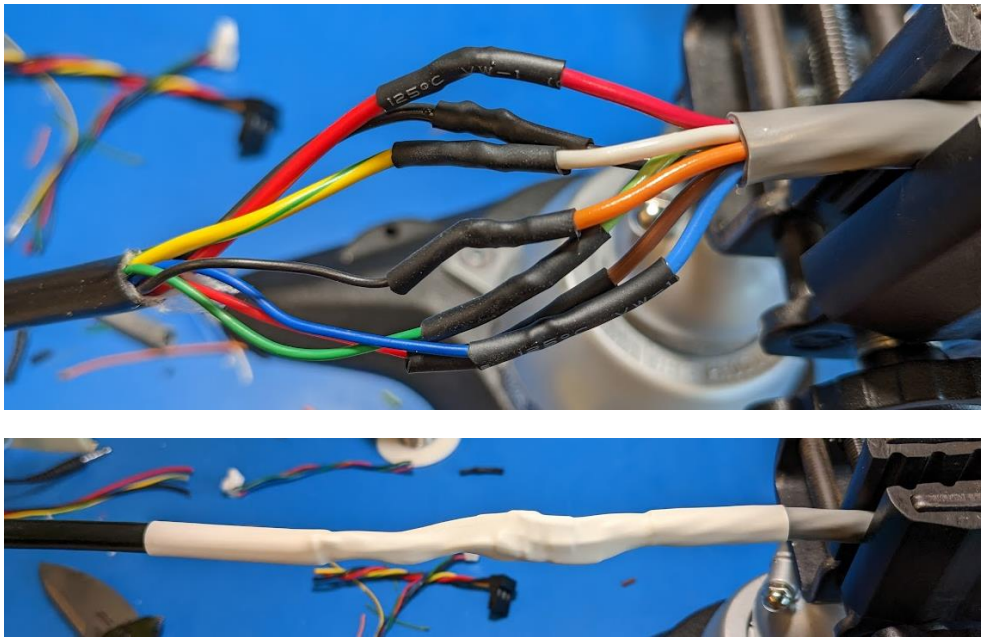

Figure 70: Completed motor wire splice (top) and heat shrink cover (bottom)

As the 3-meter dish was too large to test indoors, a smaller 1-meter dish antenna was attached to the gearing system. The antenna was connected to the top motor using an L-bracket that came with the antenna as shown in the figure below. New holes were made in the bracket to fit the required M10 bolts of the motor.

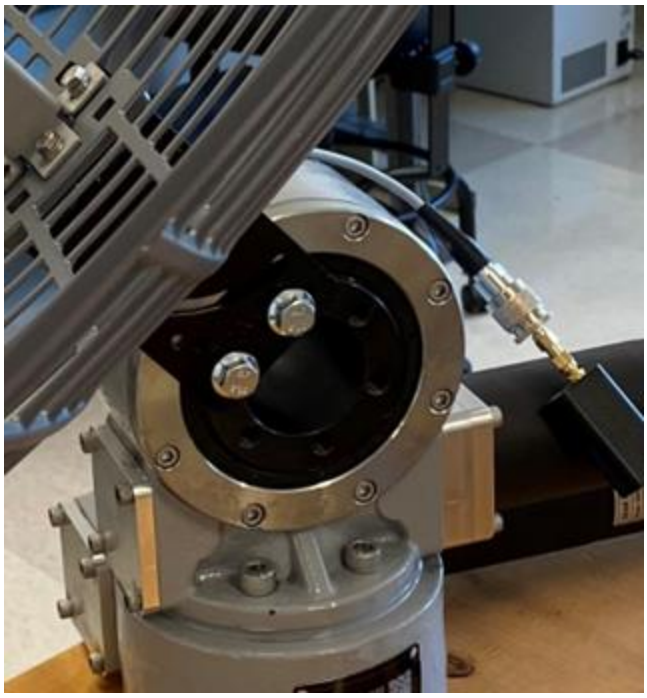

Figure 71: L-bracket for attaching antenna to motor.

To install the motor so that the azimuth axis rotation could be tested, a wooden platform was made to hold the whole system. As the motor is heavy, reinforcing L-brackets had to be added to make the platform sturdier.

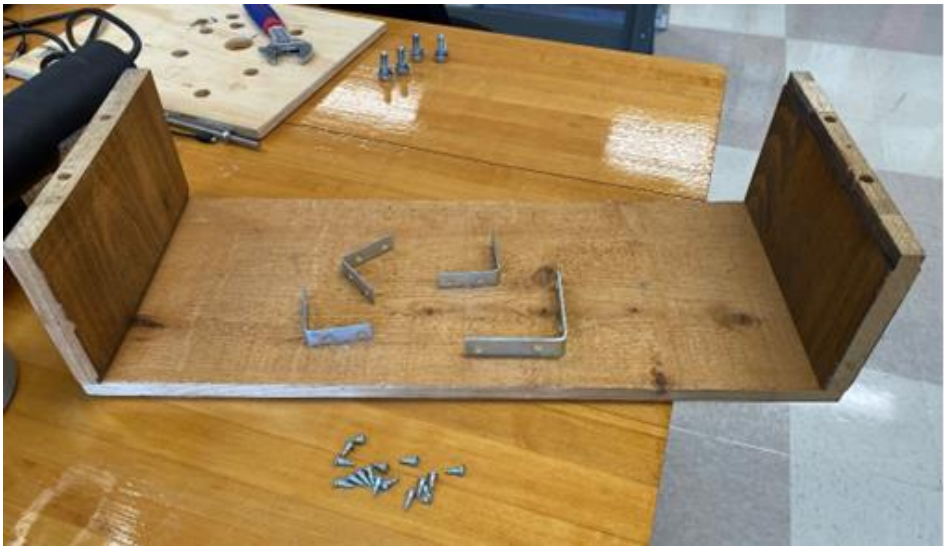

Figure 72: Components for the motor stand. The M10 bolts can be seen at the top.

When the motor and antenna were mounted to the platform, the control box was ready to connect to the motor. The entire system, including motor, the small antenna, control box, and wiring for going into and out of the control box, is shown below.

Figure 73: Final configuration of system

3.2 System Testing & Validation

The subsystems in this project were tested according to a test plan which followed the engineering requirements in the project report. The code used for the testing can be found in the diagnostic part of the code in the appendix. Test plan sheets that include the setup, inputs, outputs, and results for each test can also be found in the appendix.

3.2.1 Power Supply Test

To test the power supply, various loads were connected to ensure the 24V power supply could supply a current within its rated range (14.6A max) and maintain ripple and regulation within its specifications (150mVpp and <1%, respectively). The power supply was tested with a series of high-power resistors connected to the output and was monitored using an oscilloscope. The resistors that were connected were a 1-kOhm resistor and 2.5-Ohm power resistor.

With a very light load, the power supply output was very stable, as shown in the figure below.

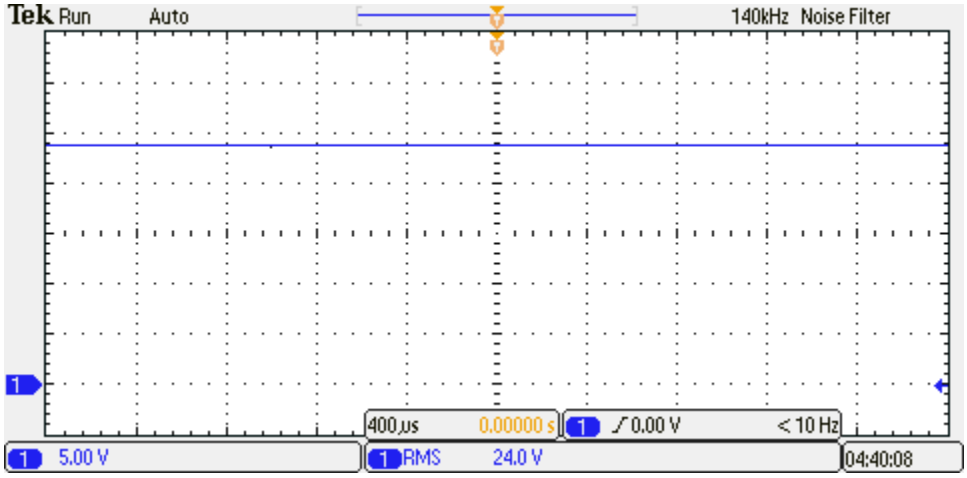

Figure 74: Mean-well power supply voltage under light load.

This power supply had a ripple voltage around 12.8mVpp as shown in the figure below.

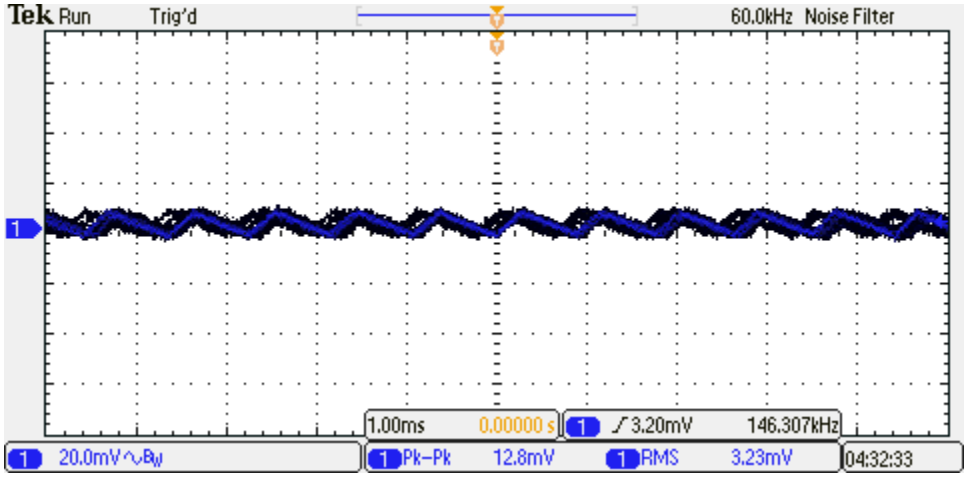

Figure 75: Mean-well power supply ripple voltage under light load.

Adding a 2.5-Ohm load to the output produced the following voltage measurement. The figure shows that the voltage has changed very little, well within the 1% regulation spec. The ripple

voltage is now a bit more noticeable, but very minimal, as shown in Figure 77. This ripple voltage is around 30mVpp, which is still well within the range given in the datasheet.

As the power supply ripple voltage was minimal and regulation was within 1%, regardless of the low load or 2.5-Ohm resistive load, it was determined that the power supply was satisfactory for the purpose of the project.

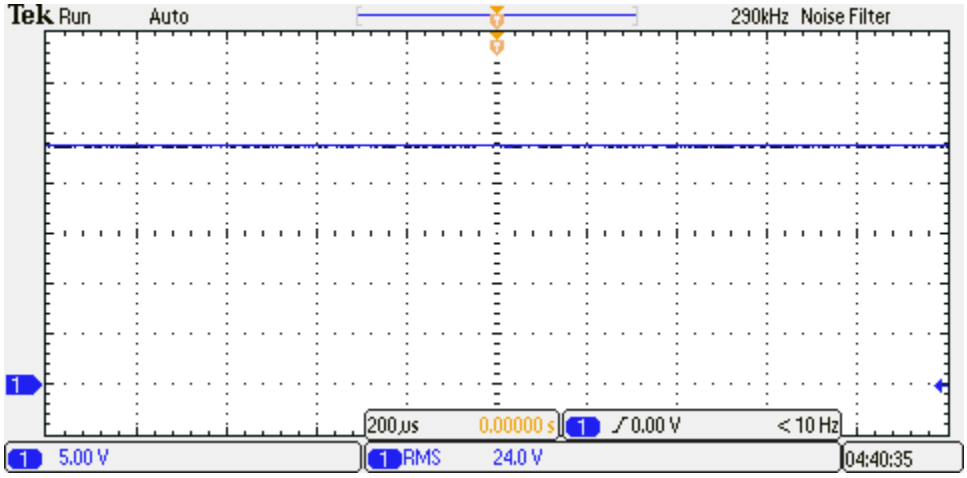

Figure 76: Mean-well power supply output under 2.5-Ohm load.

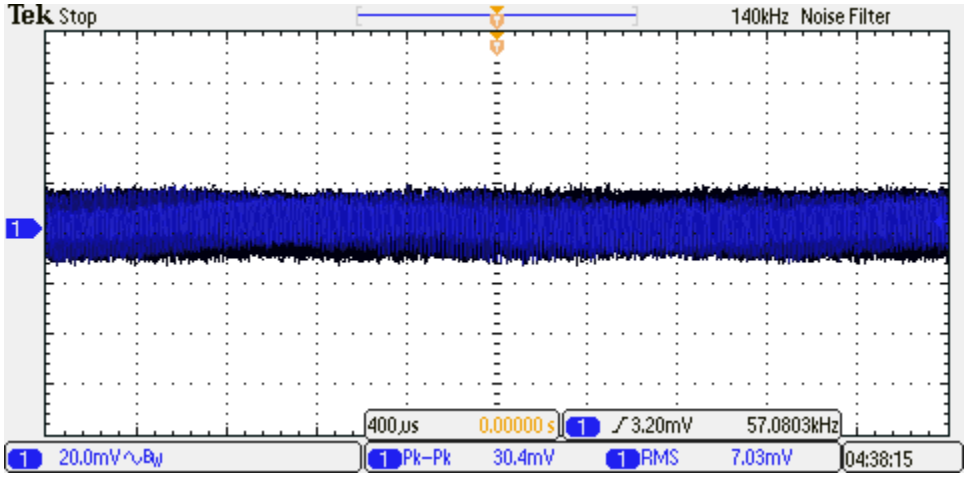

Figure 77: Ripple Voltage with 2.5-Ohm load.

3.2.2 Microcontroller Test

The heart of the system is the microcontroller. This microcontroller handles the communication between the computer and the control system, contains the control loop to drive the motors, measures and converts rotary encoder pulses into degrees, among other things. Therefore, the functionality of the microcontroller is crucial to the functionality of nearly every subsystem on the board.

The microcontroller test involved testing the solder connection, testing the programmability, UART and I2C peripherals, general-purpose input and outputs (GPIO), and analog to digital converter inputs (ADC). The surface-mount processor was installed on the custom PCB with R55-R58 omitted to isolate the H-bridge section. Only the +5V power limited with a constant-voltage, constant-current power supply was connected to the PCB. A simple diagnostic program was loaded onto the microcontroller to test the performance of the various peripherals on the microcontroller. UART terminals were established, and ADC readings were verified via the UART terminal printouts.

This test was designed to measure the current consumption of the microcontroller, the program/debug interface, GPIO lines can be pulled high/low and read, and the ADC tracks the input voltage within 10%.

The test setup for the microcontroller test is shown in the following image.

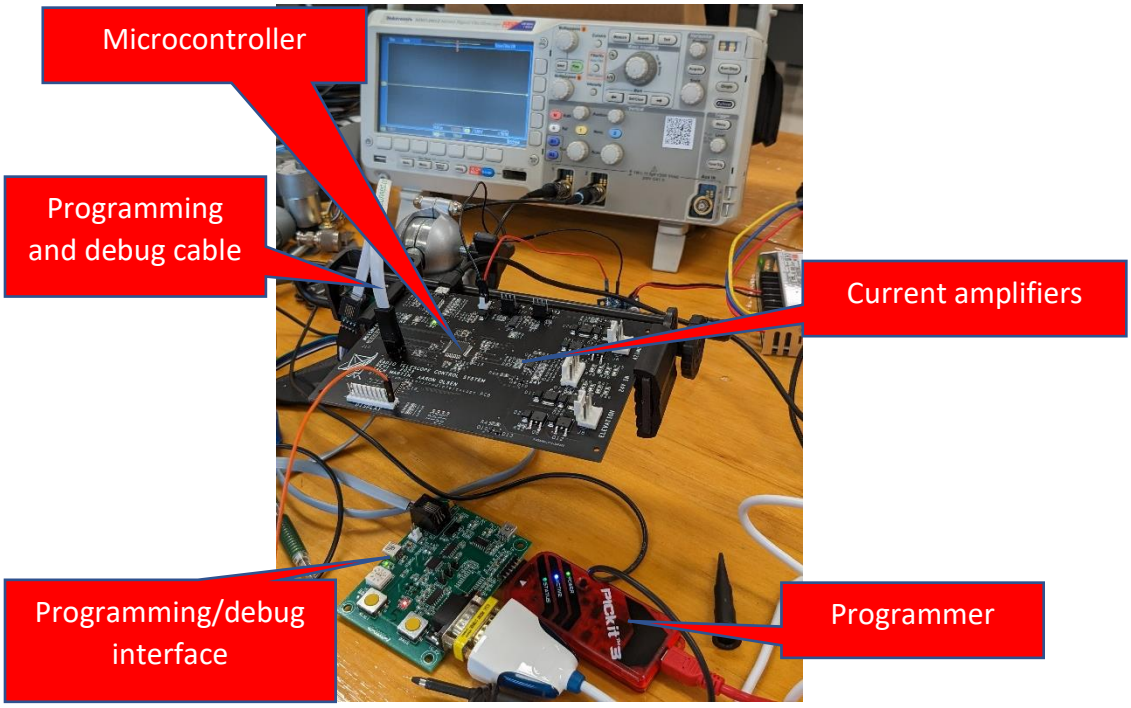

Figure 78: Microcontroller test setup

It was found that the nominal current consumption was 37mA. The debugger/programmer was able to program the PIC, with a modification in that the programming cable was pin-for-pin reversed. This was easily fixed by using a ribbon cable which reversed the pinout of the cable. Both UART peripherals were found to be working (debug and USB-UART bridge). Critical lines to the H-bridge were able to be pulled high and low. This is shown in the control interface in Figure 79. A 1 means the positive direction and a 2 means negative direction. All onboard and offboard status LEDs were functional. All inputs from the rotary encoders were able to be read from, with a slight modification in initial configuration due to the processor configuring the

azimuth encoder input as an oscillator input by default. Using the encoder values, the angles could be calculated as shown in Figure 79.

Figure 79: One example of the motors being on shown from the PC interface.

The ADCs were able to be read from with 8.6% conversion error. This may be due to noise that appeared on the ADC input, which could be remedied by adding a simple R-C low pass filter in hardware.

3.2.3 USB-UART Bridge Test

The USB-UART bridge performs the function of converting a UART communication from the microprocessor to a USB signal via a virtual COM port on the host computer. This bridge was tested with a host computer running a terminal application simply by connecting the UART TX and RX pins together on the PCB and observing whether the characters sent were reflected onto the terminal.

R21 and R22 were removed from the board, as these are series resistors that connect the TX and RX lines of the USB-UART bridge to the TX and RX lines of the microprocessor. The TX and RX pins on the USB-UART IC were then shorted together, so that the characters sent over the USB were reflected back to the terminal. The terminal on the computer sent and received the ASCII characters correctly. The RX and TX LEDs on the PCB blink during transmission. These were visually inspected while running characters across the TX and RX lines, but the LEDs are swapped. The silk screen just needs to be changed in a future revision.

3.2.4 Test LCD and Human Interface

To test the 16x2 character LCD, it was connected to an Arduino Uno and tested using a library "LiquidCrystal" designed for driving 16x2 alphanumeric LCDs over an I2C interface. The words "Radio Telescope Control System" were printed to the LCD using the appropriate commands which it did display successfully. The words cannot exceed 16 characters in the print command, or it will not display completely on the LCD. In other words, it does not increment to the next row of the LCD automatically. The new row must be selected first and another 16 characters can be printed.

The Arduino C++ library was then rewritten in C for use with the Microchip XC16 C compiler that is used for this project. This library was then tested on the custom PCB by connecting to the LCD via the display header and running a test function. With these commands, the same

message was displayed on the LCD. Each character position on the LCD could be written to successfully. This provides the user with information when operating at the location of the device. Buttons were also successfully used by checking the state of the pins to make sure they update appropriately from the code. The external status LED could also be toggled.

Figure 80: Display test result

3.2.5 Full System Test

The full system test aimed to test the fully integrated system described earlier. Code was written to receive commands from the main PC, diagnostic port, and local control interface to operate the motors. This also included displaying information to the main PC and LCD to provide the user with the current antenna altitude and azimuth angles, source of the given command, and current motor directions. The LCD allows the user at the device to know what the motor is doing and the display on the command allows the user that isn't at the device to know as well. The diagnostics will be operated at the device, so the LCD and the diagnostic screen can provide the user with information.

Tests were done for the following main PC commands: CMD_STOP, CMD_ALT_POS, CMD_ALT_NEG, CMD_ALT_STOP, CMD_ALT_RESET, CMD_AZ_POS, CMD_AZ_NEG, CMD_AZ_STOP, and CMD_AZ_RESET. These commands, shown in Figure 81, are required for choosing the two motors' directions, setting the reference (zero) point, and having an emergency stop. All commands operated successfully and provided bidirectional movement to both motors as per the design requirements. CMD_STOP is the emergency stop that stops both motors instantly. CMD_ALT_POS and CMD_AZ_POS tell the altitude and azimuth motors to rotate up and clockwise, respectively. CMD_ALT_NEG and CMD_AZ_NEG tell the altitude and azimuth motors to rotate down and counterclockwise, respectively. To stop just one of the motors, CMD_ALT_STOP or CMD_AZ_STOP are used. And to set the new position to the zero point, CMD_ALT_RESET and CMD_AZ_RESET are used.

```
Menu Options:
1 - Altitude +
2 - Altitude -
3 - Altitude Stop

4 - Azimuth +
5 - Azimuth -
6 - Azimuth Stop

7 - Enter degrees

A - Advanced Menu
Spacebar - stop all motors
=============================================
 Direction    |      Angle     |  Command
 Alt    Az    |   Alt    Az    |  Source
  0     0     |   0.0    0.0   |  PC
```

Figure 81: PC interface for the system test

The buttons and LCD were tested in the local control to control the motors and display the degree angles. Menus include the menu during PC control, elevation local control, azimuth local control, zero-out degrees menu, and the quit menu. These menus are shown in the below figures except the azimuth control. The menu is the same as the elevation menu. The elevation and azimuth menus allow movement of the motors using the buttons, the zero-out menu will reset the motors to zero, and the quit menu allows the control to go back to the PC. The degree locations are always on display.

Figure 82: Local control menu when PC control is active.

Figure 83: The first menu for local control. This is elevation control.

Figure 84: The zero-out degree menu for local control.

Figure 85: The quit menu in the local control to allow PC commands again.

Finally, a video is linked below to show the motor moving in a time lapse.

https://www.youtube.com/watch?v=-fnis7qi-ZQ

4 Project Management

4.1 Project Work Breakdown

The work breakdown structure can be seen in Figure 86. This diagram provides a graphical view of the deliverables in this project with the lead of each task. The first letter of the task leader's last name is used to conserve space in the diagram: Martin (M), and Olsen (O). The research and proposal stage provides the necessary background information and requirements and standards for the project moving forward as well as the target plan for the rest of the project. Using this research, the design stage moves to creating the schematic, simulating each section of the project design, and selecting the necessary parts based on the design. This stage also provides the PCB layout for the prototype and the basis of the firmware and computer interface used in the to-be-assembled system.

The next step is integrating the system by ordering the parts, soldering the components onto the PCB, and connecting all external modules. Upon completion of the integration, the system is moved to the testing stage where each subsystem will be tested separately for desired performance. Then, the system is tested as a whole and any problems in overall operation are debugged, and changes made in the code. Finally, the final report and presentation provides an overview of the finalized product.

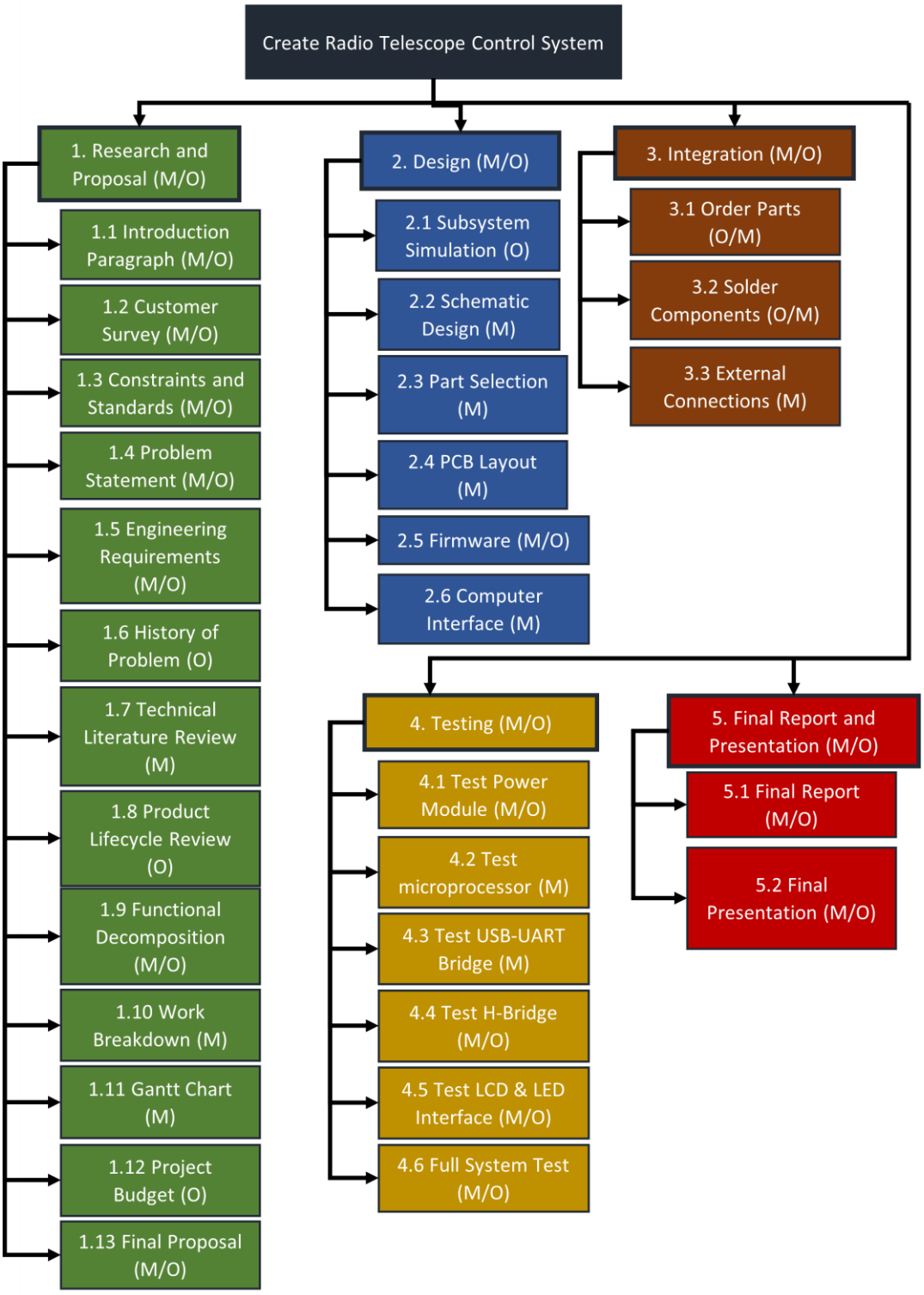

Figure 86: Work Breakdown Structure Diagram

4.2 Project Schedule

The project began in the fall semester of 2022 with the research and proposal phase and concluded in the spring of 2023 with the design, integration, and testing phases. The five main tasks include Research and Proposal, Circuit Design, Firmware Design, Integration, and Testing.

The research and proposal stages were completed by the end of the Fall 2022 semester to provide supporting information for the rest of the project. The design and integration of the project was completed throughout the spring 2023 semester, beginning with the PCB layout and completing with final touches in system configuration and program code. During the integration stage, each system was tested thoroughly to ensure the device was complying with expectations. At the end of the testing phase, the completed documentation was submitted and a presentation of the project given. The following chart shows an overview of the project schedule.

Development Stage	Research & Proposal	Circuit Design	Firmware Design	System Integration	Testing
Start Date	September 1	November 1	February 15	February 6	February 15
End Date	December 8	February 20	April 20	April 20	April 14

Figure 87: Project Schedule

In order to keep on track, the project schedule above was broken down into smaller tasks which were used to populate a Gantt chart as shown in Figure 88. This helped the team to visualize the project tasks and allocate time accordingly. Additionally, this chart was designed with tasks assigned to either or both of the project team members so that it was clear who was responsible for which task and when the task needed to be completed.

Project Lead: Zach Martin
Start Date: 9/12/2022 Monday

First Day of Week (Mon=2): 2

Tasks	Task Lead	Start	End	Duration (Days)	% Complete	Working Days	Days Complete	Days Remaining
Research and Proposal	Martin, Olsen	9/12/22	12/8/22	88	100%	64	88	0
Introduction Paragraph	Martin, Olsen	9/12/22	9/18/22	7	100%	5	7	0
Customer Survey	Martin, Olsen	9/15/22	10/6/22	22	100%	16	22	0
Constraints and Standards	Martin, Olsen	9/22/22	10/6/22	15	100%	11	15	0
Problem Statement	Martin, Olsen	9/29/22	10/17/22	19	100%	13	19	0
Engineering Requirements	Martin, Olsen	10/13/22	10/22/22	10	100%	7	10	0
History of Problem	Olsen	10/20/22	12/6/22	48	100%	34	48	0
Technical Literature Review	Martin	10/20/22	12/6/22	48	100%	34	48	0
Product Lifecycle Review	Olsen	10/27/22	12/4/22	39	100%	27	39	0
Functional Decomposition	Martin, Olsen	11/3/22	11/14/22	12	100%	8	12	0
Work Breakdown	Martin	11/10/22	12/5/22	26	100%	18	26	0
Gantt Chart	Martin	11/17/22	12/5/22	19	100%	13	19	0
Project Budget	Olsen	11/17/22	12/6/22	20	100%	14	20	0
Final Proposal	Martin, Olsen	9/12/22	12/8/22	88	100%	64	88	0
Design	Martin, Olsen	11/23/22	2/25/23	95	100%	68	95	0
Subsystem Simulation	Olsen	11/23/22	1/21/23	60	100%	43	60	0
Schematic Design	Martin	11/23/22	1/21/23	60	100%	43	60	0
Part Selection	Martin	11/23/22	1/21/23	60	100%	43	60	0
PCB Layout	Martin	1/21/23	2/11/23	22	100%	15	22	0
Firmware	Martin, Olsen	1/21/23	2/25/23	36	100%	25	36	0
Computer Interface	Martin,Olsen	1/21/23	2/25/23	36	100%	25	36	0
Integration	Maritn, Olsen	1/21/23	2/25/23	36	100%	25	36	0
Order Parts	Olsen	1/21/23	2/11/23	22	100%	15	22	0
Solder Components	Olsen, Martin	2/18/23	2/25/23	8	100%	5	8	0
External Connections	Martin	2/18/23	2/25/23	8	100%	5	8	0
Testing	Martin, Olsen	2/25/23	3/18/23	22	100%	15	22	0
Test Power Module	Martin, Olsen	2/25/23	3/11/23	15	100%	10	15	0
Test Microprocessor	Martin	2/25/23	3/11/23	15	100%	10	15	0
Test USB-UART Bridge	Martin	2/25/23	3/11/23	15	100%	10	15	0
Test H-Bridge	Martin, Olsen	2/25/23	3/11/23	15	100%	10	15	0
Test LCD and LED Interface	Martin, Olsen	2/25/23	3/11/23	15	100%	10	15	0
Full System Test	Martin, Olsen	3/11/23	3/18/23	8	100%	5	8	0
Final Report and Presentation	Martin, Olsen	1/9/23	4/15/23	97	100%	70	97	0
Final Report	Martin, Olsen	1/9/23	4/15/23	97	100%	70	97	0
Final Presentation	Martin, Olsen	1/9/23	4/15/23	97	100%	70	97	0

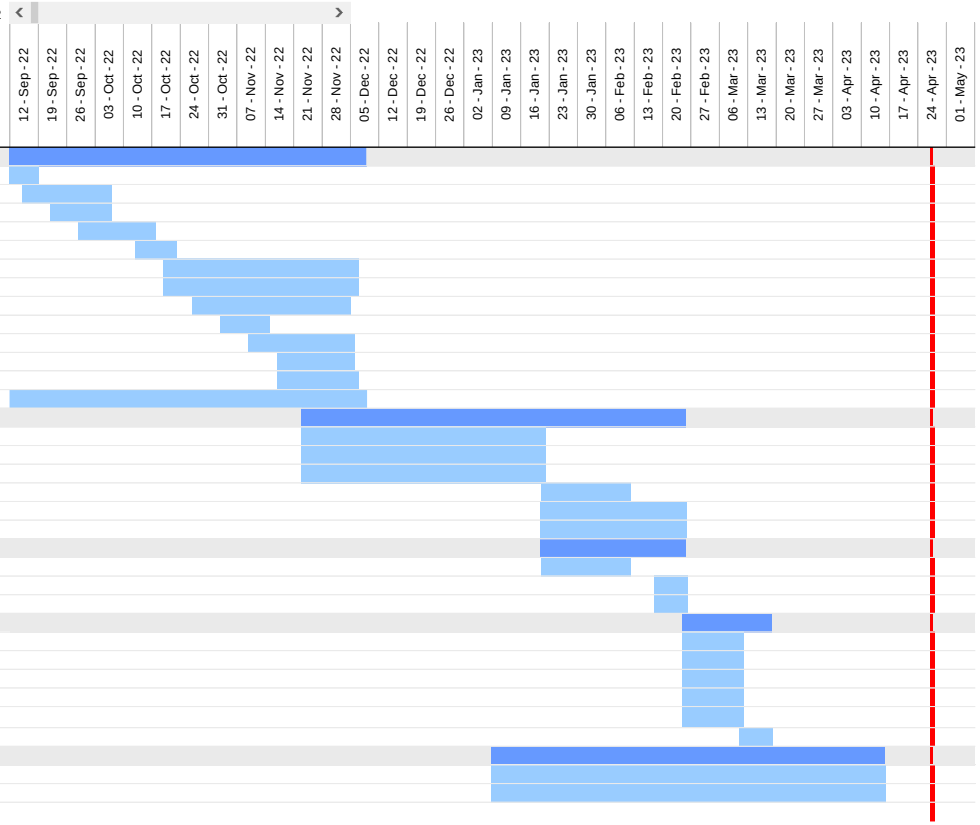

Figure 88: Project Gantt Chart

4.3 Project Budget

This document contains the project budget breakdown in Table 22. To estimate the cost of the project, several assumptions were made. The first assumption was that of the rate and hours of engineering labor. The engineering labor rate was chosen to be $30/hr, which is chosen as a rate midway between an internship pay grade ($25) and a starting engineering pay grade ($35). Of course, these estimates can vary depending on the industry and the individual. The hours worked per person was around 15 hours per week with more work happening in the second semester compared to the first. The time was distributed according to the Design, Integration, and Testing Gantt chart categories.

For the parts category of the cost analysis, there are a few things to note. First, some of the components that will be placed on the custom PCB will be sourced from personal, school, and employer contributions, so their pocket cost may be lower than the estimate. Secondly, the high-ticket item (2-Axis slewing drive) was purchased through school funding. This is because the proposed control system is intended to serve as a contribution to the overall club project and will remain in the ownership of the IEEE club as this part of the project is completed. Overall, the out-of-pocket cost was several hundred dollars for components and development tools. This cost will be split between the members of the capstone design team.

Table 22: Project Budget

Item Description			Cost
Components, Power Supply, Etc.			$ 413.37
Dual Axis Motor			$ 499.00
Dual Axis Motor Shipping			$ 432.00
Griddy Antenna			$ 179.00
Subtotal			$ 1,110.00
Labor Cost	Cost ($/hr)	Hours	
Design	30	400	$ 12,000.00
Integration	30	150	$ 4,500.00
Testing	30	100	$ 3,000.00
Total Cost			$ 20,610.00

5 Summary and Conclusion

The system designed and implemented in the pages of this document delivered a robust and expandable control system for accurate pointing of a small dish antenna for use in university radio astronomy projects. The device documented herein is at a scale and price that is much more accessible to students, researchers, and amateur astronomers. Interfacing with this device is simple for a multitude of users from many backgrounds, and can be done with simple pushbutton control, a terminal interface, or via a custom radio astronomy software program.

This system, combined with the installation of the 3-meter dish antenna and low-noise receiver, provides a method of mapping intensity of radio sources such as Hydrogen-line radiation across the sky. Its operation over a wired USB link simplifies the connectivity requirements and makes the computing requirement generic to any computer capable of running the application software. While the speed requirement was not met, the system has ample speed to provide desired results in an extended time. The final cost of the system was reduced in comparison to commercial products, and it is now easily interfaced with for the future designers and users.

5.1 Lessons Learned

One of the most important lessons learned in this project was how to coordinate within the team and with the IEEE and astronomy clubs with the project. This will be an important skill for the team members to have in the future when working on a multidisciplinary project. For the H-bridge circuit and similar applications, the transistors should be driven appropriately to have the same current passing through them. Also, future projects and iterations of this project should include hardware interlocks that protect the circuit from certain conditions. The H-bridge should be incapable of having two branches on at the same time using hardware, so any software errors do not short the 24V supply. Finally, the pinouts should be double checked before ordering the PCB to ensure that they are correct, as the programming connector had a reversed pinout.

5.2 Future Work

Since this prototype is just the beginning of the project, the other parts of the complete system need to be finished and integrated with this design. This includes the RF and programming sides of the project. Also, some revisions need to be made to the PCB for the errors discussed in this report. Some special considerations had to be made when interacting with the board in the current revision. Limit switches need to be added so the antenna does not continue rotating into an object or to any point that is undesirable. Finally, the project needs a permanent home and a new dish that is chosen for the RF side of the project.

6 References

[1] C. M. Jansky, "The Discovery and Identification by Karl Guthe Jansky of Electromagnetic Radiation of Extraterrestrial Origin in the Radio Spectrum," *Proceedings of the IRE,* pp. 13-15, 1958.

[2] K. G. Jansky, "Directional Studies of Atmospherics at High Frequencies," *Proceedings of the Institute of Radio Engineers,* vol. 20, no. 12, pp. 1920-1932, 1932.

[3] G. Reber, "A Play Entitled the Beginning of Radio Astronomy," *The Journal of the Royal Astronomical Society of Canada,* vol. 82, no. 3, pp. 93-106, 1988.

[4] K. G. Jansky, "Electrical Disturbances Apparently of Extraterrestrial Origin," *Proceedings of the Institute of Radio Engineers,* vol. 21, no. 10, pp. 1387-1398, 1933.

[5] G. Reber, "Early Radio Astronomy at Wheaton, Illinois," *Proceedings of the IRE,* vol. 46, no. 1, pp. 15-23, 1958.

[6] T. H. Legg, "A proposed new design for a large radio telescope," *Astronomy & Astrophysics Supplement Series,* pp. 369-379, 1998.

[7] G. Reber, "Radio Astronomy," *Scientific American,* vol. 181, no. 3, pp. 34-41, 1949.

[8] D. Johnson and A. Rogers, "Development of a New Generation Small Radio Telescope," Haystack Observatory, 2012.

[9] A. Farris, R. Marson and J. Kern, "The ALMA Telescope Control System," in *Int. Conf. on Accelerator & Large Expt. Physics Control Systems, Geneva*, Socorro, 2005.

[10] V. S. Netchitailo, "Center of Milky Way Galaxy," *Journal of High Energy Physics, Gravitation and Cosmology,* pp. 657-676, 2022.

[11] S. Joardar and J. Claycomb, Radio Astronomy, Mercury Learning & Information, 2015.

[12] T. Ranka, "Simulations of GMRT Servo-Mechanical System," National Centre For Radio Astrophysics - Tata Institute of Fundamental Research, 2009.

[13] S. Bagde, S. Sabhapathy, B. C. Joshi, A. Kumar and B. Thiyagarajan, "GMRT Servo System: Motivations and challenges for the upgrades," in *URSI AP-RASC*, New Delhi, 2019.

[14] National Centre for Radio Astrophysics, "Servo System for GMRT Antennas," [Online]. Available: http://www.ncra.tifr.res.in/ncra/gmrt/sub-systems/servo-system-for-gmrt-antennas. [Accessed 4 April 2023].

[15] P. Bhalerao, S. Dahake and R. Labade, "Design of DC Servo Motor Control For GMRT FPS at Prime Focus of 45m Dish Antenna," *Journal of Computing Technologies,* 2012.

[16] J. Tatum, Celestial Mechanics, Victoria: Libre Texts, 2020.

[17] Z. Z. Abidin, F. Ramadhani, J. C. Algaba, N. M. Shah, M. Dahari and W. Z. A. W. Mokhtar, "Control system performance of a 7.3-meter radio telescope converted from telecommunication antenna to radio astronomy purposes in Malaysia," *J. Astron. Telesc. Instrum. Syst.,* no. 8(3) 037001, 2022.

[18] F. I., "Sharjah Five-Meter Radio Telescope," *Journal of Instrumentation,* vol. 15, no. P01033, 2020.

[19] AstroShop, "Advanced Radio Telescope Spider 500A with Waterproof Mount," [Online]. Available: https://www.astroshop.eu/telescopes/radio2space-advanced-radio-telescope-spider-500a-with-waterproof-mount/p,54711. [Accessed 11 November 2022].

[20] Green Bank Observatory, "National Radio Quiet Zone," 12 February 2021. [Online]. Available: https://greenbankobservatory.org/about/national-radio-quiet-zone/. [Accessed 4 April 2023].

[21] National Radio Astronomy Observatory, "Very Large Array," [Online]. Available: https://public.nrao.edu/telescopes/vla/. [Accessed 4 April 2023].

[22] I. Glass, "The Square Kilometre Array radio telescope: A media darling," *South African Journal of Science,* vol. 114, no. 9/10, 2018.

[23] S. S. Sami, Z. A. Obaid, M. T. Muhssin and A. H. Hussain, "Detailed modelling and simulation of different DC motor types for research and educational purposes," *International Journal of Power Electronics and Drive Systems,* p. 703~714, 2021.

[24] G. C. Bower, "Focus on First Sgr A* Results from the Event Horizon Telescope," *The Astrophysical Journal Letters,* 2022.

[25] Camera Concepts & Telescope Solutions, "The Itty Bitty Radio Telescope Kit," [Online]. Available: https://camera-concepts.shoplightspeed.com/radio-astronomy-the-itty-bitty-radio-telescope-kit.html. [Accessed 12 November 2022].

Appendix A: Customer Survey

Radio Telescope Capstone Survey

This project is a contribution to a small-scale radio telescope project.

A radio telescope is used in a similar way to a traditional optical telescope to view objects in space. It measures the location of objects in space by the intensity of the radio frequency signals generated at that position. Intensity measurements are then plotted onto a 2-D image such as the ones in the image below.

* Required

Example Images from Various Sizes and Types of Radio-Telescopes

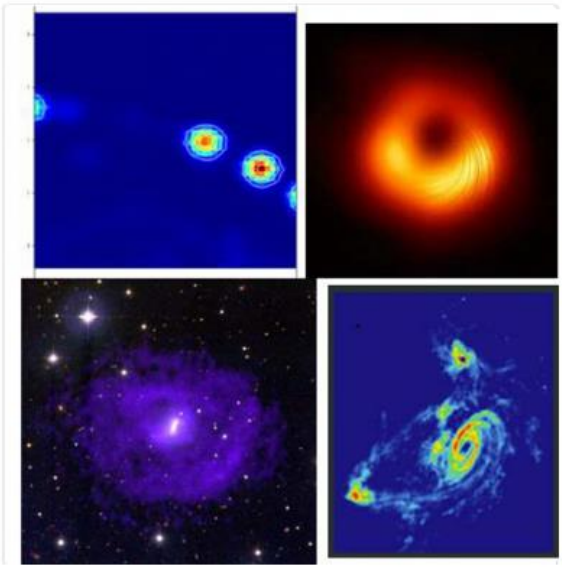

There are many things that can be measured with radio astronomy. One most likely to produce results is the "Hydrogen Line," a spectral line at 1.42 GHz that can be used to map Hydrogen content in the universe. Other materials could be mapped similarly, as shown in the example table below.

Please rank the options for measurement below by your level of interest in their measurement.*

Measurement Subject	Frequency
Pulsars -- rotating neutron stars	Various
Deuterium (DI)	327.3840 MH
Hydrogen (HI)	1420.406 MH
Methyladyne (CH)	3263.794 – 33
Formaldehyde (H2CO)	4829.660 MH
Methanol (CH2OH)	6668.518 MH
Ionized Helium Isotope (3HeII)	8665.650 MH
Cyclopropenylidene (C3H2)	18.343 GHz

Hydrogen

Pulsars

Deuterium

Hydroxyl radical

Methyladyne

Formaldehyde

Methanol

Helium Isotope

Cyclopropenylidene

How would you like to power this device? *

- Portable (12 Volt Battery) (More portable)
- 120 Volt AC Utility power (More stationary)

Please rank the following features by priority. *

Small Size/Portability
Speed: capture images within several minutes
Plot Size: Larger picture, longer capture time
Low Cost: May sacrifice resolution and sensitivity
Accuracy: slower speed, longer capture time

How quickly would you like a result? *

- < 5 minutes
- 5 - 10 minutes
- greater than 10 minutes

What is a reasonable price for a small scale radio telescope? *

- $1,000-$2,000
- $2,000-$5,000
- $5,000-$10,000
- Other

How accurate should the rotational system be in degrees?

- <0.2 degrees
- 0.2 to 0.5 degrees
- 0.5 to 1 degree

The device will scan automatically to capture a section of the sky. Should there be a way to control it locally for individual user measurements and adjustments?

- Yes
- No

How would you use a radio telescope? *

University research

Student research

Personal interest/hobby

Additional comments or feature requests:

Appendix B: Engineering Requirements Development

Radio Telescope Capstone Survey

18	05:33	Active
Responses	Average time to complete	Status

1. Example Images from Various Sizes and Types of Radio-Telescopes

2. There are many things that can be measured with radio astronomy. One most likely to produce results is the "Hydrogen Line," a spectral line at 1.42 GHz that can be used to map Hydrogen content in the universe. Other materials could be mapped similarly, as shown in the example table below.

   Please rank the options for measurement below by your level of interest in their measurement.

Rank	Options
1	Hydrogen
2	Deuterium
3	Pulsars
4	Methyladyne
5	Methanol
6	Hydroxyl radical
7	Helium Isotope
8	Formaldehyde
9	Cyclopropenylidene

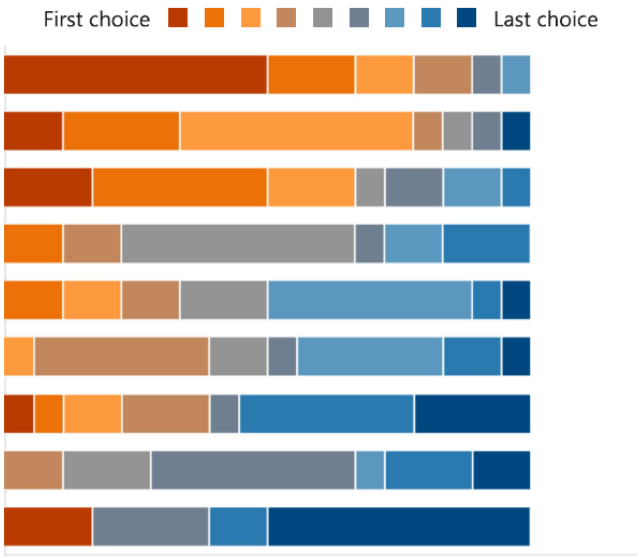

3. How would you like to power this device?

Portable (12 Volt Battery) (More ...	9
120 Volt AC Utility power (More ...	9

4. Please rank the following features by priority.

Rank	Options
1	Accuracy: slower speed, longer ...
2	Speed: capture images within se...
3	Plot Size: Larger picture, longer ...
4	Small Size/Portability
5	Low Cost: May sacrifice resoluti...

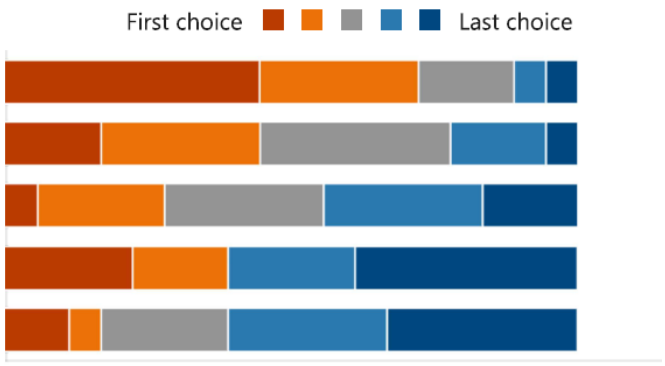

5. How quickly would you like a result?

< 5 minutes	8
5 - 10 minutes	8
greater than 10 minutes	2

6. What is a reasonable price for a small scale radio telescope?

$1,000-$2,000	6
$2,000-$5,000	7
$5,000-$10,000	2
Other	3

7. How accurate should the rotational system be in degrees?

<0.2 degrees	5
0.2 to 0.5 degrees	11
0.5 to 1 degree	2

8. The device will scan automatically to capture a section of the sky. Should there be a way to control it locally for individual user measurements and adjustments?

Yes	16
No	2

9. How would you use a radio telescope?

University research	5
Student research	4
Personal interest/hobby	9

10. Additional comments or feature requests:

6
Responses

Latest Responses

"Not at this time."

" 100M-3G capability for more information reception"

2 respondents (**33**%) answered **pictures** for this question.

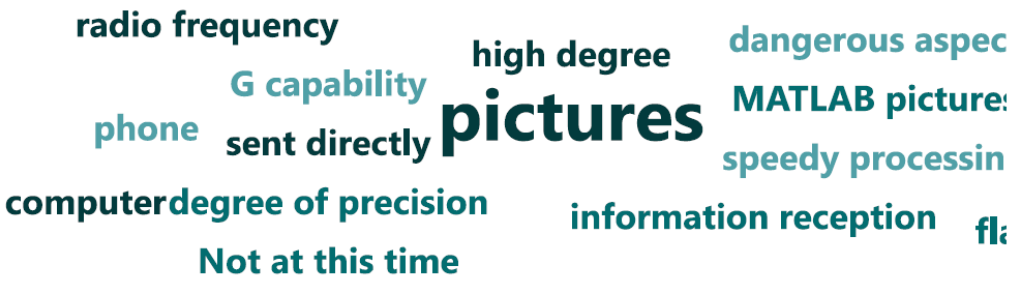

Appendix C: Final Schematics, Layout, and Parts List

This section contains the information necessary to replicate the custom control board circuitry. The information following and the OrCAD configuration files can be downloaded from the following link: https://github.com/drkntz/radiotelescope-PCB

Schematics

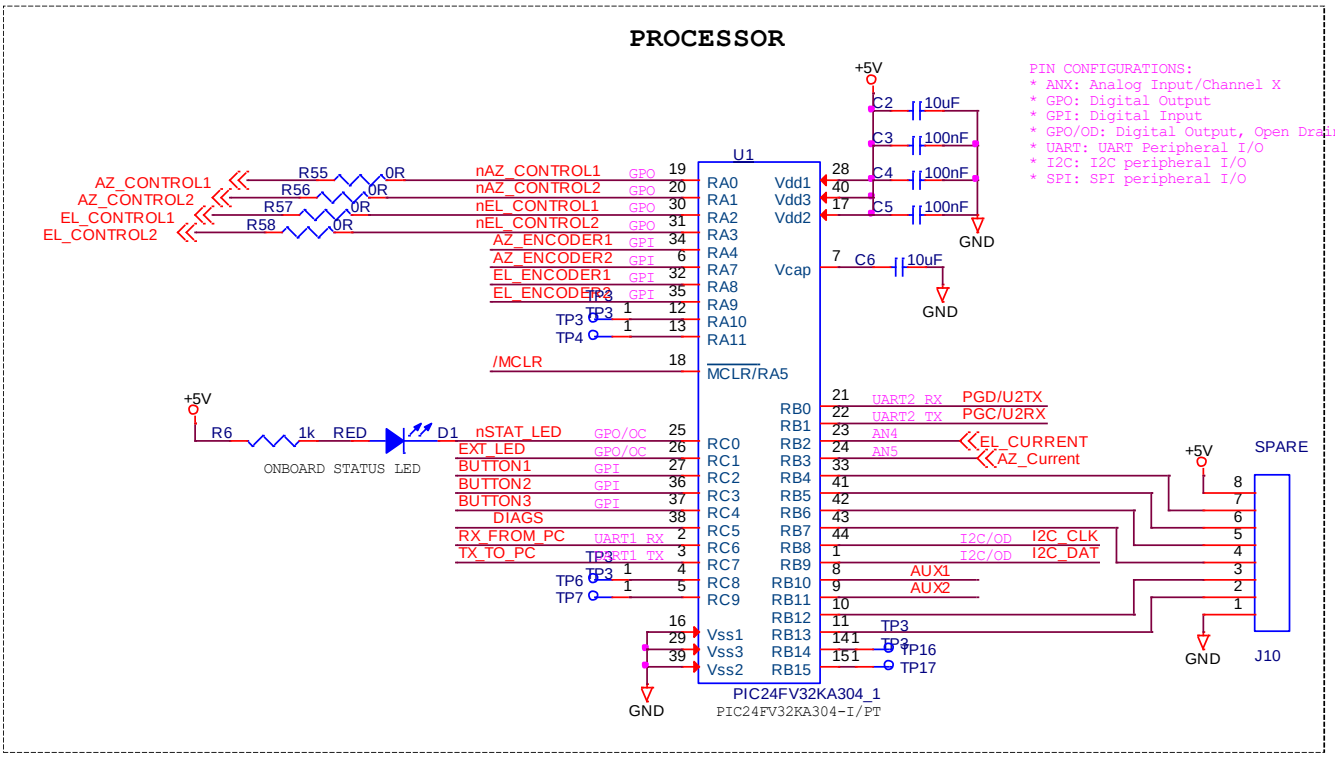

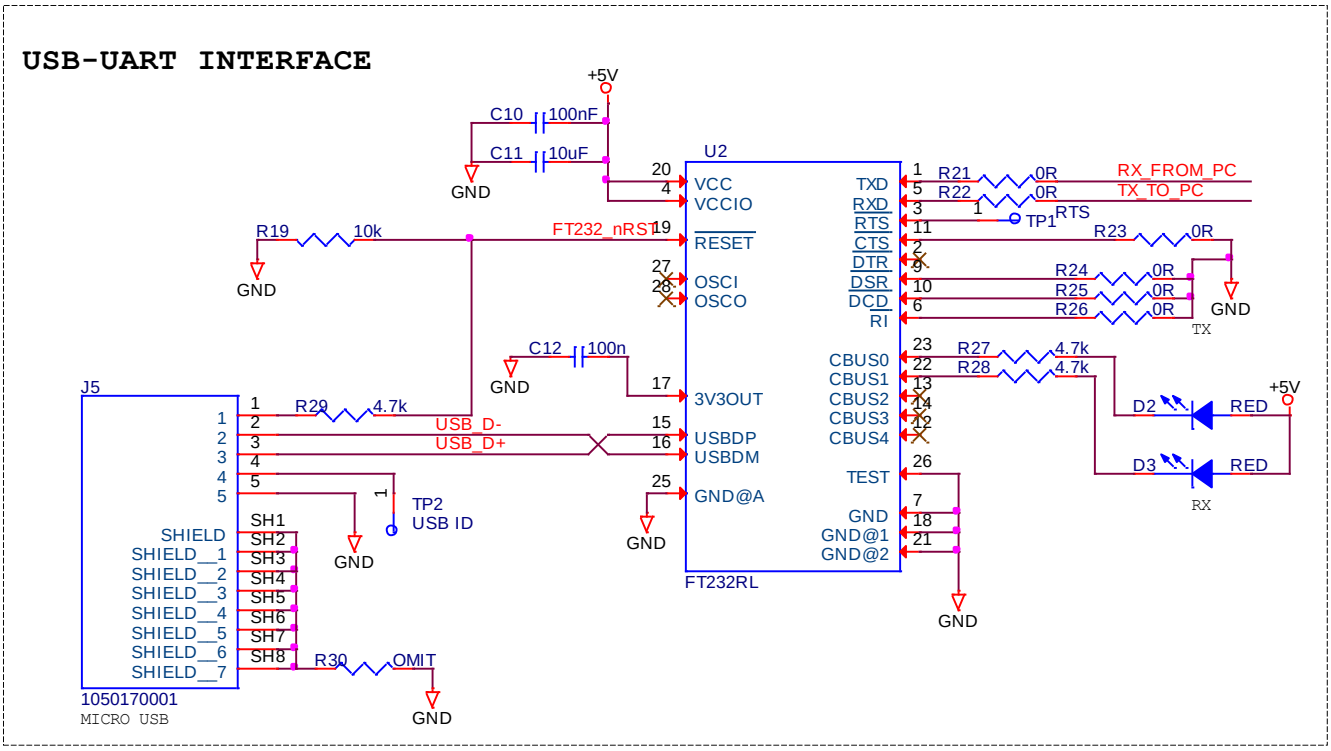
USB-UART INTERFACE
+5V
C10 100nF
C11 10uF
GND
U2
VCC
VCCIO
RESET
OSCI
OSCO
3V3OUT
USBDP
USBDM
GND@A
TXD
RXD
RTS
CTS
DTR
DSR
DCD
RI
CBUS0
CBUS1
CBUS2
CBUS3
CBUS4
TEST
GND
GND@1
GND@2
FT232RL
R19 10k
FT232_nRST
R21 0R
R22 0R
RX_FROM_PC
TX_TO_PC
TP1
RTS
R23 0R
R24 0R
R25 0R
R26 0R
TX
C12 100n
R27 4.7k
R28 4.7k
D2 RED
D3 RED
RX
J5
R29 4.7k
USB_D-
USB_D+
TP2
USB ID
SHIELD
SHIELD__1
SHIELD__2
SHIELD__3
SHIELD__4
SHIELD__5
SHIELD__6
SHIELD__7
R30 OMIT
1050170001
MICRO USB

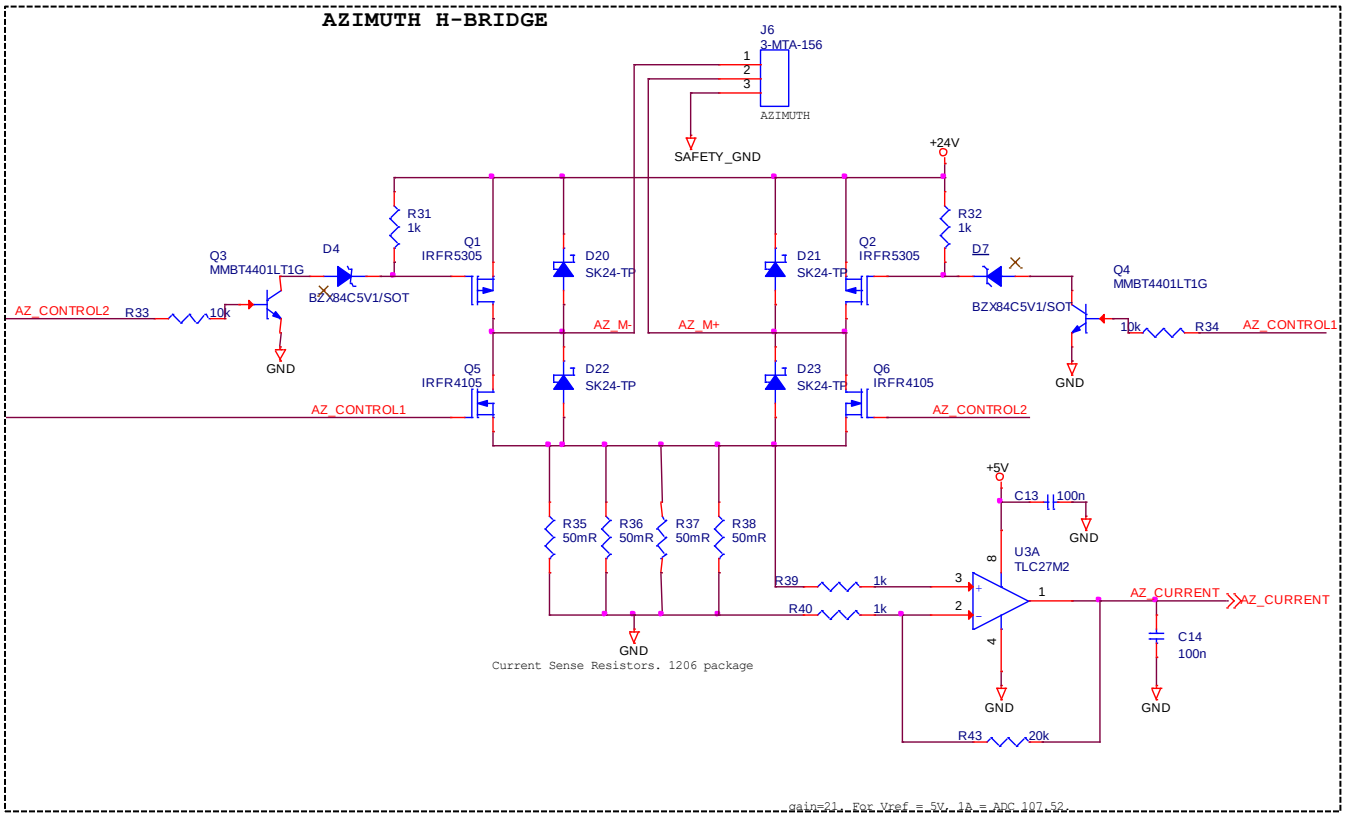
AZIMUTH H-BRIDGE
J6
3-MTA-156
AZIMUTH
SAFETY_GND
+24V
R31 1k
R32 1k
Q1 IRFR5305
Q2 IRFR5305
Q3 MMBT4401LT1G
Q4 MMBT4401LT1G
D4 BZX84C5V1/SOT
D7 BZX84C5V1/SOT
D20 SK24-TP
D21 SK24-TP
D22 SK24-TP
D23 SK24-TP
AZ_CONTROL2
R33 10k
AZ_M-
AZ_M+
R34 10k
AZ_CONTROL1
Q5 IRFR4105
Q6 IRFR4105
R35 50mR
R36 50mR
R37 50mR
R38 50mR
Current Sense Resistors. 1206 package
C13 100n
U3A TLC27M2
R39 1k
R40 1k
AZ_CURRENT
C14 100n
R43 20k
gain=21. For Vref = 5V, 1A = ADC 107.52

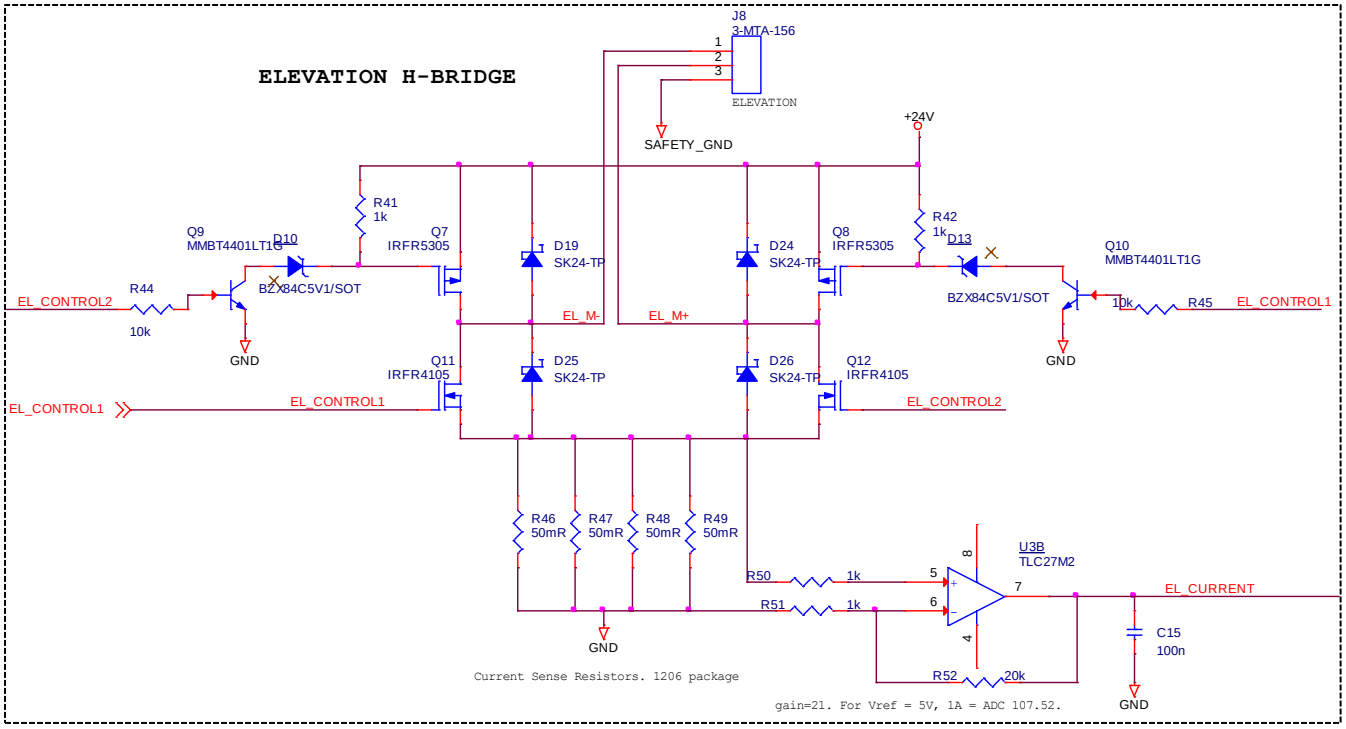
ELEVATION H-BRIDGE
J8
3-MTA-156
ELEVATION
SAFETY_GND
+24V
R41
1k
Q9
MMBT4401LT1G
D10
BZX84C5V1/SOT
Q7
IRFR5305
D19
SK24-TP
D24
SK24-TP
Q8
IRFR5305
R42
1k
D13
BZX84C5V1/SOT
Q10
MMBT4401LT1G
EL_CONTROL2
R44
10k
GND
EL_M-
EL_M+
10k
R45
EL_CONTROL1
Q11
IRFR4105
D25
SK24-TP
D26
SK24-TP
Q12
IRFR4105
EL_CONTROL1
EL_CONTROL1
EL_CONTROL2
R46
50mR
R47
50mR
R48
50mR
R49
50mR
U3B
TLC27M2
R50
1k
R51
1k
EL_CURRENT
C15
100n
R52
20k
GND
Current Sense Resistors. 1206 package
gain=21. For Vref = 5V, 1A = ADC 107.52.

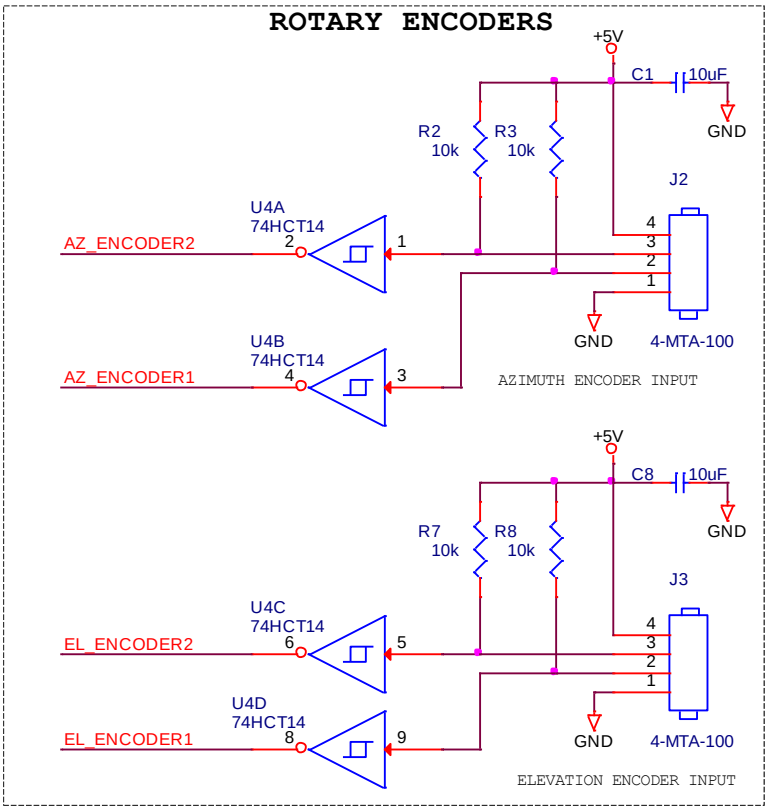
ROTARY ENCODERS
+5V
C1
10uF
GND
R2
10k
R3
10k
J2
U4A
74HCT14
AZ_ENCODER2
U4B
74HCT14
AZ_ENCODER1
GND
4-MTA-100
AZIMUTH ENCODER INPUT
+5V
C8
10uF
GND
R7
10k
R8
10k
J3
U4C
74HCT14
EL_ENCODER2
U4D
74HCT14
EL_ENCODER1
GND
4-MTA-100
ELEVATION ENCODER INPUT

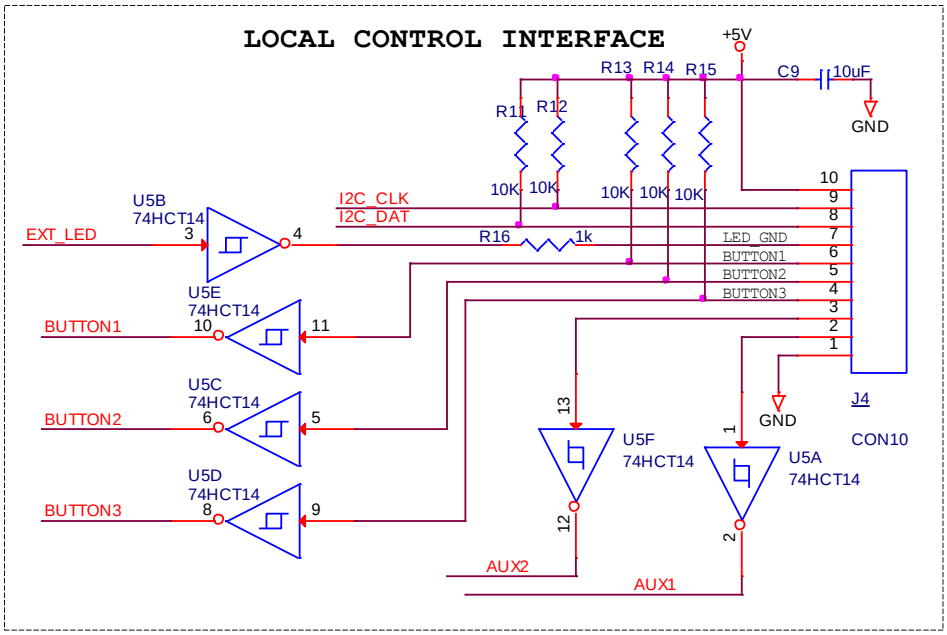
LOCAL CONTROL INTERFACE
+5V
R13 R14 R15
C9 10uF
GND
R11 R12
10K 10K
10K 10K 10K
I2C_CLK
I2C_DAT
U5B
74HCT14
EXT_LED
3
4
R16 1k
LED_GND
BUTTON1
BUTTON2
BUTTON3
10
9
8
7
6
5
4
3
2
1
J4
CON10
U5E
74HCT14
BUTTON1
10
11
U5C
74HCT14
BUTTON2
6
5
U5D
74HCT14
BUTTON3
8
9
13
U5F
74HCT14
12
AUX2
1
U5A
74HCT14
2
AUX1

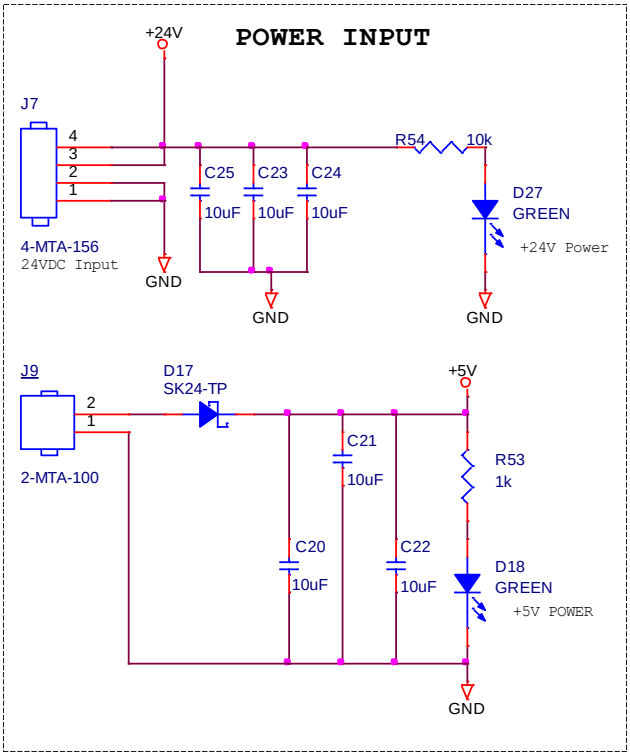
POWER INPUT
+24V
J7
4
3
2
1
4-MTA-156
24VDC Input
GND
C25 C23 C24
10uF 10uF 10uF
GND
R54 10k
D27
GREEN
+24V Power
GND
J9
2
1
2-MTA-100
D17
SK24-TP
+5V
C21
10uF
R53
1k
C20
10uF
C22
10uF
D18
GREEN
+5V POWER
GND

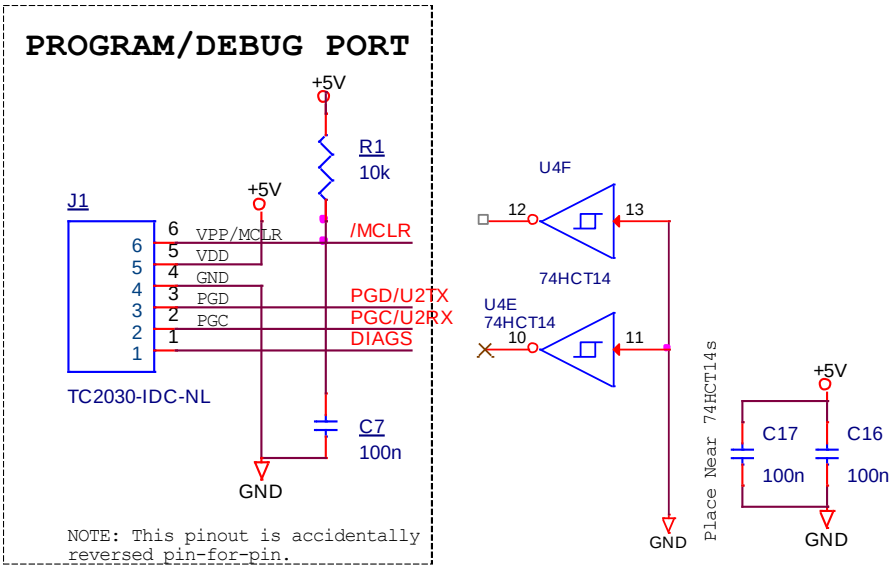

Layout

Dimensional Drawing

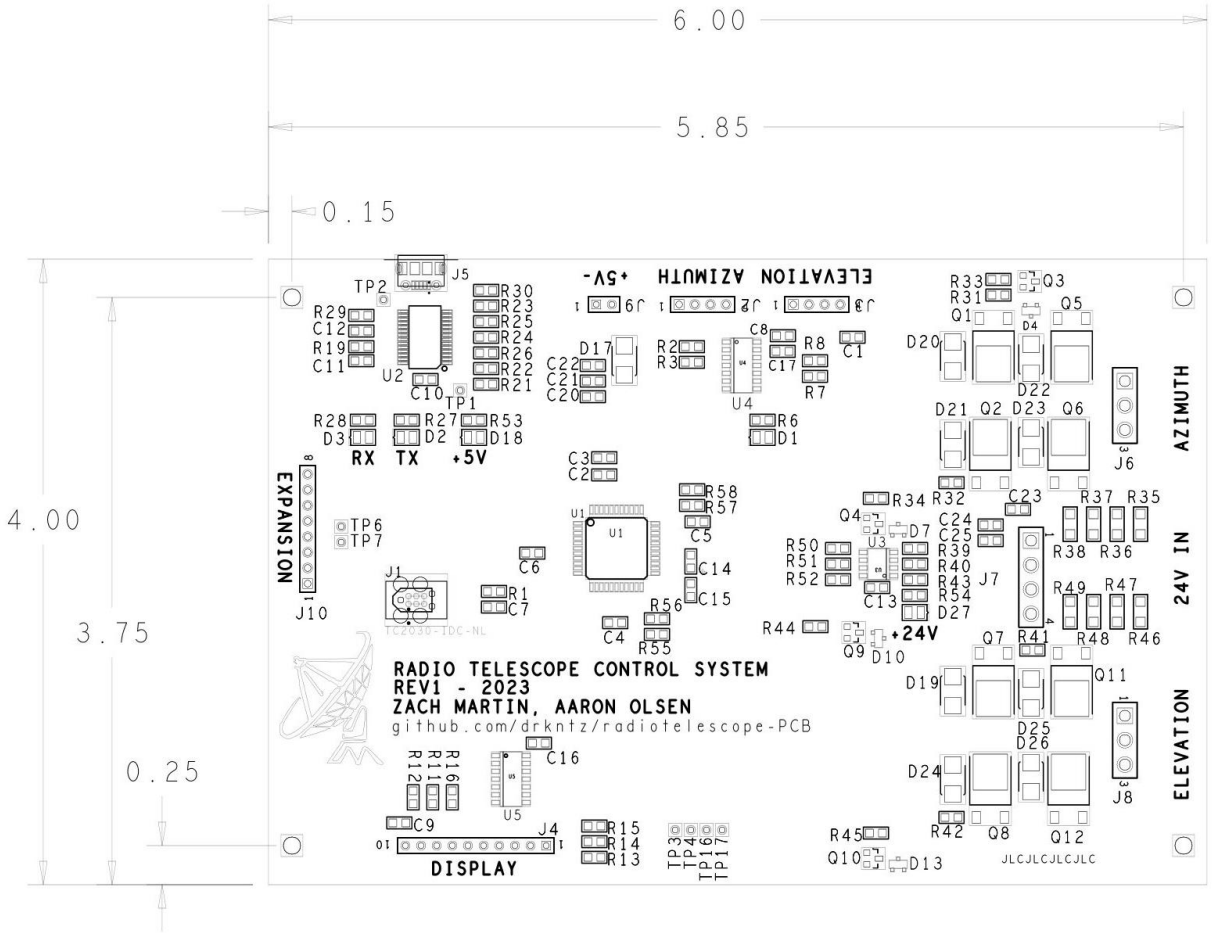

Top Layer

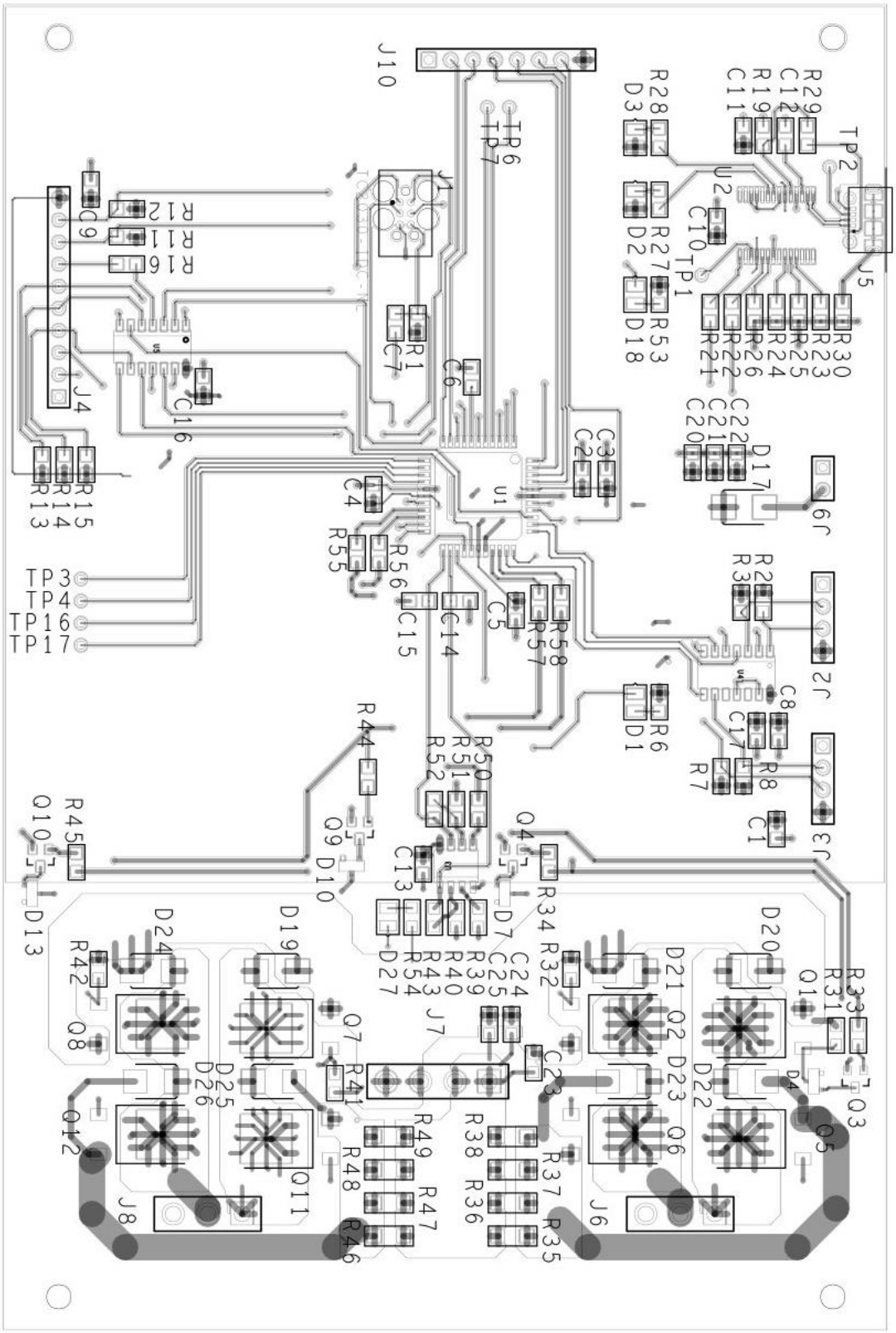
J10
TP6
TP7
J1
R28
D3
R29
C12
C11
R19
TP2
J5
U2
C10
TP1
R27
D2
R53
D18
R30
R23
R25
R24
R26
R22
R21
C22
C21
C20
D17
J9
C9
J4
C16
R1
C7
C6
C3
C2
U1
R13
R14
R15
C4
R55
R56
C15
C14
C5
R57
R58
TP3
TP4
TP16
TP17
R2
R3
J2
C8
C17
R7
R8
C1
J3
D1
R6
R44
R50
R51
R52
Q4
R45
Q10
Q9
D10
C13
D7
R34
R32
C24
C25
R39
R40
R43
R54
D27
D13
D24
D19
D20
D21
Q2
D23
Q6
R33
R31
Q1
Q3
Q5
D22
D4
R42
Q8
Q7
R41
J7
C23
D25
D26
Q12
Q11
R49
R48
R47
R46
R38
R37
R36
R35
J8
J6

Bottom Layer

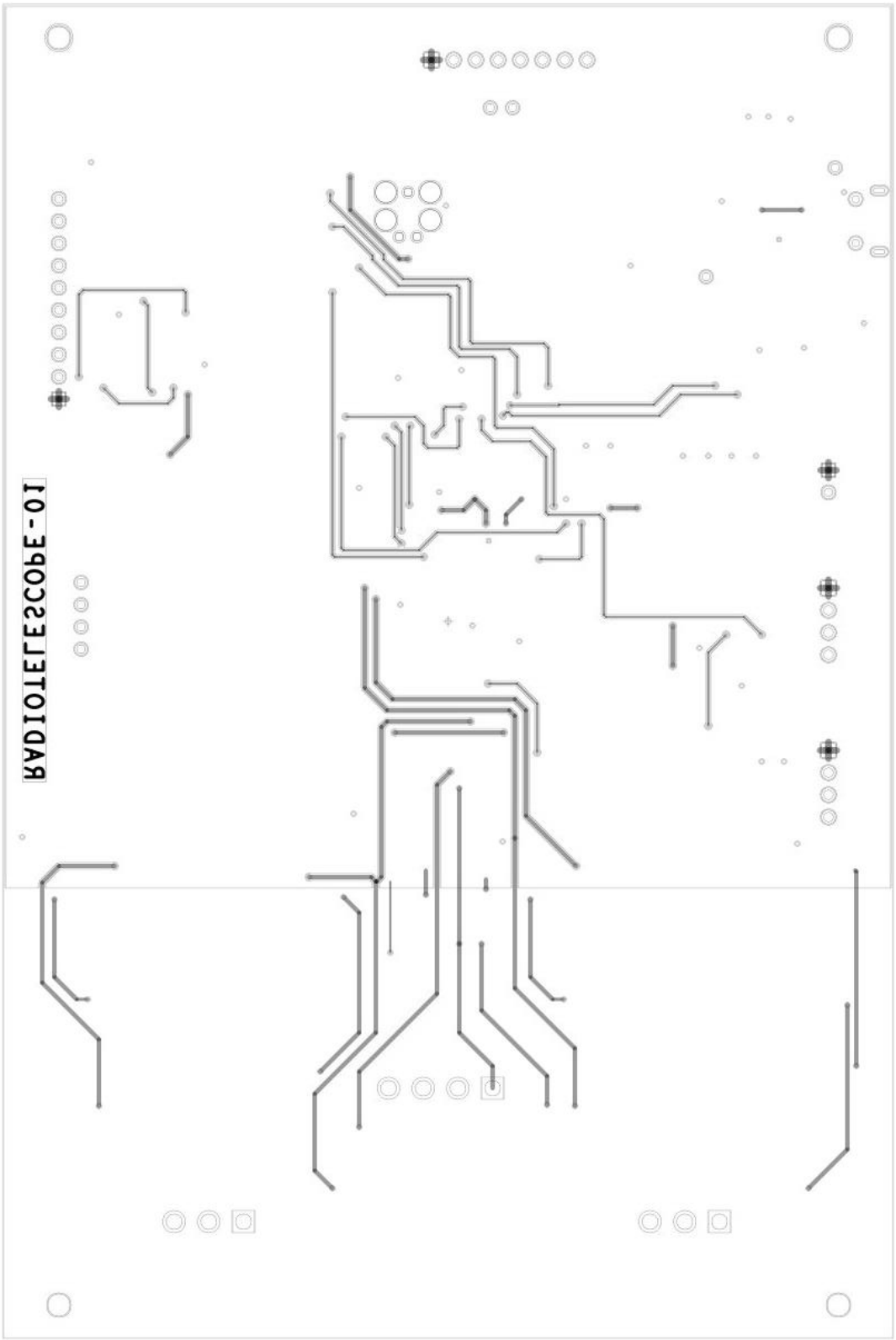

Silk Screen

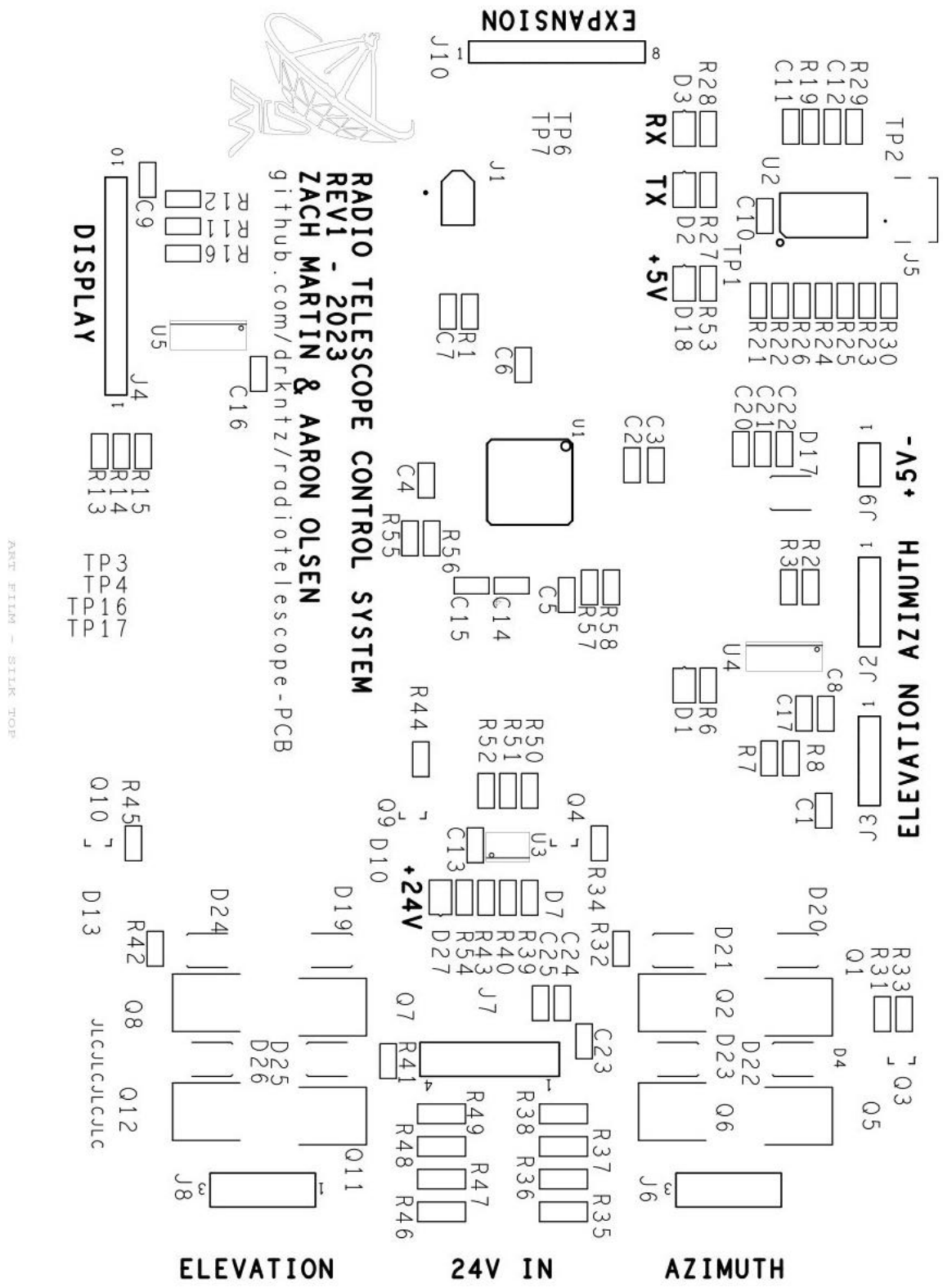
RADIO TELESCOPE CONTROL SYSTEM
REV1 - 2023
ZACH MARTIN & AARON OLSEN
github.com/drkntz/radiotelescope-PCB
EXPANSION
ELEVATION AZIMUTH
RX TX +5V -5V
DISPLAY
+24V
ELEVATION
24V IN
AZIMUTH
ART FILM - SILK TOP

Top Solder Mask

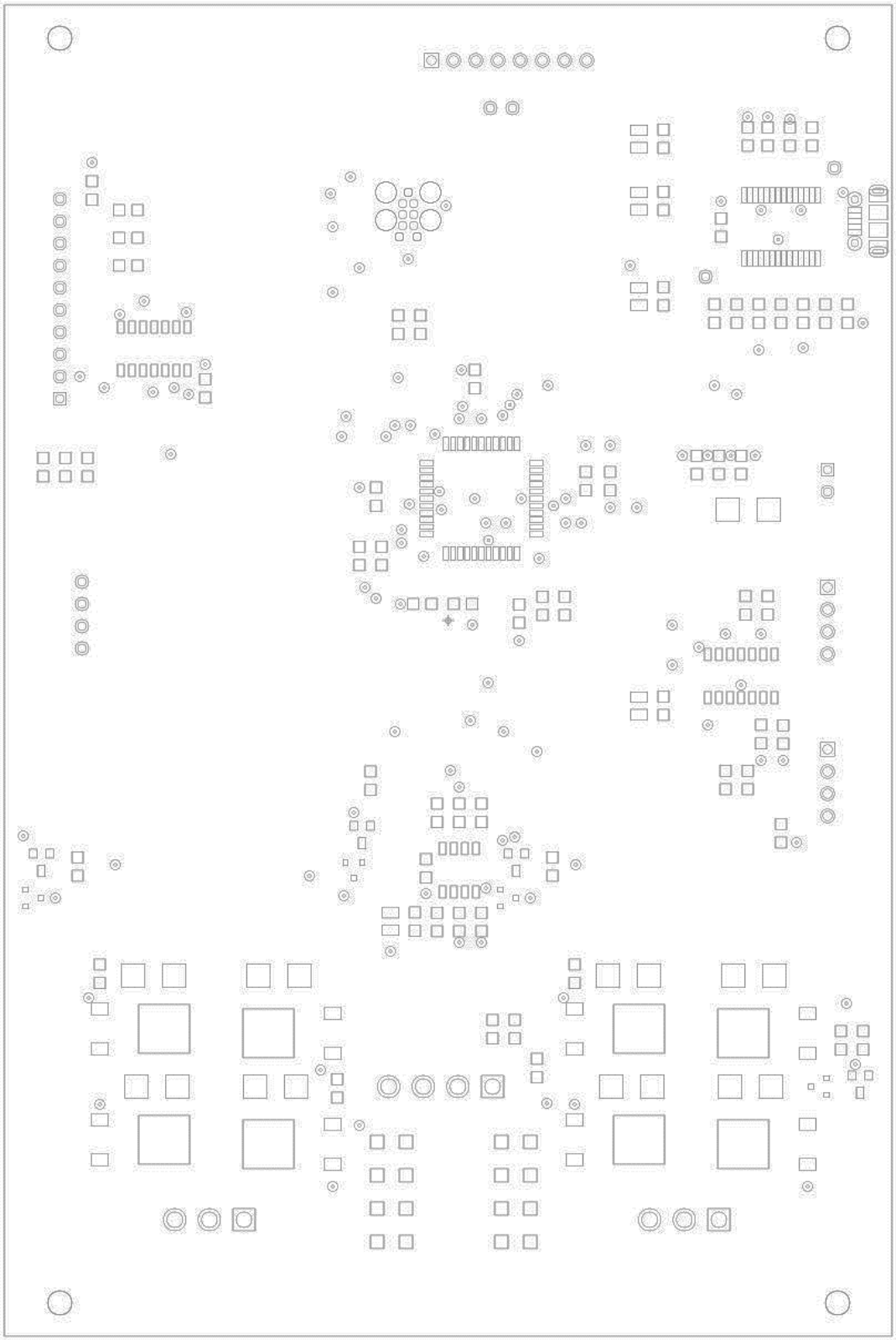

Bottom Solder Mask

Parts List

Table 23: Bill of Materials for the Entire Project.

Team Members:	Aaron Olsen, Zach Martin
Project Name:	Radio Telescope Control System
Date:	2/3/2023

Item Description	Manufacturer	Vendor or Source	Units/Batch	Price/Unit	Price	Quantity	Cost
PIC24FV32KA304 (Processor)	Microchip	Digikey	1	$ 4.90	$ 4.90	1	$ 4.90
FT232RL (USB-Serial Converter)	FTDI	Amazon.com	1	$ 6.49	$ 6.49	1	$ 6.49
LCD Display	GeeekPi	Amazon.com	1	$ 10.99	$ 10.99	1	$ 10.99
Printed Circuit Board	JLCPCB	JLCPCB	5	$ 8.00	$ 40.00	1	$ 40.00
74HCT14 (Inverters)	Texas Instruments	Digikey	1	$ 0.54	$ 0.54	2	$ 1.08
3-647609-4 (4-MTA-100 Male Header)	TE Connectivity	Mouser	1	$ 0.95	$ 0.95	2	$ 1.90
644518-2 (2-MTA-100 Male Header)	TE Connectivity	Mouser	1	$ 0.81	$ 0.81	1	$ 0.81
3-644615-3 (3-MTA-156 Male Header)	TE Connectivity	Mouser	1	$ 0.53	$ 0.53	2	$ 1.06
644752-4 (4-MTA-156 Male Header)	TE Connectivity	Mouser	1	$ 0.49	$ 0.49	1	$ 0.49
MMBT4401LT3G (NPN Transistor)	Onsemi	Digikey	1	$ 0.15	$ 0.15	4	$ 0.60
IRFR5305TRPBF (p-Channel MOSFET)	Infineon Technologies	Digikey	1	$ 1.55	$ 1.55	4	$ 6.20
IRFR4105TRPBF (n-Channel MOSFET)	Infineon Technologies	Digikey	1	$ 1.25	$ 1.25	4	$ 5.00
1-640456-0 (10-MTA-100 Male Header)	TE Connectivity	Mouser	1	$ 0.51	$ 0.51	1	$ 0.51
61300811121 (8-pin 0.1" Spacing Male Header)	Wurth Elektronik	Digikey	1	$ 0.40	$ 0.40	1	$ 0.40
1050170001 (Micro-USB Port)	Molex	Digikey	1	$ 1.41	$ 1.41	1	$ 1.41
LRS-350-24 (24-Volt Power Supply)	Mean Well	Amazon.com	1	$ 37.92	$ 37.92	1	$ 37.92
Rocker Switch Power Socket Inlet Module Plug	3Dman	Amazon.com	1	$ 7.99	$ 7.99	1	$ 7.99
03130 18 AWG Replacement Power Cord	C2G	Amazon.com	1	$ 8.45	$ 8.45	1	$ 8.45
24-Volt to 5-Volt Buck Converter Module	UCTRONICS	Amazon.com	1	$ 14.99	$ 14.99	1	$ 14.99
PICkit3	Comidox	Amazon.com	1	$ 38.95	$ 38.95	1	$ 38.95
3-640441-4 (4-MTA-100 Female Header)	TE Connectivity	Mouser	1	$ 0.26	$ 0.26	2	$ 0.52
3-640441-2 (2-MTA-100 Female Header)	TE Connectivity	Mouser	1	$ 0.20	$ 0.20	1	$ 0.20
3-644501-3 (3-MTA-156 Female Header)	TE Connectivity	Mouser	1	$ 0.64	$ 0.64	2	$ 1.28
3-640429-4 (4-MTA-156 Female Header)	TE Connectivity	Mouser	1	$ 0.73	$ 0.73	1	$ 0.73
BZX84B5V1HE3-TP (5.1 V Zener Diode)	Micro Commerical Co	Digikey	1	$ 0.27	$ 0.27	4	$ 1.08
B240-13-F (40 V Schottky Diode)	Diodes Incorporated	Digikey	1	$ 0.44	$ 0.44	9	$ 3.96
Enclosure	QILIPSU	Amazon	1	$ 30.99	$ 30.99	1	$ 30.99
TC2030-MCP-SOFT 6-Pin Cable with RJ12 Modular Plug	Tag-connect	Tag-connect.com	1	$ 41.34	$ 41.34	1	$ 41.34
TLC27M2CDR (Dual operational amplifier)	Texas Instruments	Digikey	1	$ 1.13	$ 1.13	1	$ 1.13
ERJ-HP6F2002V (20k Ohm SMD Resistor 0805)	Panasonic	Mouser	1	$ 0.36	$ 0.36	2	$ 0.72
ERJ-8BWFR100V (0.1 Ohm SMD Resistor 1206)	Panasonic	Mouser	1	$ 0.62	$ 0.62	8	$ 4.96
ERJ-HP6D4701V (4.7k Ohm SMD Resistor 0805)	Panasonic	Mouser	1	$ 0.44	$ 0.44	3	$ 1.32
ERJ-6GEYJ102V (1k Ohm SMD Resistor 0805)	Panasonic	Mouser	1	$ 0.10	$ 0.10	11	$ 1.10
ERA-6VEB1002V (10k Ohm SMD Resistor 0805)	Panasonic	Mouser	1	$ 0.68	$ 0.68	16	$ 10.88
GRM21BR6YA106ME43L (10 uF SMC Capacitor 0805)	Murata Electronics	Mouser	1	$ 0.38	$ 0.38	12	$ 4.56
C2012X7T2E104K125AE (100 nF SMC Capacitor 0805)	TDK	Mouser	1	$ 0.43	$ 0.43	11	$ 4.73
150080RS75000 (Red LED SMD 0805)	Wurth Elektronik	Mouser	1	$ 0.19	$ 0.19	3	$ 0.57
150080VS75000 (Green LED SMD 0805)	Wurth Elektronik	Mouser	1	$ 0.19	$ 0.19	2	$ 0.38
M10 Bolts x 25		True Value	1	$ 3.19	$ 3.19	4	$ 12.76
M10 Lock Washer		True Value	1	$ 0.33	$ 0.33	4	$ 1.32
Female M12 8 Pin Plug (A133880-ND)	TE Connectivity	Digikey	1	$ 10.11	$ 10.11	2	$ 20.22
Male M12 bulkhead pigtail connector (839-10-04035-ND	Tensility International Corp	Digikey	1	$ 11.69	$ 11.69	2	$ 23.38
Waterproof Pushbutton Switch (EG4570-ND)	E-Switch	Digikey	1	$ 5.02	$ 5.02	5	$ 25.10
Dual Axis Motor	Luoyang Jiawei Bearing Manufacturer Co., Ltd.	Alibaba	1	$ 499.00	$ 499.00	1	$ 499.00
Dual Axis Motor Shipping	Luoyang Jiawei Bearing Manufacturer Co., Ltd.	Alibaba	1	$ 432.00	$ 432.00	1	$ 432.00
Griddy Antenna	Waveform	Waveform	1	$ 179.00	$ 179.00	1	$ 179.00
Various screws, nuts, etc.			1	$ 30.00	$ 30.00	1	$ 30.00
Subtotal							$ 1,523.37
Labor Cost				Cost ($/hr)		Hours	
Design				$ 30.00		400	$ 12,000.00
Integration				$ 30.00		150	$ 4,500.00
Testing				$ 30.00		100	$ 3,000.00
Total Cost							$ 21,023.37

Appendix D: Program Code

The program code for this project involved writing custom firmware in the C language as well as incorporating Microchip Code Configurator (MCC)-generated drivers. These MCC-generated drivers generally handled the interfacing between the program code and the hardware peripherals, such as UART, timers, pins, and i2c. The following files note which are generated by MCC and which by the project authors. In some cases, the MCC files had to be modified after generation.

The entire program for the embedded microprocessor is several thousand lines long and spans over sixty pages. Therefore, the program code was removed from the appendix to keep the document size down. However, the program code for this project, including the microchip MPLAB X project settings, can be downloaded at the following URL: https://github.com/drkntz/radiotelescope-firmware.

Appendix E: Datasheets

SVH3 Motor

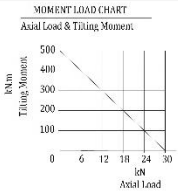

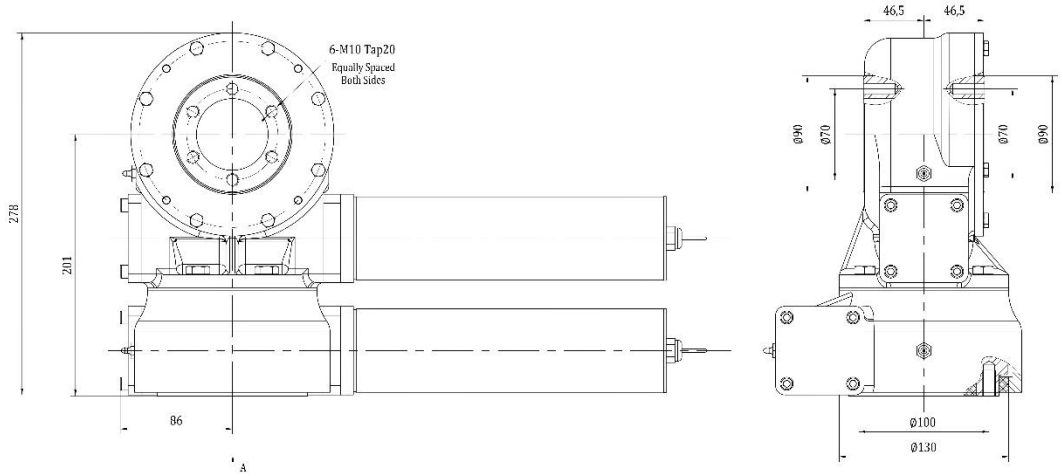

Wire Define	
Pin 1 (black)	motor −
Pin 2 (red)	motor + 24V
Pin 3 (yellow)	hall GND
Pin 4 (brown)	hall + (5-12V)
Pin 5 (blue)	hall A
Pin 6 (green)	hall B
Pin E (gray)	GND

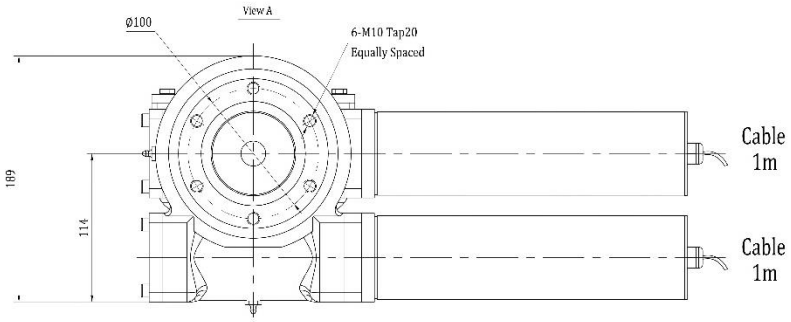

Slewing Drive Performance Parameters（Elevation direction）		
Rated Output Speed	0.048rpm	
Output Torque	716N.m	528 lbf.ft
Tilting Moment	1100 N.m	811 lbf.ft
Holding Torque	2200N.m	1479 lbf.ft
Static Axial Rating	30 kN	6750 lbf
Static Radial Rating	15 kN	3375 lbf
Dynamic Axial Rating	9.6 kN	2160 lbf
Dynamic Radial Rating	8.4 kN	1890 lbf
Gear Ratio	62:1	
Precision	≤0.12°	

MOMENT LOAD CHART

Axial Load & Tilting Moment

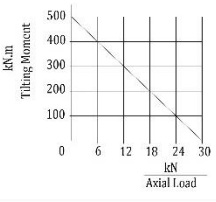

Slewing Drive Performance Parameters（Horzontal）		
Rated Output Speed	0.048rpm	
Output Torque	716N.m	528 lbf.ft
Tilting Moment	1100 N.m	811 lbf.ft
Holding Torque	2200N.m	1479 lbf.ft
Static Axial Rating	30 kN	6750 lbf
Static Radial Rating	15 kN	3375 lbf
Dynamic Axial Rating	9.6 kN	2160 lbf
Dynamic Radial Rating	8.4 kN	1890 lbf
Gear Ratio	62:1	
Precision	≤0.12°	

24VDC Planetary Reducer Motor Performance Data（24H/30/33）	
Rated Output Torque	33 N.m
Rated Output Speed	3 rpm
IP Class	IP 65
Gear Ratio	575:1
Rated Current	<1.9 A

MAGNETIC PULSE GENERATOR DATA		
Output type	-	voltage output
pull-up resistor	-	yes
Output signal	-	2 square wave signals
Phase quadrature	-	90 °
Impulses per revolution	ppr	2,channels A and B
Operating voltage	VDC	DC5-24
Operating current	mA	max. 12
Deviation of pulse width	-	max. 15 °
Deviation of phase shift	-	max. 15 °
Output voltage(low level)	VDC	max. 0.4 (20mA)
SIGNAL RISE TIME	ns	85
SIGNAL DECAY TIME	ns	60
Operation temperature	℃	-40 - +85

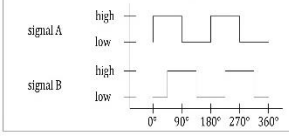

24VDC Planetary Reducer Motor Performance Data（24H/30/33）	
Rated Output Torque	33 N.m
Rated Output Speed	3 rpm
IP Class	IP 65
Gear Ratio	575:1
Rated Current	<1.9 A

MAGNETIC PULSE GENERATOR DATA		
Output type	-	voltage output
pull-up resistor	-	yes
Output signal	-	2 square wave signals
Phase quadrature	-	90 °
Impulses per revolution	ppr	2,channels A and B
Operating voltage	VDC	DC5-24
Operating current	mA	max. 12
Deviation of pulse width	-	max. 15 °
Deviation of phase shift	-	max. 15 °
Output voltage(low level)	VDC	max. 0.4 (20mA)
SIGNAL RISE TIME	ns	85
SIGNAL DECAY TIME	ns	60
Operation temperature	℃	-40 - +85

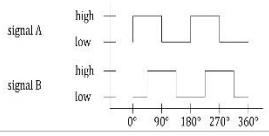

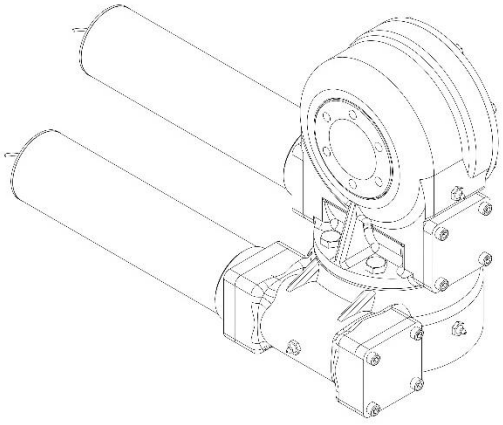

REV	DATE	REVISER	REVISER
DESIGNED BY	2020/10/27	Li Ming	Luoyang Jiawei Bearing Manufacturer Co., Ltd.
CHECKED BY	2020/10/27	Rui Wang	
APPROVED BY	2020/10/27	Shane Zhang	

WEIGHT	SCALE	Slewing Drive	
	1 : 3		
SYMBOLE ISO	SIZE	A3	SVH3-62B-RC-24H3033	REV
	SHEET	1 / 1		B

Mean Well LRS-350-24 (24-Volt Power Supply):
https://www.meanwell.com/productPdf.aspx?i=459

5 Volt Regulator:

https://github.com/drkntz/12-5_Volt_Regulator

PIC24FV32KA304 Microprocessor:
https://ww1.microchip.com/downloads/aemDocuments/documents/OTH/ProductDocuments/DataSheets/30009995e.pdf

Appendix E: Test Plans

Table 24: Power Supply Test

Test Author:	Aaron Olsen, Zach Martin		
Test Name:	Mean-Well 24 VDC Power Supply	**Test ID #:**	1
Description:	Examines the power supply voltage output, current output, and ability to rotate the motor.	**Test Type:**	☐ Component X Subsystem ☐ System
Name of Tester:	Aaron Olsen, Zach Martin	**Date:**	3/21/2023
Hardware/Software Version:	HW V1.0	**Time:**	2:30 p.m.

Test Setup: Connect various loads to power supply to ensure it can provide rated current (< 14.6A) and monitor regulation (<1%) and ripple (150mVpp max). This test will be conducted by powering on the power supply, attaching a power resistor to the output, and monitoring the output voltage on the oscilloscope as the load changes. A power resistor will be attached which provides a load of approximately 10A.

	INPUTS		**OUTPUTS**		**Pass**	**Fail**	**N/A**	**COMMENTS**
Test	Power Input	Load	Vout (DC)	Ripple				
1	120VAC	1k ohm resistor	24.0V	12.8mVpp	X			
2	120VAC	2.5 ohm power resistor	24.0V	30.4mVpp	X			

Test Summary: Power supply passed test with little to note. Ripple voltage was low, current output is OK, drives both light and heavy loads with no perceptible change in voltage regulation (within 1%).

Table 25: Microcontroller Test

Test Author:	Zach Martin		
Test Name:	Microcontroller Test	**Test ID #:**	2
Description:	This test examines current consumption, program function, UART terminal connection, GPIO and ADC peripherals.	**Test Type:**	X Component ☐ Subsystem ☐ System
Name of Tester:	Zach Martin, Aaron Olsen	**Date:**	3/28/23
Hardware/Software Version:	HW V1.0, SW V1.0	**Time:**	5:30PM

Test Setup: The surface-mount processor will be installed on the custom PCB, with R55-R58 omitted to isolate the H-bridge section. Only the +5V power limited to 100mA will be applied via a bench power supply to J9. 24V input will remain disconnected. A simple diagnostic program will be installed on the PIC via a PICKIT3 flash programmer. A UART terminal will be established using the debug connections, and the terminal will be used to toggle GPIO lines. A voltage will be applied to the ADC inputs and verified via the UART terminal.

	INPUTS		OUTPUTS		Pass	Fail	N/A	COMMENTS
1	+5V DC	100mA Max	Current consumption 37mA nominal		X			Green +5V LED turns on
2	PICKIT3 flash program		Program flash complete with modification		X			Had to modify the program connection at header J1: pinout was inverted from 1-6 to 6-1.
3	Debug UART via J1		Debug UART RX and TX characters		X			Uart2 via J1 works after inverting J1 connection as shown above.
4	USB to UART via J5		Main UART to USB RX and TX characters		X			
5	AZ Control 1 High	AZ Control 1 Low	High	Low	X			

6	AZ Control 2 High	AZ Control 2 Low	High	Low	X			
7	EL Control 1 High	EL Control 1 Low	High	Low	X			
8	EL Control 2 High	EL Control 2 Low	High	Low	X			
9	Status LED High		Status LED High		X			
10	AZ input 1 High	AZ input 1 Low	High	Low	X			Had to change the code as it expected the AZ1 encoder input to be an oscillator by default
11	AZ input 2 High	AZ input 2 Low	High	Low	X			
12	EL input 1 High	EL input 1 Low	High	Low	X			
13	EL input 2 High	EL input 2 Low	High	Low	X			
5	100mV into U3 amplifier		2.3V output	ADC read 2500mV	X			8.6% ADC error. Output of U3 amplifier is very noisy. Should add series resistance to C14 and C15 to form LPF
Test Summary: Test passed with modification. PCB current consumption is low at 37mA nominal, debug UART works, GPIO works, ADC input works with 8.6% error and noisy reading from U3 amplifier. J1 pinout was reversed and had to be modified by reversing the pinout on the programming cable.								

Table 26: USB-UART Bridge Test

Test Author:	Zach Martin		
Test Name:	USB-UART Bridge Test	**Test ID #:**	3
Description:	This is a “Loop-back” test. Characters sent over UART TX will be returned via RX.	**Test Type:**	X Component ☐ Subsystem ☐ System
Name of Tester:	Zach Martin, Aaron Olsen	**Date:**	3/8/23
Hardware/Software Version:	HW V1.0, SW V1.0	**Time:**	6PM

Test Setup: R21 and R22 will be removed from the PCB to isolate the USB-UART system. A wire will be used to short the TXD and RXD pads. +5V, 100mA is applied. A USB cable will be connected between the computer and the PCB, and a UART terminal will be established. Characters sent from the computer will be “looped back” and visible as a received character on the terminal. The TX/RX LED status will be observed during the test, both with and without wire jumper.

	INPUTS	**OUTPUTS**		**Pass**	**Fail**	**N/A**	**COMMENTS**
Test	Keyboard input	Output					
1	ASCII Characters 0-9, A-Z	Ascii Characters 0-9, A-Z		X			Rx’d character = Tx’d character
2	ASCII Characters	RX LED	TX LED			X	RX/TX LEDs both work, but are swapped

Test Summary: Received characters were observed to match the sent characters over the UART. RX and TX LEDs are swapped on the PCB. This does not affect the functionality of the PCB.

Table 27: H-Bridge Test

Test Author:	Zach Martin, Aaron Olsen		
Test Name:	H-Bridge Test	**Test ID #:**	4
Description:	This test tests the performance of the H-bridge subsystem built from discrete components. Switching transients, performance under various resistive and inductive loads, and thermal performance are tested.	**Test Type:**	☐ Component X Subsystem ☐ System
Name of Tester:	Zach Martin, Aaron Olsen	**Date:**	3/28/23
Hardware/Software Version:	HW V1.0, SW V1.0	**Time:**	10AM

Test Setup: Tests are performed with a functional PIC processor. 5V and 24V current limited to 100mA were applied to the PCB. 1.1k resistive load was applied to the output. The PIC was used to switch the H-bridges between forward, reverse, and off states. The oscilloscope was used to observe the transient waveforms at the load resistor and the waveforms at each of the H-Bridge Transistors' gates. The temperature of the H-bridge components was monitored with a FLIR IR camera to observe overheating. The output of the current sense amplifier was monitored on the oscilloscope at the output filter capacitor (C14 and C15). The test was repeated with the motor attached and unloaded.

	INPUTS				**OUTPUTS**		**Pass**	**Fail**	**N/A**	**COMMENTS**
Test	Vin	R_{LOAD}	Axis	Direction	I_{LOAD}	Temp				
1	24VDC	1kΩ	AZ	CW	~25mA	~25C (Ambient)	X			
2	24VDC	1kΩ	AZ	CCW	~25mA	~25C (Ambient)	X			
3	24VDC	1kΩ	ALT	CW	~25mA	~25C (Ambient)	X			
4	24VDC	1kΩ	ALT	CCW	~25mA	~25C (Ambient)	X			
5	24VDC	8Ω	AZ	CW	3A	35C	X			

6	24VDC	8Ω	AZ	CCW	3A	35C	X			
7	24VDC	8Ω	ALT	CW	3A	35C	X			
8	24VDC	8Ω	ALT	CCW	3A	35C	X			
9	24VDC	4Ω	AZ	CW	6A	150C		X		6A can be driven, but N-Channel MOSFET gets too hot
10	24VDC	4Ω	AZ	CCW	6A	150C		X		"
11	24VDC	4Ω	ALT	CW	6A	150C		X		"
12	24VDC	4Ω	ALT	CCW	6A	150C		X		"
13	24VDC	2.4 Ω	ALT	CW	10A	Over 160C		X		Cannot drive a 10A load without overheating. Observed smoke from transistor
14	24VDC	DC Motor	ALT	CW	300mA	~35C	X			Can easily drive motors.
15	24VDC	DC Motor	ALT	CCW	300mA	~35C	X			
16	24VDC	DC Motor	AZ	CW	300mA	~35C	X			
	24VDC	DC Motor	AZ	CCW	300mA	~35C	X			

Test Summary: Test passed with load currents below 6A, but we ran into thermal issues with load currents of 6-10A. This may be due to either lack of thermal conductivity between transistor solder pads and surrounding plane (we did have thermal reliefs which increase thermal resistance) or this could be due to the N-Channel MOSFETs not getting driven hard enough. The P-Channel MOSFETs were observed to be much cooler when compared to the N-Channel. The P-Channel MOSFETS were driven to ~18V, much past the threshold voltage, while the N-Channel MOSFETS were driven to ~5V, just beyond the threshold voltage. The on-state resistance may have been higher in the N-Channel. The H-bridge has no trouble with driving the motors in either direction.

Table 28: Test LCD and Human Interface

Test Author:	Zach Martin, Aaron Olsen		
Test Name:	Test LCD and Human Interface	**Test ID #:**	5
Description:	Use I2C to display characters on LCD using Arduino library and Arduino first, then using the microcontroller on the PCB with the library converted onto the microcontroller. Test LED control from microcontroller. Receive three button inputs to the microprocessor.	**Test Type:**	☐ Component X Subsystem ☐ System
Name of Tester:	Aaron Olsen, Zach Martin	**Date:**	4/6/2023
Hardware/Software Version:	HW V1.0, SW V1.0	**Time:**	6:30PM

Test Setup: An Arduino Uno was connected to a computer and the LCD I2C pins were connected to the Uno (5 V, GND, SDA, and SCL). SDA and SCL were connected to the SDA and SCL pins on the Uno. A test program was run on the Uno to verify the display function. The Arduino C++ library was adapted to C code to run on the PIC, which was tested in a similar way to write a character to each position of the LCD display.

	INPUTS		OUTPUTS	Pass	Fail	N/A	COMMENTS
1	Arduino Uno and LCD	The words “Radio Telescope Control System”	Printed “Radio Telescope Control System”	X			
2	PIC and LCD	The words “Radio Telescope Control System”	Printed “Radio Telescope Control System”	X			

Test Summary: The microcontroller can send characters to the display with no issue. We discovered that we can modify the Arduino driver fairly easily to drive the display, using a print function that we already wrote for the UARTs.

Table 29: Full System Test

Test Author:	Zach Martin, Aaron Olsen		
Test Name:	Full System Test	**Test ID #:**	6
Description:	With all systems connected properly, the main PC sends commands to the processor over the USB-UART communication path. These commands are interpreted and give proper outputs to the H-bridge and LCD. The H-bridge will move in desired directions based on the given command.	**Test Type:**	☐ Component ☐ Subsystem X System
Name of Tester:	Aaron Olsen, Zach Martin	**Date:**	4/16/2023
Hardware/Software Version:	HW V1.0, SW V2.0	**Time:**	6:30PM

Test Setup: All subsystems are connected according to the level-two functional decomposition. This includes the 24 V DC power supply, 5 V DC converter, PCB, main PC connected with USB, and motor. The motor had the test antenna and mount connected.

	INPUTS		OUTPUTS	Pass	Fail	N/A	COMMENTS
1	Main PC	CMD_STOP	Stops both motors	X			
2	Main PC	CMD_ALT_POS	Rotates antenna up in altitude	X			
3	Main PC	CMD_ALT_NEG	Rotates antenna down in altitude	X			
4	Main PC	CMD_ALT_STOP	Stops just the altitude motor	X			
5	Main PC	CMD_ALT_RESET	Resets altitude degrees to zero	X			
6	Main PC	CMD_AZ_POS	Rotates azimuth motor clockwise	X			
7	Main PC	CMD_AZ_NEG	Rotates azimuth motor counterclockwise	X			
8	Main PC	CMD_AZ_STOP	Stops just the azimuth motor	X			

9	Main PC	CMD_AZ_RESET	Resets azimuth degrees to zero	X			
10	Local Control	Button interrupt	Stops the program			X	
Test Summary: All basic commands from the main PC operated successfully in starting and stopping each motor as well as setting the zero point for the encoders. The motor turns on and off in a reasonable amount of time and the LCD updates according to the desired information on motor direction, antenna angles, and which source is giving the command (main PC, local, diagnostic).							